ACTA AGROPHYSICA

MECHANICAL PROPERTIES OF GRANULAR AGRO-MATERIALS. CONTINUUM AND DISCRETE APPROACH

Joanna Wiącek, Marek Molenda,
Józef Horabik

190

Instytut Agrofizyki
im. Bohdana Dobrzańskiego PAN
w Lublinie

Rozprawy i Monografie
2011 (1)

Opiniował do druku
Prof. dr hab. Jerzy Weres

Adres redakcji

Instytut Agrofizyki im. Bohdana Dobrzańskiego PAN, Wydawnictwo
ul. Doświadczalna 4, 20-290 Lublin, tel. (81) 744-50-61, www.ipan.lublin.pl

Streszczenia i pełne teksty prac dostępne są na stronie internetowej czasopisma
www.acta-agrophysica.org

Czasopismo jest umieszczone w następujących bazach:
Thomson Scientific Master Journal List
Polish Scientific Journals Contents – Life Sci.
Biblioteka Główna i Centrum Informacji Naukowej Uniwersytetu Przyrodniczego w Poznaniu
Instytut Bibliotekoznawstwa i Informacji Naukowej Uniwersytetu Śląskiego w Katowicach
Lonicera – serwis botaniczny

ISSN 1234-4125
ISBN 978-83-89969-51-4

Acta Agrophysica są do nabycia w dziale Wydawnictw Instytutu Agrofizyki PAN w Lublinie. Prenumeratę instytucjonalną można zamawiać w dziale Wydawnictw Instytutu Agrofizyki PAN w Lublinie oraz w oddziałach firmy Kolporter S.A. na terenie całego kraju. Informacje pod numerem infolinii 0801-205-555 lub na stronie internetowej http://www.kolporter-spolka-akcyjna.com.pl/prenumerata.asp

Wydanie I. Nakład 200 egz., ark. 10,6
Skład komputerowy: Wanda Woźniak
Druk: *ALF-GRAF*, ul. Abramowicka 6, 20-391 Lublin

CONTENTS

BASIC NOTATION

c – cohesion (kPa),
D – diameter (m),
e – coeficient of restitution,
E – Young modulus (MPa),
E_e – effective elstic modulus (MPa),
FF – flow function,
k – pressure ratio,
K – spring constant (N m^{-1}),
m – mass (kg),
N – normal force (N),
p – normal pressure (MPa),
q – tangential pressure (MPa),
Q – volume flow rate (m^3 h^{-1}),
R – radius (mm),
S – porosity,
t – time (s),
Δt – time increment (s),
T – tangent force (N),
V – volume (m^3),
w – moisture content, wet basis (%),
ε_1, ε_2,, ε_3 – principal strains,
ε – total strain,
λ – aspect ratio
μ, – coefficient of friction,
ν – Poisson's ratio,
φ – angle of internal friction (deg),
ρ – density (kg m^{-3}),
σ_1, σ_2, σ_3 – principal stresses (kPa),
σ – normal stress (kPa),
τ – shear stress (kPa).

1. INTRODUCTION

In the second half of the 20th century granular mechanics appeared to have a strong appeal both to scientists and to industrial practitioners. Granular materials have properties between those of solids and liquids, and arguments have been made that they should be treated as an additional state of matter in their own right (Jaeger *et al.* 1996). In important industries, such as chemical, pharmaceutical, cosmetics, food or agricultural, numerous operations involve processing granular materials as raw materials or final products. In the last two decades of the 20th century globalisation has put industrial firms handling particulate materials under severe pressure to reduce costs while enhancing the quality of their products.

One of the first propositions of mathematical description of the behaviour of granular material was published over 100 years ago (1895) – Janssen's method for the evaluation of loads exerted by grain on storage silos. The method was based on analytical solution of numerical equations describing the balance of forces on differential slice of grain filling the silo. Since that time numerous questions of granular mechanics have been solved based on mechanics of continuum and exact analytical solutions of differential equations relating load and deformation. An immense amount of knowledge was gathered and numerous solutions of engineering questions have been proposed. Regarding loads on silos, a broad outline of analytical methods available at the end of 20th century has been given by Drescher (1991). Granular mechanics made another step in progress with the proliferation of computers, when methods of approximate solutions of sets of differential equations entered in common use. This allowed to use material models based on non-linear continuum, contrary to those used up to the 1970's that were generally based on the linear continuum concept (e.g. Jenike and Johanson 2005). The finite element method (FEM), commercialised at the world market as several huge software packages, became a basic designer tool in many applications including granular mechanics. Since the 1980's till the end of the century many attempts have been undertaken to develop FEM computational models to represent the behaviour of granular materials in silos. In this method the material is represented as a continuum with an appropriate constitutive law, usually based on a semiempirical interpretation of static tests on relatively small samples. Mark *et al.* (1999) presented results of an international collaborative project performed to compare predictions of several silo phenomena by numerical simulations. The authors concluded that different programs gave very different predictions. The scatter showed that much further research is needed on the prediction of the filling state in silos if FEM is to be a useful tool. FEM cannot represent the filling process at all. A serious shortcoming of continuum calculations is the necessity to assume an initial unstressed surface profile at the angle of repose and an initial

unstressed density for the bulk solid. Continuum models cannot predict the packing structure of the deposit and pose problems in identifying and managing discontinuities.

The mechanics of continuum and analytical methods gave many acceptable interpretations of effects observed in the laboratory as well as satisfactory solutions of practical industrial problems used in the design of equipment and process control in all cases where the behaviour of granular material was close to solid state or fluid. Continuum calculations by definition could not tackle problems in that discontinuity, inhomogeneity or particle size have a considerable influence. Based on earlier investigations of arrays of disks or spheres, Cundal and Strack (1979) concluded that the numerical technique may be the most powerful way of modelling assemblies of such particles. The method termed Discrete (or Distinct) Element Method (DEM) is based on tracking the motion of each individual particle and obtaining detailed information about the system behaviour. For simulations, the trajectory and rotation of each particle in a system are obtained using a numerical time integration scheme. The contact forces in each contact point are evaluated at each step and are resolved into normal and tangential components. Newton's second law of motion is then used to determine the motion of each particle from any unbalanced force. The flexibility of numerical modelling that extended to loading configuration, particle size, size distribution and properties of the particles were regarded by the authors as an advantage over physical modelling. The authors compared force vectors observed in a photoelastic experiment with those obtained in a numerical simulation and concluded that DEM was a valid tool for fundamental research into the behaviour of granular assemblies. Since then substantial progress has taken place in DEM modelling, amplified by increase in computing power and proliferation of computing resources throughout the world. Simulations of Cundall and Strack were performed for approximately 150 two-dimensional particles. Today simulations of several thousands of 3D spheres or ellipsoids are conducted. Still a long way remains to be covered, regarding that the mass of 1000 seeds of wheat is approximately 40 g, thus a 40 kg sack contains approximately one million kernels. The success of DEM examination of granular material relies on proper use of concepts from several branches of science and engineering, such as: mechanics of continuum, impact mechanics, contact mechanics, strength of materials or programming.

The main objective of this book was to present the evolution and current state of study of the mechanical properties of granular solids with special focus on agro and food biologically based granular materials. The main features of biologically based materials that make them different from mineral materials are strong influence of moisture content on mechanical behaviour and high deformability of granules. These differences bring about certain peculiar behaviours and enforce ad-

justments of contact models and calculation techniques. This work reviews currently available solutions and presents problems that have a chance to be solved in the nearest future. Out of these only narrow portions of knowledge are presented in this book that are directly tied with the phenomena to be analysed, encountered by the authors in their laboratory examinations or in practice.

2. CLASSIFICATION OF GRANULAR MATERIALS

The term *granular materials* includes a large group of materials of particular physical, chemical and mechanical properties. Granular material is a three- phase system consisted of grains creating a skeleton and liquid and gases which fill intergrain space (Łukaszuk and Horabik 2002).

According to Herrmann (2002) granular media is a system consisted of macroscopic grains of sizes range from several meters to several microns. The granular materials can be found in kitchen (sugar, salt), geophysics (sand, gravel) and also in astrophysics (asteroids), which prove their commonness.

Peculiar nature of granular media which have some properties of gases, liquids and solids causes that granular materials are considered to be the fourth state of matter (Jaeger *et al.* 1996). The facts which prove the rightness of that opinion are following: existing of static friction, inelastic collisions and very small energy of thermal motions in comparison to potential energy of gravtational field. The granular materials behave like a liquid or like solid dependenly on parameters such as density of system, moisture et al. As the consequence of rise of angle of inclination of surface of sandpile having a feature of solid to value higher than dump angle the flow begins typical for liquids.

The variety of granular materials and their different properties result in difficulties in defining and describing these materials. The classification of materials of different and variable physicochemical, mechanical and geometrical properties is a difficult task. A lot of standards which normalise and order the most important properties of materials were proposed. The parameters which are taken into account for classification of granular materials are: size of particles, shape, density, flowability, abrasiveness, toxicity et al.

CEMA-Conveyor Equipment Manufacturer's Association and ISO (Chattopadhyay *et al.* 1994) are the most popular classification systems. The former classifies materials according to their bulk density, size, flowability, abrasiveness and other mixed properties. ISO classification includes particle size, flowability and several mixed properties.

The general classification of granular materials according to size recognises fine-grained and coarse-grained materials.

The *British Pharmacopoeia* recommends following division of powders (Barbarosa-Cánovas and Vega-Mercado 1996):

- coarse-grained,
- moderately coarse-grained ,
- moderately fine-grained,
- fine-grained,
- very fine-grained.

Based on ISO classification, MHEA (Mechanical Handling Engineers' Association, U.K.) (Chattopadhyay *et al.* 1994) divided granular material into 10 classes according to dimension of particles (D), however Chattopadhyay *et al.* proposed five following groups:

- dust $D \leq 0.42$ mm,
- grain $D \leq 3.35$ mm,
- lump $D \leq 40$ mm,
- clump $D \leq 200$ mm,
- block $D > 200$ mm.

The classification according to shape of particles proposed by ISO is as follows:

- sharp-edged, with three dimensions similar,
- sharp-edged, with one of the dimensions cleary greater than the other two,
- sharp-edged, with one or three dimensions cleary smaller than the other two,
- round-edged, with three dimensions similar,
- round-edged, with one or three dimensions cleary smaller than the other two,
- fibrous, stringy, curly, linked.

Based on Carr's classification (1965) and BS-2955 (1958) Chattopadhyay *et al.* proposed detailed classification taking into account shapes of three-, two- and onedimentional particles and particles of irregular shapes.

The density which is a ratio of mass and volume of particle is one of parameters characterizing granular materials and influencing highly their mechanical characteristics.

The classification of materials according to bulk density (ρ) is as follows (Horabik 2001):

- light $\rho < 600$ kg m^{-3},
- medium 600 kg m^{-3} $< \rho \leq 1100$ kg m^{-3},
- heavy 1100 kg m^{-3} $< \rho \leq 2000$ kg m^{-3},
- very heavy $\rho > 2000$ kg m^{-3}.

The flowability defined as a motion of particles with reference to neighbouring particles or along surfaces is a next parameter describing granular materials (Peleg 1985). It has a huge influence on processes occurring during storage and handling of materials in industry and agriculture. The conventional classifications of materials according to flowability origin from classification proposed by Jenike (1964). It was based on flow function (*FF*).

Chattopadhyay *et al.* extended Jenike's classification adding two extreme classes:

- fluidlike flooding
- very free flowing $FF > 10$,
- free flowing $10 > FF > 4$,
- average flowing $4 > FF > 2$,
- poor flowing $2 > FF$,
- sluggish/interlocked.

The abrasiveness of materials defines ability of particles to destroy surfaces of devices remaining in contact with particles as a result of its displacement. The knowledge of abrasiveness of grains enables designer to choose proper material while designing devices and to limit damages and waste.

The classification of materials according to abrasiveness proposed by Chattopadhyay *et al.* includes four following classes:

- mildly abrassive,
- moderately abrasive,
- extremely abrasive,
- very sharp, gouges soft materials like rubber.

Among classifications presented above recommended by ISO and CEMA there are also classifications taking into account different properties affecting processes which granular materials are subjected to. These are for example:

- friablility,
- stickiness,
- toxicity,
- explosiveness,
- flammability,
- higroscopic properties.

3. MECHANICS OF GRANULAR MEDIA – CONTINUUM APPROACH

The microstructure of engineering materials is discontinuous. However, for a majority of engineering problems it is not necessary to take into account the discontinuous nature of the material because engineering problems take material in large quantities. The quantities are large enough for the microstructure of the material to be described by averaged material properties, which are continuous.

The physical and mathematical formulation of the contact mechanics is built upon the mechanics of materials and continuum mechanics. The description of single contact between two bodies appears to be insufficient to describe the mechanical behaviour of multi-particle systems, such as granular matter. Numerous problems of technology of granular materials have been successfully solved using the continuum approach. Processes involving the behaviour of static deposit or slow motion of the material were treated using the mechanics of solids. In the case of rapid flow of granular materials in ducts or chutes fluid mechanics have found successful applications. The importance of mechanical behaviour of granu-

lar media for various branches of technology resulted in numerous theoretical models and experimental methods of investigation of granular materials, dispersed in books and articles of various disciplines.

The granular material considered as a solid reveals a low extension strength or none at all. The materials have relatively high compressibility under compression and variable shear strength. The shearing of loose material results in an increase in their density, while shearing of a dense material causes its loosening. Shear deformation leads to plastic flow. A static medium revealing initially the features of solid phase behaves as a liquid when the energy delivered to the system overcomes friction.

The first development of the mechanics of granular materials was based on continuum mechanics. Its objective was the search for constitutive equations, i.e. relationships connecting stresses and strains in the material under mechanical load. The different deformability of materials under stress results in the necessity of deriving constitutive equations for specific classes of materials. Physical properties are material parameters of constitutive equations.

The mechanical properties of materials are based on interactions at the molecular level, however real systems are much bigger and in certain applications the question of non-homogeneity arises. The continuum concept, which is a basic model of material in the mechanics of deformable bodies, encountered difficulties with the description of more complex granular materials. The mechanics of solids assumes continuum of matter and displacements of particles under external forces on macroscopic level. It gives a basis to models which describe the behaviour of complex systems through deriving equations of motion for a representative volume. The representative volume is a minimum volume for which the properties of material can be averaged.

The assumption of continuum of granular materials enables researchers to apply terms originating from continuum mechanics (such as strain, stress etc.) to describe the mechanical properties of granular materials. The model of material which assumes its continuum played an important role in the development of technology and for numerous applications still remains a useful description of material behaviour.

Based on the available results, the viscous-elasto-plastic model seems to be the most suitable to describe the nature of granular materials for some applications in the silo technique. The difficulties with mathematical description of materials and low significance of viscosity and elasticity of some materials result in assumptions which treat granular media as plastic media. That approach is the basis of the ideal plastic model and the plastic model with hardening and softening presented in chapter 3.3.

Among models based on constitutive equations the empirical and theoretical models are distinguished. The former are created on the basis of experimental data providing knowledge about the behaviour of material under stress. The latter

ones originate from physical laws (first principles) which are used to describe the behaviour of systems in the micro- and macroscopic scale. The development of mechanics of granular media resulted in numerous models and some of them are more popular than others. The Coulomb criterion of plasticity, plastic model with hardening and softening, macroscopic and microscopic models are the most popular. The inclusion of new effects (particle rotations, friction, force distribution in contact points etc.) results in more accurate descriptions of material behaviour. The ability to describe mathematically granular materials enables researchers to numerically model observed effects and to foresee their behaviour in practice. In the case on numerical techniques, the models based on the continuum approach (e.g. FEM (Akin 1994, Goodey *et al.* 2003) and the discrete approach (e.g. DEM (Cleary and Sawley 2002, Yu 2004)) are frequently used.

The elastic-plastic models of Coulomb-Mohr and Drucker, presented in chapter 3.1., are among the simplest ones. In spite of their simplicity, they may be applied in FEM codes to analyse strains for design needs. The application of these models in commercial codes resulted in an increase in the accuracy of engineering design. The disadvantages of that group of material models are difficulties with measuring the material constant in laboratory tests.

The models originating from Molecular Dynamics (e.g. DEM) and based on rheological contact models have a more sound physical basis than those mentioned above, but they have not found any commercial application yet.

3.1. The flow condition

The plasticisation is a process of material evolution from elastic or rigid state to plastic state (Bednarski 1995). The finding of the yield condition is a main task of the mechanics of granular media.

The following criteria are the most popular among the plasticity criteria formulated based on the terms used in the continuum mechanics (Horabik 2001):

- Coulomb-Mohr plasticity criterion,
- Drucker-Prager plasticity criterion,
- Lade-Duncan plasticity criterion.

The Coulomb-Mohr plasticity criterion assumes that shear strength τ is a linear function of normal stress σ

$$\tau = \sigma tan\varphi + C, \tag{1}$$

where φ is the internal friction angle and C is cohesion.

Resistance resulting from internal friction and cohesion is overcome by strains in the moment of yield strength.

The Coulomb-Mohr plasticity criterion expressed through principal stresses is a set of 6 equations, two of which are as follows:

$$\sigma_1 - \sigma_2 = (\sigma_1 + \sigma_2) \cdot sin\varphi + 2C \cdot cos\varphi$$
$$\sigma_2 - \sigma_3 = (\sigma_2 + \sigma_3) \cdot sin\varphi + 2C \cdot cos\varphi \quad (2)$$

These equations describe 6 surfaces which create a pyramid in the space of main components of stress. The axis of the pyramid lies on the axis of isotropic stresses.

The Coulomb-Mohr plasticity criterion has a shape of a triangle on a deviator surface whose sides join at a point of the same value of internal friction angle (φ = *const.*) (Fig. 1). Depending on the value of the internal angle, the ratio of triangle sides has different values (Cudny and Binder 2005).

The Coulomb–Mohr plasticity criterion is a basis for more advanced constitutive models, however their application is a challenge.

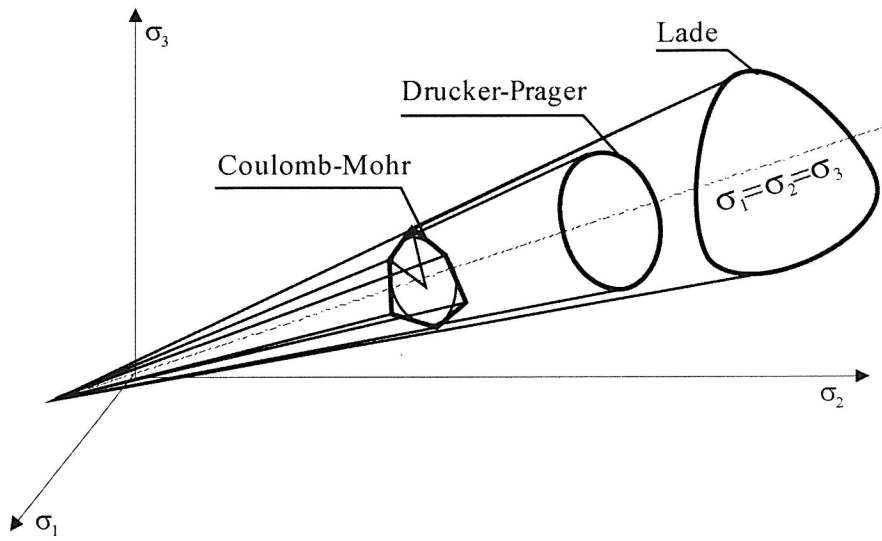

Fig. 1. Plasticity criteria: Coulomb-Mohr, Drucker-Prager and Lade-Duncan in principal stress space

The application of the Drucker-Prager criterion in numerical calculations enables researchers to avoid several problems occurring during the application of the Coulomb–Mohr plasticity criterion. This allows for defining the direction of the normal to plasticity surface in each point of the surface.

The Drucker-Prager criterion has the following form:

$$F = J_2^{\frac{1}{2}} + \frac{1}{3}\alpha I_1 - k^* = 0, \tag{3}$$

where:

$$I_1 = \sigma_1 + \sigma_2 + \sigma_3,$$

$$J_2 = \frac{1}{6}[(\sigma_1 - \sigma_2)^2 + (\sigma_2 - \sigma_3)^2 + (\sigma_3 - \sigma_1)^2]$$

$$k^* = \frac{(6 \cdot c \cdot cos\varphi)}{\left[3^{\frac{1}{2}} \cdot (3 - sin\varphi)\right]},$$

$$\alpha = (6 \cdot \sin\varphi) / \left[3^{\frac{1}{2}} \cdot (3 - sin\varphi)\right].$$

The plasticity surface in the main components of stress is a surface area of a cone with axis lying on line $\sigma_1 = \sigma_2 = \sigma_3$.

The experimental tests conducted for ground samples reveal the lack of possibility to apply the criterion to practical applications for ground materials with high angles of internal friction (Cudny and Binder 2005).

The Lade-Duncan (Lade *et al.* 1987) criterion formulated on the basis of experimental tests is defined by means of the first and third stress tensors (I_1, I_2):

$$F = \frac{I_1^3}{I_3} - k^* = 0, \tag{4}$$

where:

$$k^* = (-3 - sin\varphi)^3 / [(-1 - sin\varphi) \cdot (-1 + sin\varphi)].$$

The plasticity surface in the space of the main components of stress is the surface area of a cone with a smooth base and triple axial symmetry.

The shape of the contour of the Lade–Duncan criterion is close to the circular shape of the Drucker-Prager criterion for low angles of internal friction. It is in accordance with the Coulomb-Mohr plasticity criterion for stresses corresponding to triaxial compression only (Zhang *et al.* 1994).

3.2. The plastic flow rule

The plastic flow rule is a relationship between components of tensor of plastic deformation increment or components of tensor of velocity of plastic deformation and components of stress tensor which occur during ideal plastic body displacement processes (Bednarski 1995). The rules are formulated on the basis of assumptions. The experimental verification of these assumptions is needed because of frequent disagreement of theory and experiment. That disagreement depends on both the type of material and the test conditions.

The theory of plastic flow assumes the existence of plastic potential $G(\sigma_{ij})$ in the stress space. The existence of plastic potential was confirmed through experimental tests.

The relationship between components of tensor of plastic deformation increment $d\varepsilon_{ij}$ with components of stress tensor result in the following plastic flow rule:

$$d\varepsilon_{ij} = d\lambda\left[\partial G(\sigma_{ij})/\partial\sigma_{ij}\right], \tag{5}$$

where $d\lambda$ is a parameter depending on energy of plastic deformation.

The plastic potential $G(\sigma_{ij})$ is frequently taken to be identical with the yield condition $F(\sigma_{ij})$, which makes physical and geometrical interpretation of the rule easier, and in such a case we speak about the so-called associated flow rule:

$$d\varepsilon_{ij} = d\lambda\left[\partial F(\sigma_{ij})/\partial\sigma_{ij}\right]. \tag{6}$$

The models which take into account material hardening ensure a higher accuracy of description of the plastic flow process. The development of such models resulted in many varieties of models but all of them assume that the material has not a single yield condition but a whole family of yield conditions (Horabik 2001):

$$F\left(\sigma_{ij}, x\right) = 0. \tag{7}$$

The density of material ρ, volumetric weight γ, porosity p or its index e can be a yield parameter x (Dresher 1991). The form of function F depends on the type of material and it is measured experimentally.

The stiffness of granular materials depends on both the actual state of stress and the stress path. The hypoplastic models which are an alternative for elasto-plastic models allow for general description of a nonlinear stress-strain relationship (Kolymbas 2000). The constitutive equations allow for taking into account non-elastic properties of materials and, contrary to the elasto-plastic models, they

do not require the recognition of elastic and plastic deformations and plastic and hardening rules. Herle and Gudehus (1999) pointed out that simple experimental tests (e.g. measurement of angle of repose, measurement of maximal and minimal density and shear and compression tests) are sufficient to calculate the parameters of the hypoplastic model.

3.3. Plastic model with hardening and softening

Models of plastic flow with material hardening and softening attempt to predict overall change of the material state from any initial state to any other final state or to critical state when material yield without volume change. Special attention is payed in the models to very important role of density ρ, which is treated as hardening parameter (Drescher 1991). It is assumed that the material has no single yield condition but a whole family of such conditions:

$$F(\sigma_{ij}, \rho) = 0. \tag{8}$$

Density ρ is strictly related to volumetric deformation and dependent on the major principal stress $\rho(\sigma_1)$. The most important contribution in the development of the model of granular material with hardening and softening is that by Roscoe (1970). In the model, for the particular values of density ρ we obtain, in the plane (τ,σ), yielding conditions separating the plastic states of the material from its elastic or rigid states. As higher density is related to higher strength, the yield condition is a monotonically increasing function of density. For a fixed density ρ the yield condition represents in the stress space an enclosed surface that, in the case of a cohesionless material, passes through the origin of the system of coordinates whose axis of symmetry is the axis of isotropic stress. In axis-symmetrical state of stress the yielding condition can be written in the system of coordinates (p,q):

$$F(p, q, \rho) = 0, \tag{9}$$

where:

$$p = \frac{1}{3}(\sigma_1 + 2\sigma_2),$$

$$q = \sigma_1 - \sigma_2,$$

$$\sigma_1 \neq \sigma_2 = \sigma_3.$$

In Figure 2 the critical line separates the area of compaction where plastic strain is accompanied by an increase in density $\rho > \rho_1$ and therefore expansion of

the yield curve from the area of dilation in which strain is accompanied by volume increase of the material, decrease in density $\rho < \rho_2$, i.e. in effect shrinking of the yield curve. The change in density is defined by the law of conservation of mass:

$$d\rho = \rho d\varepsilon_p, \tag{10}$$

where:

$$d\varepsilon_p = \frac{dV}{V} = d\varepsilon_1 + 2d\varepsilon_2,$$

$$d\varepsilon_q = \frac{2}{3}(d\varepsilon_1 - d\varepsilon_2).$$

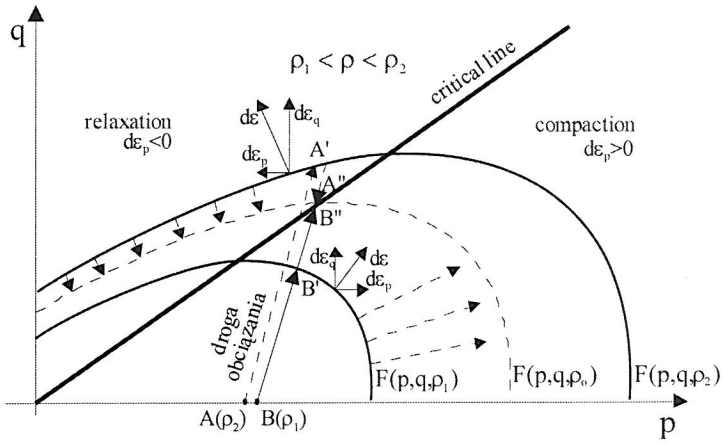

Fig. 2. Yield curves with compaction and dilation regimes

The critical line represents the state of stress in the material that causes yielding without changes in density, therefore corresponds to steady flow. The above model comprises hardening, softening, or flow in the critical state of stresses. The hardening or softening are determined by the sign of the partial derivative $\partial F/\partial p$. If the following relations occur in the process under study:

$$F(p, q, \rho) = 0, \tag{11}$$

$$dF(p, q, \rho) = 0,$$

then the yield condition is fulfilled. If we also have the inequality:

$$\frac{\partial F}{\partial p} dp + \frac{\partial F}{\partial q} dq > 0, \tag{12}$$

which means that the angle between the direction of stress increment (dp, dq) and the direction of the normal to the yield curve is less than 90° and

$$\frac{\partial F}{\partial p} > 0, \tag{13}$$

then, on the grounds of the assumption of coaxiality of the principal stresses and strain increments, the increase of volumetric deformation is positive ($d\varepsilon_p > 0$). In such a case material hardening takes place. Density increases ($d\rho > 0$), and the yield curve expands. Such plastic strain is called stable strain. In this case the flow rule presents a unique description of plastic strain of the material.

In a case when the partial derivative equals zero:

$$\frac{\partial F}{\partial p} = 0 \tag{14}$$

the strain increment $d\varepsilon_q$ tends to infinity, and increase of volumetric strain $d\varepsilon_p$ is indeterminate. This is the case of critical yielding. The material is in the state of steady flow at constant material density. Therefore, neither hardening nor softening of the material take place.

In the case of the inequality of:

$$\frac{\partial F}{\partial p} < 0 \tag{15}$$

it follows from the flow rule that the increase in the volumetric strain is negative ($d\varepsilon_p < 0$), and therefore density decreases ($d\rho < 0$) and material softening takes place. The material yields, and the yield curve shrinks due to the decreasing density ρ:

$$\frac{\partial F}{\partial \rho} d\rho > 0. \tag{16}$$

As the total differential of the yield condition $F(p,q,\rho)$ equals zero:

$$\frac{\partial F}{\partial p}dp + \frac{\partial F}{\partial q}dq + \frac{\partial F}{\partial \rho}d\rho = 0, \tag{17}$$

therefore, taking into account relation (43), vector (dp, dq) must be pointed into the interior of the initial yield curve:

$$\frac{\partial F}{\partial p}dp + \frac{\partial F}{\partial q}dq < 0. \tag{18}$$

This is a case of experimentally observable unstable yielding with softening. Stable or unstable behaviour of a material can be observed at the same density of the material but at different stress paths. The model predicts stable and unstable behaviour of material also for the case of the same stress path but different initial densities.

The model with density controlled hardening and softening does not describe correctly all the mechanical processes that take place in granular materials. It provides a unique description only for the stress paths on which compaction of the material occurs. This substantiates the adoption of the associated flow rule. The model does not describe accurately the transition of the material from stable state to steady flow in critical state, nor does it uniquely describe unstable states of the material.

Density hardening is an example of isotropic hardening, that is such a process in which the yield curve expands uniformly, while retaining its shape.

There are also hypotheses of anisotropic hardening, assuming that in the course of plastic strain the yield curve does not change its shape and size, but moves as a rigid object towards the increase of plastic strain (Voyiadjis *et al.* 1995). Such a hardening is called kinematic hardening. The yield condition in an advanced stage of the process of kinematic hardening of the material can be described by means of the function:

$$F(\sigma_{ij} - \alpha_{ij}) = 0, \tag{19}$$

where tensor α_{ij} represents the displacement of the yield condition, and therefore the kinematics of the hardening.

3.4. Constitutive models of granular materials

The developement of mechanics of granular materials resulted in many constitutive models describing real systems (nonlinearly elastic, viscoelastic, elasto-plastic, viscoplastic and hypoplastic).

Among the more advanced elasto-plastic models that find a broader application for granular materials of plant origin the models of Ghaboussi-Momen and

Lade should be mentioned. They were applied by Zhang *et al.* (1994) to describe the stress- strain relationship for wheat grain mass.

Mentioned models assume that total strain ε_{ij} is a sum of elastic ε^{e}_{ij} and plastic strains ε^{p}_{ij}:

$$\varepsilon_{ij} = \varepsilon^{e}_{ij} + \varepsilon^{p}_{ij}. \tag{20}$$

The model of Ghaboussi and Momen adopts the Drucker-Prager yield condition and it describes phenomena typical for isotropic and kinematic hardening. It describes especially well the anisotropy of material, the hysteresis of stress-strain cycle and the evolution of hysteresis loop in the course of multiple loadings.

The model of Lade presents plastic strain as a sum of plastic strain related with the compaction of material ε^{c}_{ij} and the plastic strain related to dilation of material ε^{d}_{ij}:

$$\varepsilon^{p}_{ij} = \varepsilon^{c}_{ij} + \varepsilon^{d}_{ij}. \tag{21}$$

The model of micropolar media allows for taking into account the rotations of particles, moment stress during the generation of strain and mean grain diameter as a characteristic length. It treats granular body as a continuum of undeformable grains (Rymarz 1993). On the basis of Cosserat's theory the constitutive equations dependent on particle size are derived. It provides an opportunity to model the structure of media. Increase in the interest in the theory resulted in development of that approach and its application in research of granular materials.

The Cosserat model proposed by Mühlhaus and Vardoulakis (1987) which takes into account the constitutive elasto-plastic relationship of Drucker-Prager and isotropic hardening and softening is a useful tool in the investigation of shear bands in granular materials. As a consequence of joining two theories, the model taking into account both the continuum features of media and the characteristic dimension was proposed. The constitutive equations of Mühlhaus are characterised with a high number of functions and material parameters which have to be measured by means of experimental methods.

The micropolar models based on assumptions of the continuum mechanics provide an opportunity to model processes in numerous systems. The application of that method into the FEM code (Tejchman and Wu 1995, Tejchman 1998) allows for the description of effects occurring in complex systems of real sizes.

Presented models found an application in both analytical and numerical methods which are used in investigations of granular materials. The constitutive mod-

els are applied through the finite element method (FEM) proposed in the 40's of the 20th century (Desai and Abel 1972, Akin 1994, Kleiber 1995). The development of that numerical technique resulted in a wide spectrum of methods initially to solve simple linear problems for one- and two-dimensional systems and recently to solve non-linear problems for objects of complex 3D geometries.

The most important feature of FEM is discretisation which consists in the division of an area into a finite number of geometrically simple elements (for example triangles in 2D and cubes in 3D systems), joined with nodes placed on the sides of the elements. The solution of differential equations provides values of physical magnitudes for the nodes. They are next used to calculate the values of quantities for points placed outside the nodes.

FEM is a useful tool to investigate objects of complex shapes where the application of analytical methods is not sufficient. The division of an object into very small elements improves the accuracy of results but it also results in an increase in computational effort. It is worth to remember that multiple approximations increase the magnitude of errors. The magnitude of error depends on assumptions made while formulating the problem to be solved and the accuracy of material parameters. Application of procedures allowing for avoiding errors is therefore a very important task.

The prove of popularity and large potentiality of FEM is a variety of commercial FEM codes on the market and the problems which are solved with that method (e.g. investigation of structure strength, modelling of deformation, strain, displacement processes, liquid flow, investigations of kinematics and dynamics of devices, examination of electromagnetic and electrostatic interactions).

Comparing the results obtained through the application of Lade's model in FEM code with experimental data for cohesionless granular materials, Zhang and Whiten (1996) revealed a satisfying accordance of obtained results. The application of the model does not make sense in the case of materials subjected to highly fluctuating loads.

The application of the Drucker–Prager constitutive model in the FEM code enabled Zahlan *et al.* (2001) to observe strain distribution in a sample of powder subjected to load. Tejchman used FEM code based on Cosserat's theory to model silo filling and discharge processes and shearing of granular material.

The finite element method is therefore a useful tool to investigate granular media, including granular plant materials (Lu *et al.* 1997, Mark *et al.* 1999, Goodey *et al.* 2003).

4. GEOMETRIC STRUCTURE OF GRANULAR MEDIUM

The packing structure of a granular assembly has a crucial significance for properties of the system. The results of geotechnical studies have shown that natural sand deposits formed under gravity are usually anisotropic. Allen (1969) proved that in the course of sand deposit formation grains of sand tend to orient themselves with their long axes parallel to the horizontal plane. The result of this is the formation of deposits with a high degree of geometric arrangement of particles. Oda (1972) examined the effect of the anisotropy of a deposit on its mechanical properties and conducted a series of laboratory tests on sand samples. The author showed that knowledge of the structure of particle packing is necessary for the determination of the stability of non-cohesive soils subjected to external loads. Mechanical phenomena, such as the anisotropy of response to loading, stress-strain relations, strain hardening, strength and porosity, turned out to be dependent on the structure of packing (Oda 1976, 1978). Ever since those experiments it has been known that two samples of the same sand with the same porosity need not have identical mechanical properties. The author distinguished two elements of the packing structure: 1) spatial orientation of the long axes of non-spherical granules (characterized by two parameters) and 2) packing density.

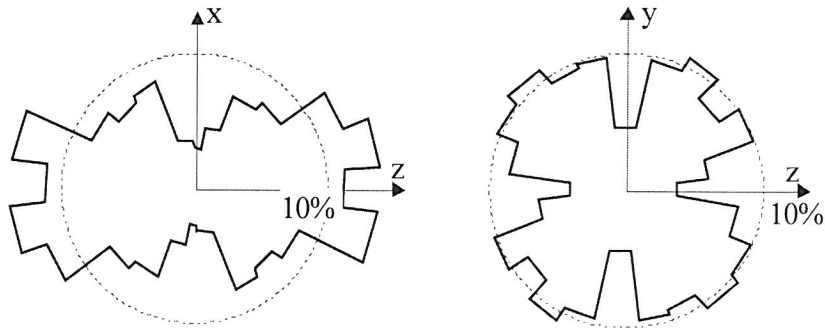

Fig. 3. Distribution of density of probability of angle of inclination to horizontal line of long axis of sand grains (Oda 1976)

Figure 3 (Oda 1976) presents the density distribution of probability of sand grains long axis inclination angle. The sample was formed by pouring sand into a mould filled with water, then compacted by tapping on the walls of the mould. V-section is the vertical section and H-section is the horizontal section of the sample. In the vertical section, the density of probability in the horizontal direction is notably higher, while in the horizontal section no distinct orientation of long axes of the granules is observed. The manner of characterizing the geometric structure of

a granular material illustrated in Figure 3 has been later frequently used by other researchers, especially in the case of 2D models.

Konishi *et al.* (1982) performed an elasto-optical study of biaxial deformation of 2D systems of particles in the form of rods with oval cross-section. The authors recorded force values at various strain stages while taking elasto-optical photographs. They estimated the effect of anisotropy related to the sample forming method, friction between the particles, and their form on the response of the material to mechanical loading. They used particles with two section forms and three size classes. The length ratio of the long to short axes of the elliptical cross-section was 1.1 in the first group, and 1.4 in the second. The dimension of the long axis of the cross-section ellipse in the first group was 14.8, 9.9 and 6.3 mm, and in the second – 16.0, 10.7 and 7.1 mm. To examine the effect of interparticle friction two series of measurements were performed; one with non-lubricated particles with internal friction angle of 52° and another with particles lubricated with talcum, for which the internal friction angle was 26°. Samples were poured into a cubicoid mould with different angles θ of mould bottom inclination to the horizontal. The sample, compressed horizontally with a constant force, had freedom to deform vertically. Measurements included vertical loads as well as vertical and horizontald deformation of the sample. Elasto-optical photographs showed that the load is transmitted by columns of particles oriented in the direction of maximum compressive stress. The points of contact around the columns transmited only a limited amount of the load applied, but ensured stability of the columns that transmited most of the load. The distribution of forces obtained is highly similar to that presented earlier by Drescher and De Josselin de Jong (1972) in their work concerned with verification of the theoretical model of granular medium flow.

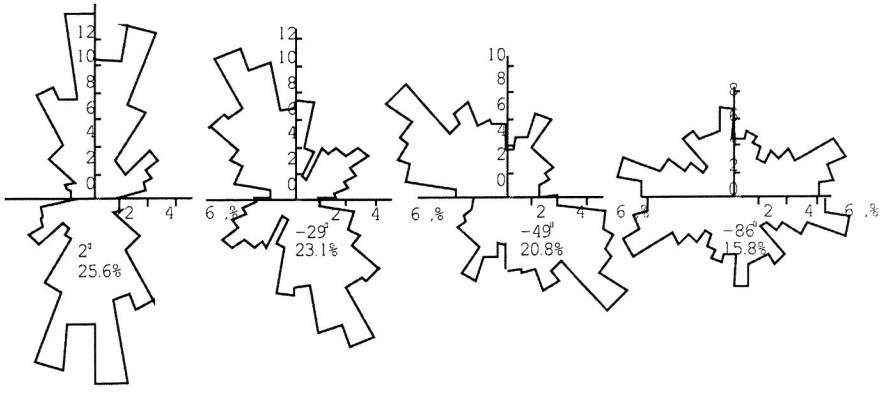

Fig. 4. Probability density disribution of angle of contact normals in the assembly of rods of cross section (ratio of length of axes 1.4 (Konishi 1982))

Konishi *et al.* (1982) applied the distribution of unit normal directions at contact points for the description of the packing structure of particles. Figure 4 presents the obtained distributions of contact normal directions for the particular variants of the experiment in an undeformed sample. The authors adopted an approximation of the distribution of normal directions by means of an ellipse. The long axis of the ellipse in undeformed state is perpendicular to the plane of deposit pouring. The effect was more pronounced in the case of flatter particles and in the case of lubricated particles that display higher anisotropy.

The numbers in Figure 4 represent the direction of the long axis of the ellipse (higher) and the degree of anisotropy (lower). The parameters were calculated according to the relation (Oda *et al.* 1980):

- long axis direction:

$$\bar{\beta} = \frac{1}{2} arctg\left(\frac{A}{B}\right), \tag{22}$$

- degree of anisotropy:

$$M = \sqrt{A^2 + B^2} \cdot 100, \tag{23}$$

where:

$A = \int E(\beta) \cdot sin\beta d\beta,$

$B = \int E(\beta) \cdot cos\beta d\beta,$

$E(\beta)$ – distribution of probability density.

With progressing deformation, some of the contacts disappear and new ones come into existence. The distribution of contact normal directions changes. The main axes of the ellipses that describe the distribution rotate so that more contact normals assume a direction close to that of the maximum compressive stress. This tendency is more pronounced for spherical particles than for flatter particles. Kanatani (1981) proposed the characterization of the spatial distribution of particles by means of the packing tensor. He performed a quantitative estimation of the distributions of contact normal directions obtained by Konishi *et al.* (1982). Figure 5 presents the experimental distributions and Kanatani's approximations (Kanatni 1984) up to the fourth order, for material prior to loading and subjected to load.

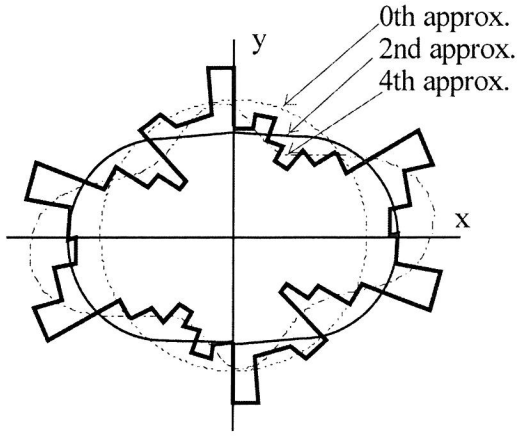

Fig. 5. Probability density distribution of angle of inclination of contact normals and their approximations (Kanatni 1984)

4.1. Anisotropy of seed layers

The studies on the effect of the anisotropy of a seed sample on the angle of internal friction (Molenda *et al.* 1995) were undertaken in the Institute of Agrophysics PAS in Lublin. Selected for the studies were seeds of what, barley, rye, as well as rapeseeds. The seed of the species chosen represent shapes varying from the spherical (rape) to a strongly elongated ellipsoid (rye). The seed moisture varied from 10.5% to 12%, and in the case of rapeseed it was 8%.

To achieve a specific orientation of seeds in the sample the researchers made use of the phenomenon of the formation of an angle of natural repose and the effect of grains arranging themselves usually with the long axis towards the generatrix of the cone formed by the seed. The method of sample preparation for the triaxial compression test is illustrated in Figure 6. Grain was poured with a steady flow from the funnel through a rectangular outlet of 8 x 24 mm in size into a rubber diaphragm placed in a two-part cylindrical mould. The funnel, placed at the wall of the mould, was lifted up as the mould was filled with grain, so that the outlet hole was always positioned about 20 mm above the top of the freely formed surface of grain poured. After complete filling of the mould, the cylindrical top cover of the sample was fixed in place. Next, vacuum was generated within the grain sample, which gave the sample rigidity of shape, and that permitted its placement inside a pressure chamber without risk of disturbing the spatial structure of the medium created in the course of sample formation. The angle between the freely formed surface of poured grain and the base of the sample was varied by tilting the mould away from the vertical. As grains tend to orient themselves so that their long axes is parallel to the generatrix of the cone of natural repose, varying the tilt of the mould with relation to the vertic-

al resulted in a change of the preferred spatial orientation of the grains with relation to the sample-related system of reference. For further tests six values of sample inclination were chosen: $\beta = -20^\circ$, -10°, 0°, 10°, 20° and 30° (Fig. 6). The angle of natural repose of the grain was about 20°. Additionally, for purposes of comparison, grain was poured into a vertical mould ($\beta = 0^\circ$), positioning the outlet hole of the funnel along the sample axis of symmetry and not close to the mould wall as before. Every time the same quantity of grain filled the whole volume of the mould, therefore every time the same density of the medium was obtained.

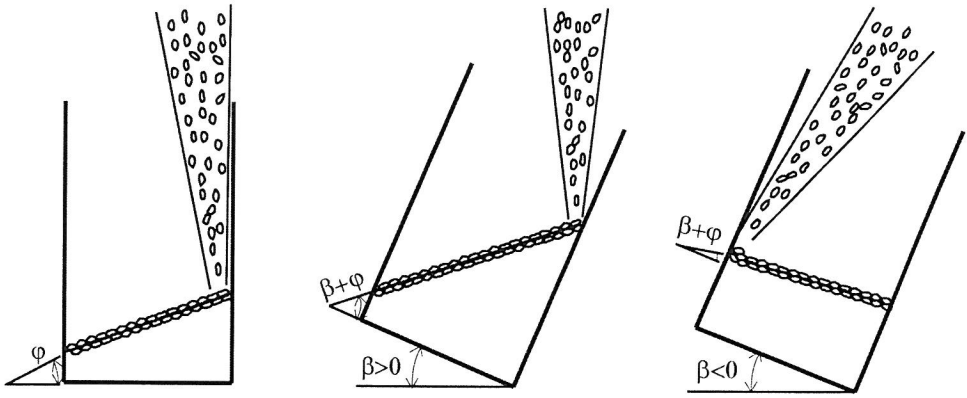

Fig. 6. The method of sample preparation for the triaxial compression test (Molenda and Horabik 2005)

To estimate the degree of arrangement of the long axes of the grains, the samples prepared according to the method described above were flooded with polyesther resin. Once the resin was set, the samples were cut along horizontal and vertical planes. The sections obtained were used to determine the measure of grain arrangement after (Oda 1978), in accordance with the formula:

- preferred angle of inclination of long axes of grains with relation to chosen system of coordinates:

$$\bar{\theta} = \frac{1}{2} arctg \left(\frac{\sum_{i=1}^{n} sin2\theta_i}{\sum_{i=1}^{n} cos2\theta_i} \right), \tag{24}$$

- intensity of parallel orientation of the long axes

$$V \cdot M = \sqrt{\left(\sum_{i=1}^{n} \sin 2\theta_i\right)^2 + \left(\sum_{i=1}^{n} \cos 2\theta_i\right)^2} \cdot \frac{100}{n}, \tag{25}$$

where:
n – number of measurements,
θ_i – the angle of inclination of the long axis of a given grain with relation to the adopted system of reference.

The value of the expression $V \cdot M$ varies within the range from 0 to 100%. The value of 0% corresponds to totally random orientation of the long axes of the grains, while 100% represents ideally parallel orientation of the long axes of the grains. For angle $\beta = 20^\circ$ and for the vertical sample section, the measures had values of $\theta = 38^\circ$, $V \cdot M = 65\%$, respectively, and therefore the sample was characterized by considerable anisotropy.

The effect of spatial orientation of grains of three cereals and of rape on the angle of internal friction was examined with the triaxial compression method and with the direct shear method. The methods were chosen due to their popularity in experimental studies on the mechanics of granular materials. It was assumed that comparison of the two methods would permit formulation of conclusions on their applicability in studies on agricultural materials.

The procedure of sample preparation for the direct shear test was identical as in the case of the triaxial compression test. In the direct shear tests five levels of normal load σ were applied, equal to the values of stress σ_3 in the triaxial compression test. The speed of mutual displacement of two sample halves was 1.3 $mm \cdot s^{-1}$. Each variant of the experiment was repeated three times.

A preliminary study of the effect of sample preparation, performed with the method of triaxial compression on rye seeds within an expanded range of the angle of sample inclination $\beta = -40^\circ$, -20°, 0°, 20° and -40°, permitted the conclusion that the manner of grain pouring into the mould had a significant effect on the mechanical characteristics obtained. The highest values of strength were obtained for grain samples poured into vertical mould. Those samples were also characterized by the highest uniformity of deformation. As a rule, no distinct plane of shear was observed. The sample swelled uniformly, assuming barrel shape. The behaviour of samples poured into mould tilted from the vertical by an angle β was totally different. Such samples lost the uniformity of deformation much sooner, and a clearly defined shear plane was formed. With increasing value of angle β, the maximum value of the ratio of main stresses decreased. A marked orientation of the shear plane occurred regularly in every experiment. On the basis of the obtained maximum values of main stresses

σ_1/σ_3, the value of the angle of internal friction φ was calculated on the basis of the Coulomb-Mohr yield condition. Figure 7 presents the values of the angle of internal friction for various values of angle β of mould inclination from the vertical. The highest values of the angle of internal friction were obtained for the case of samples poured into vertical mould, and especially when grain was poured into the mould along the axis of symmetry. With increasing angle of sample inclination β, the angle of internal friction φ decreased significantly.

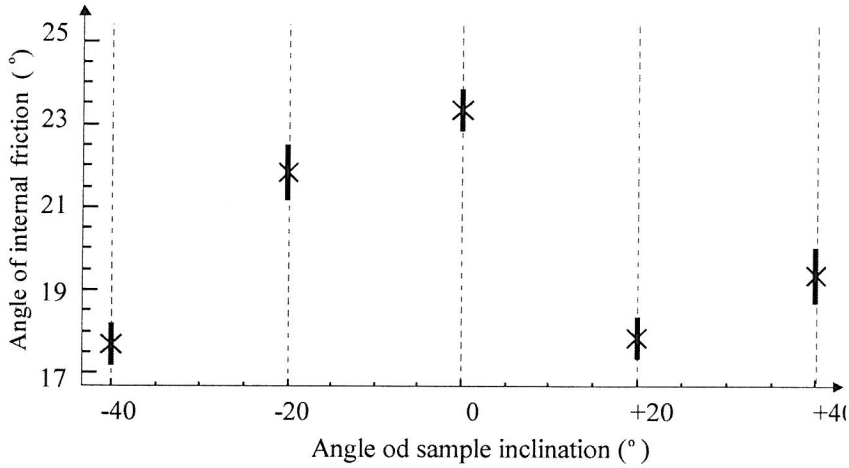

Fig. 7. The values of the angle of internal friction of rye samples for various values of angle β of mould inclination from the vertical (Molenda and Horabik 2005)

According to the Coulomb yield criterion, the slip plane is inclined at the angle $\alpha = \pm(\pi/4+\varphi/2)$ to the plane of the higher main stress. Figure 8 presents the theoretical slip planes and the plane of free surface of grain sample, inclined to one of them at angle γ_1. Figure 8a refers to the triaxial compression test at sample inclination angles β: 10°, 20° and 30°, while Figure 8b refers to angles β: 0°, –10° and –20°. While in the case of an isotropic medium there are many possible orientations of the slip plane, in the case of an anisotropic material the slip plane is determined by the direction of the lowest strength.

In a material composed of spherical granules there may occur anisotropy of concentration of normal directions to the points of grain contact. In a hexagonal structure, the normal directions to the points of contact are mutually inclined at 60°, and therefore the angle of inclination of the normal directions to the slip plane is described by the equations presented in Figure 8c.

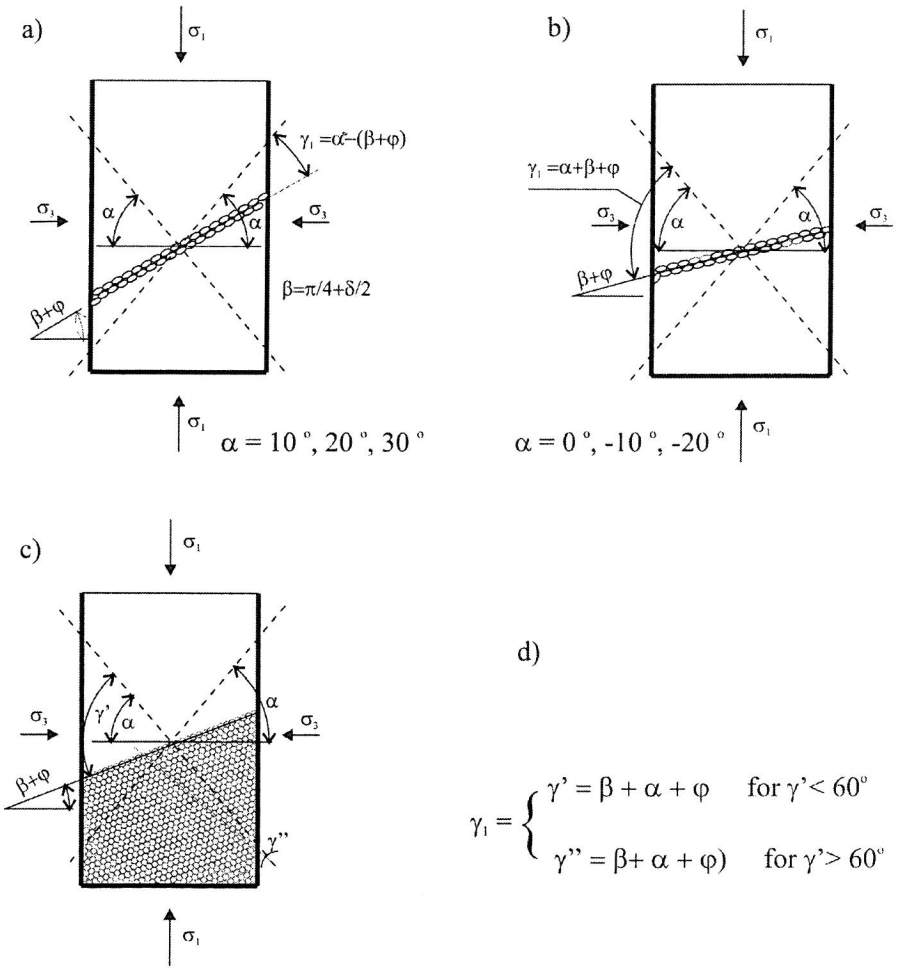

Fig. 8. Sample of granular material in triaxial compression test: a), b) – non-spherical grains, c) – spherical grains (Molenda and Horabik 2005)

Figure 9 presents the stress condition realized in the direct shear apparatus. Point P in the Mohr graph illustrates the values of normal stress σ and maximum tangential (shear) stress τ measured in a horizontal shear plane. Point P is not identical with point T – the point of tangency of the Coulomb-Mohr yield criterion of strength with the Mohr circle (Schott and Britton 1984). Therefore, the plane in which the Coulomb-Mohr yield criterion is fulfilled does not coincide with the horizontally enforced shear plane, but is inclined to it at the angle $\delta/2$. The angle of long granule axis preferred inclination γ_2 was referred not to the plane in which the Coulomb-Mohr yield criterion is fulfilled, but to the horizontal shear plane.

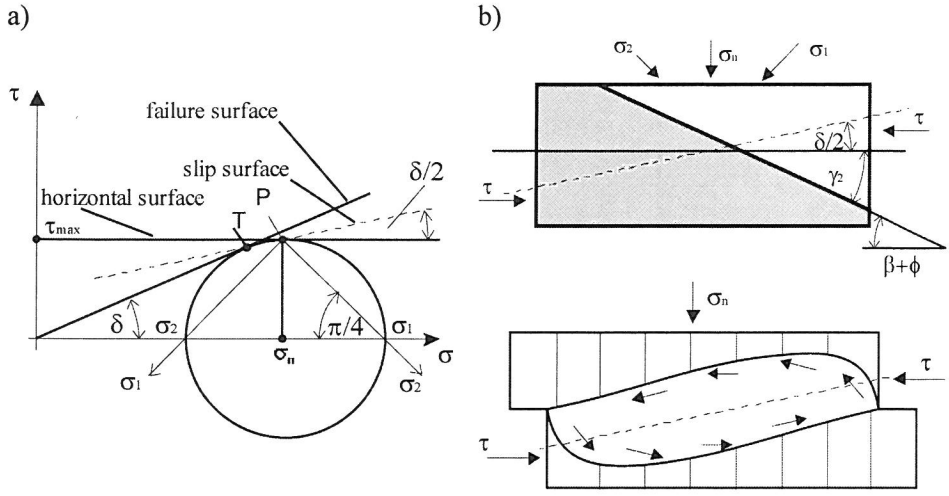

Fig. 9. Sample of granular material in direct shear test: a) diagram of Mohr for state of stress in the sample, b) orientation of preferred direction of long axis of grains against theoretical slip plane γ_2, c) image of deformation of the sample (Molenda and Horabik 2005)

The results of the measurements are presented in Figure 10 as graphs of the relation of the angle of internal friction φ to the angle of slip plane inclination to the direction of grain long axes or to the normal direction of the normals at contact points. The closest agreement of the relations $\varphi(\gamma_1)$ and $\varphi(\gamma_2)$ was obtained in the case of rapeseed. In both the tests performed on rapeseed the maximum of the angle of internal friction, $\varphi = 29^\circ$, occurred at similar values of the angles $\gamma_1 \approx \gamma_2 \approx 35^\circ$. Considering the fact that the plane of the higher principal stress σ_1 is inclined to the slip plane at an angle $\alpha = \pi/4+\varphi/2$ it is easy to note the agreement of the obtained maximum of the angle of internal friction with the results obtained by Oda (1972, 1977). The author found that in the course of non-dilatational hardening of granular material the normal directions to the points of contact concentrate around the direction of the higher main stress, and that the direction gradually rotates with increasing tangential (shear) stress. The main axes of the ellipse characterizing granule packing tend towards a position coaxial with the directions of the main stresses.

In the case of non-spherical grains, a different relation was observed between the angle of internal friction and the angle between the direction of granule long axis orientation and the direction of slip for the tests of triaxial compression and of direct shearing. In the triaxial compression test, the angle φ increased with increasing values of angle γ_1 – of granule long axis inclination to the slip plane. The trend was observed for all the cereal species under study. The relation $\varphi(\gamma_2)$ obtained in the direct shear test had an approximately parabolic form, with a minimum for the angle

$\gamma_2 \approx 25^\circ$. The divergence between the relations $\varphi(\gamma_1)$ and $\varphi\ (\gamma_2)$ results from differences in the mechanisms of sample deformation in the tests compared. In the triaxial compression test, the slip plane forms freely, conforming to the state of stress and to the structure of the material, while in the direct shear test the slip direction is forced. In the latter test, the process of shearing is additionally complicated by the non-uniform state of deformation and by the anisotropy of the material; the displacement and the rotation of individual grains are forced.

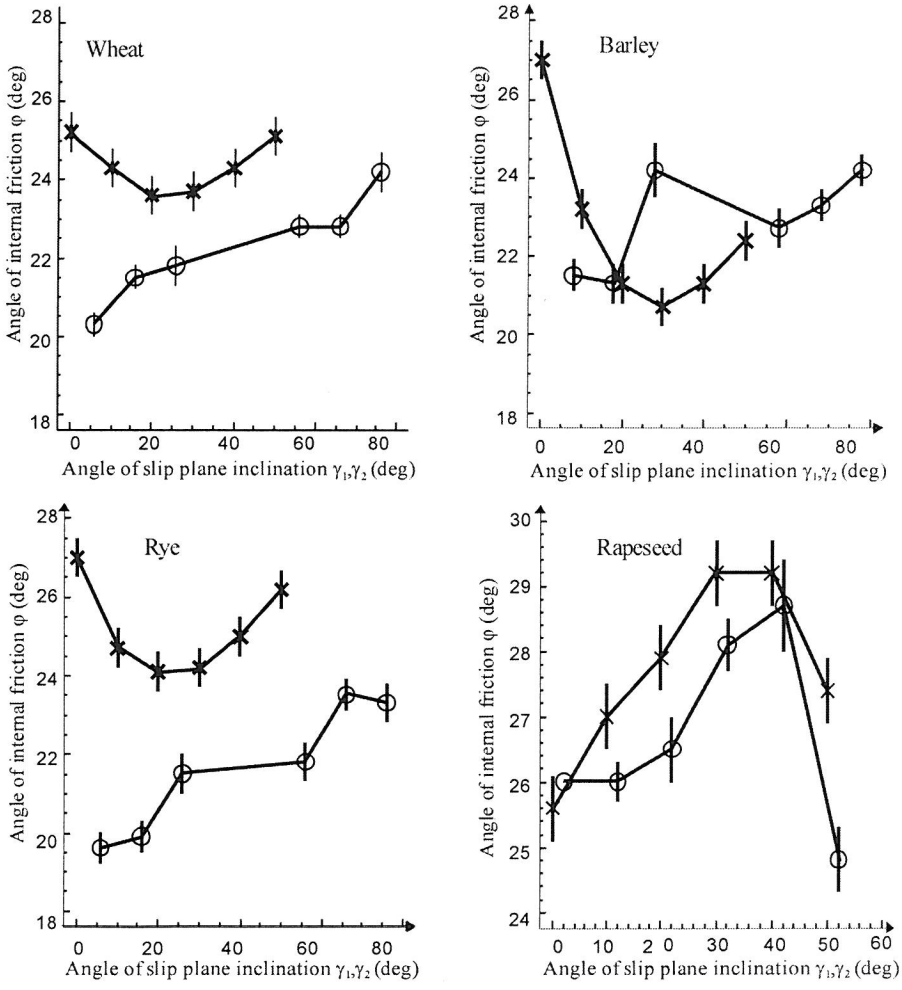

Fig. 10. Influence of the angle of slip plane inclination γ_1 and γ_2 on the angle of internal friction φ in direct shear test × and triaxial compression test (Molenda and Horabik 2005)

The results of the experiments described above permit the formulation of several methodological remarks concerning the measurement techniques. Due to the relatively large dimensions of the grains, it is recommended to increase the size of samples with relation to those routinely used for soils. It appears that the sample dimensions used in the studies presented here (triaxial sample: $D = 150$ mm, $H = 300$ mm, direct shear test sample: $D = 210$ mm, $H = 120$ mm) are sufficient. Especially worthy of recommendation for measurement of the angle of internal friction is the triaxial compression method, though in the case of spherical granules the less complex direct shear test yields similar results. The recommendation of the triaxial compression method is also supported by the fact that the method has been frequently used for the determination of theoretical and empirical parameters of models describing the stress-strain relation. The method was used by Zhang *et al.* (1986) and by Li *et al.* (1989) for the determination of parameters of the elasto-plastic model adapted by the authors for the description of the stress-strain relation in wheat grain. In that model, formulated by Lade *et al.* (1987) for cohesionless sand, the total increase of strain caused by increase in stress equals the sum of three components: increase in elastic strain, increase in plastic strain caused by normal stress, and increase in plastic strain caused by stress deviator. The values of model parameters determined in the triaxial compression test permit an accurate drescription of the response of a medium to other loading conditions. For the description of anisotropy and hysteresis in the stress-strain relation in the case of multiple loading of wheat grain, Zhang *et al.* (1986) used an elasto-plastic model that included the density and kinematic hardening of the medium. The determination of the values of the parameters of the model also involved the application of the triaxial compression test. Likewise, the method of triaxial compression was applied by Zhang and Jofriet (1993) for the determination of parameters of an elasto-plastic model describing the stress-strain relation for soybean and maize seeds.

5. LABORATORY TESTING OF MECHANICAL PROPERTIES

5.1. Density of granular materials

Density, which is mass divided by volume, is one of the fundamental parameters of granular materials. Knowledge of the exact value of the density of a deposit of granular material is very important for numerous practical applications. The density of a material has a significant effect on its mechanical characteristics. It is one of the three basic parameters, along with the friction coefficient and the pressure ratio, that are used in the determination of granular material pressure against the structure of the bin or silo. It is also necessary for accurate estimation of container capacity.

With relation to their bulk density, granular materials are classified as:

- light (peat, sawdust, bran, cereal meal, dried plant material) $\rho < 600$ kg m^{-3},
- medium (cereal grain, fertilizers, soil) $600 < \rho \leq 1100$ kg m^{-3},
- heavy (mineral raw materials, sand, gravel) $1100 < \rho \leq 2000$ kg m^{-3},
- very heavy (minerals, stone) $\rho > 2000$ kg m^{-3}.

5.1.1. Bulk density

A popular method for the determination of the bulk density is based on measurement of the mass of granular material poured freely into a cylindrical container of constant volume, typically 0.25 or 1 dm^3 (Britton and Moysey 1986, PN-73/R-74007, PN-74/Z-04002.07). The values of bulk density of typical agricultural materials differ significantly from the density of those materials in silos (Britton and Moysey 1986, Chang *et al.* 1983). That density is a function of moisture, pressure, degree of contamination, manner and rate of filling, and falling height of the grain (PN-B-03254-2002). Cereal grain density usually varies within a relatively broad range, depending on the species and cultivar, manner of bin or silo filling, height of deposit, degree of contamination of the grain, and other factors.

Tapped density provides information on the susceptibility of a granular material to compaction through vibrations. The relevant standard provides for a measurement consisting in bringing a known mass of a granular material to the lowest volume possible through the application of vibrations of constant amplitude and frequency (PN-74/Z-04002.07). The tapped density of cereal grain is higher than the bulk density by several percent, and in some cases even by over twenty percent (Ślaska-Grzywna 1995).

Chang *et al.* (1983) showed that distributed filling of silo increases the density of granular material by from 5.1 to 9.2% as compared to filling from centrally located spout of conveyor. Stephens and Foster (1976) observed increases in density of the order of 3 to 5% above the bulk density values in condensed filling from spout of a conveyor, and 7% in the case of distributed filling. Versavel and Britton (1984) showed that density depends on the falling height, the degree of contamination, and on the filling rate. The researchers noted a considerable increase in density, of the order of 8-10%, and in the case of high filling rates a decrease in density. Similar relations were found by Schott and Britton (1984) in laboratory studies. With increasing grain falling height the kinetic energy of the grain increases, which increases the packing density of the material (Moysey 1984). That effect disappears above a certain height, due to increasing aerodynamic drag during the free fall of the grain.

In view of the wide range of variation and considerable number of factors affecting density, attempts are made at developing methods for the determination of „apparent density" that would correspond to the density of a material in a silo.

Therefore, it is necessary to search for general rules applicable to the determination of the actual density of granular media in containers that would be common for as extensive a class of materials as possible. Basing on experimental results obtained so far it is recommended to estimate the density of a granular material in a silo by assuming an average density increase of 6% with relation to the density value determined from the mass of 1 hectoliter (Britton and Moysey 1986). It appears, however, that application of more accurate methods for the prediction of density of granular material deposit is a necessity.

The density of granular material is a monotonically increasing non-linear function of pressure. The function most frequently used for the description of the relation is a power, exponential or logarithmic function. Gu *et al.* (1992) made a detailed analysis of empirical relationships used, determining for each the range of pressure values for which a given function best describes the change in density.

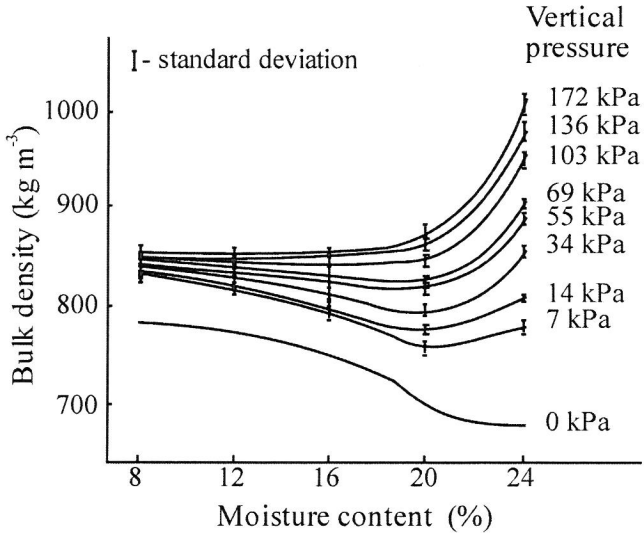

Fig. 11. Bulk density values for wheat as a function of moisture content and pressure (Thompson and Ross 1983)

In the case of materials of plant origin, another parameter – apart from pressure – that significantly affects the density of a deposit is the moisture content of the material. Thompson and Ross (1983) made an in-depth study of the density of wheat grain deposit within the range of pressures from 0 to 170 kPa. They found that within the grain moisture range from 8% to 12% a half of the change in the density of the medium was attributable to reorientation of the grains, and the other half their elastic deformation. Increase in the grain moisture caused

an increase in the contribution of deformation of the grains in the change of the density of the medium. At grain moisture level of 24% the contribution of deformation of the grains was about 70% of the change in density. For vertical pressure values below 100 kPa the authors found a distinct minimum of density at grain moisture levels within the range of 20-24%. With increasing pressure, the minimum shifted slightly towards lower values of moisture (Fig. 11). The authors described the relation with a non-linear function. A similar course of the relation was determined – for maize kernels – by Clower *et al.* (1973) and by Loewer *et al.* (1977). The curve marked with the symbol 0 kPa in Figure 5.1 presents bulk density decreasing with increasing grain moisture content.

5.1.2. Experimental methods

Eurocode 1 (2003) recommends direct application of bulk specific gravity of granular materials, determined experimentally under oedometric compression, for the calculation of pressure. It is also recommended to use the value of vertical pressure that will exist in the bottom part of the silo as the consolidation pressure. If the information is not available, pressure value of 100 kPa is recommended for use as reference pressure. Bulk specific gravity determined in this manner is used for the determination of the upper limit of load. A sample of the material tested is placed in a cylindrical container with diameter D that is greater than the maximum grain size by a factor of at least 40. Height H of the sample should be in the range of 0.3-0.4D. After the filling of the container, without any vibration and application of compacting loads, the upper surface of the sample is loaded with normal force generating the reference pressure σ_r (corresponding to maximum vertical pressure p_v or to 100 kPa). Then the top plate of the apparatus is rotated three times by 10° right and left for additional compaction of the material. Bulk specific gravity is determined as the quotient of the weight of consolidated sample and its volume.

5.2. Compressibility and elasticity

Granular materials in storage get compacted under their own weight and/or under external loads. Compaction increases through a change in packing and through deformation of the grains. The resultant strain ε_p is the sum of reversible deformation ε^e, caused by the elastic deformation of grains and thus disappearing with the removal of the load, and of the permanent deformation ε^p related to the change of mutual orientation of grains:

$$\varepsilon_p = \varepsilon^e + \varepsilon^p \tag{26}$$

Figure 12 presents the curve of cyclic loading of wheat grain sample under the conditions of oedometric compression. Irrespective of the type of material tested (cereal grain, sand, soil), the stress-strain curves display qualitative similarity (Hueckel and Dresher 1972, Li *et al.* 1989, Morland *et al.* 1993). The wide hysteresis loop during the first loading (curve 0AB) is dominated by plastic deformation with less contribution of elastic strain. During repeated loading of the sample, at a load value below the previous maximum, the material is stiffer than before (curve BC), while after exceeding the maximum value of the previous loading (section CD) the stiffness of the material decreases and the material behaves as if never subjected to loading. The behaviour of the material along the curve sections AB, BC, DE can be described by the modulus of elasticity K and along the curve 0ADG by the modulus of compressibility E_i. The values of the moduli are strain dependent.

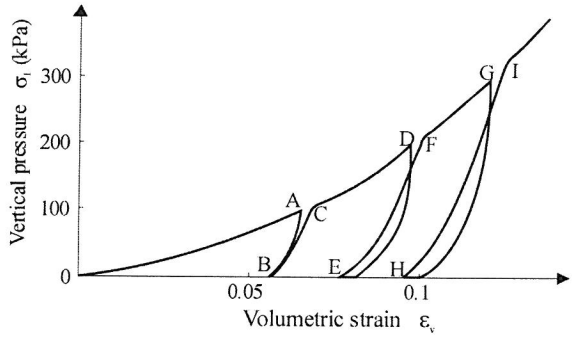

Fig. 12. Stress-strain relation during loading-unloading cycles of wheat grain in oedometric test (Molenda and Horabik 2005)

Zhang *et al.* (1988) determined the modulus of volumetric elasticity K and the modulus of plasticity H_o of wheat grain in bulk in the triaxial compression test at constant value of minor principal stress σ_3 from the following power relations:

$$K = K_0 P_a \left(\frac{\sigma_3}{P_a}\right)^A, \tag{27}$$

$$H_0 = B P_a \left(\frac{\sigma_3}{P_a}\right)^C, \tag{28}$$

where:
A – exponent of the modulus of elasticity,
B – constant of the modulus of plasticity,
C – exponent of the modulus of plasticity,
K_0 – constant of the modulus of elasticity,
P_a – atmospheric pressure,
σ_3 – minor principal stress.

The modulus of compressibility E_i was determined on the basis of the resultant material strain, sum of reversible (elastic) and irreversible (plastic) strain (Zhang *et al.* 1988):

$$\frac{1}{E_i} = \frac{1}{K} + \frac{1}{H_0}. \tag{29}$$

Volumetric elasticity of granular material is closely related to the elasticity of individual grains. Modulus of elasticity of seeds of individual plant species varies within a broad range. In the case of wheat, Young modulus determined for cylindrical samples cored from the grain endosperm falls within the range of 0.2-3 GPa depending on the cultivar (Glenn *et al.* 1991) – Figure 13. With increasing grain moisture, Young modulus decrease to stabilize at moisture levels above 22% (Delwiche 2000). Modulus of elasticity depends on the protein content and on the type of endosperm (Koper and Grundas 1987). For vitreous grains, the values of the modulus are about 30% higher than for mealy grains (Grundas and Hnilica 1987, Woźniak 2001). Multiple wetting and drying of grain causes internal cracks in the grain endosperm structure, which reduces the values of modulus of elasticity even by 40% (Woźniak 2001). In the case of maize kernels, modulus of elasticity decreases with increasing moisture, from 600 MPa at moisture content of 10% to 50 MPa at moisture of 35% (Kragelsky *et al.* 1977). Modulus of elasticity of rape seeds at moisture content of 6-8% is about 40 MPa, and with increasing seed moisture drops to the level of several MPa (Stępniewski 1997). Modulus of elasticity of pea seeds falls within the range of 100-400 MPa depending on the cultivar and the seed moisture content (Dobrzański 1990).

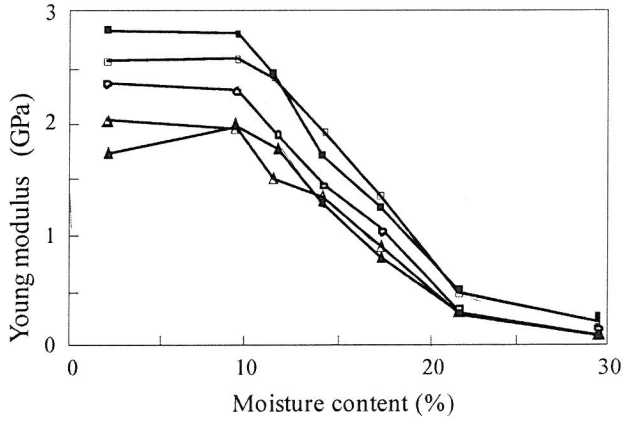

Fig. 13. Young modulus of wheat endosperm as influenced by moisture content (Glenn *et al.* 1991)

Direct linking of the modulus of volumetric elasticity of a granular material with the elastic properties of elementary grains by means of a quantitative mathematical formula is extremely complicated. Theoretical studies are usually focused on the search for general conditions that would permit the determination of modulus of volumetric elasticity of a system of elastic granules. Walton (1987) derived the relationship of effective modulus of volumetric elasticity of a random system of spheres K on the basis of elastic reactions taking place within the area of elementary contact:

$$K = K_1 E^{\frac{2}{3}} |p|^{\frac{1}{3}}, \tag{30}$$

where:

$$K_1 = \frac{1}{6}\left(\frac{3\upsilon^2 N_t^2}{\pi^2(1-\nu^2)^2}\right)^{\frac{1}{3}},$$

$$\upsilon = \frac{4\pi R^3 n}{3V},$$

E – Young modulus,
K_1 – material parameter,
n – number of granules in volume V,
N_t – mean number of contacts per individual granule,
p – pressure,
R – radius,
V – volume,
υ – solid fraction,
ν – Poisson constant.

For the description of the stress-strain relation within the area of elementary contact of the bodies he applied the Hertz formula that is commonly used for the case of contact of an elastic sphere with flat rigid surface (Mindlin 1949, Moshenin 1978, Tsang-Mui-Chung *et al.* 1984).

Relating the modulus of elasticity of a material deposit with the Young modulus and Poisson coefficient of the granules of the medium and with the average pressure and the material packing parameters permits correct physical interpretation of elastic reactions in a bulk of granular material. Studies by Horabik and Molenda (1989) showed that the Hertz formula permits also the description of the behaviour of grain within a broad range of moisture content (Fig. 14). At the current stage of the research, the application of the relation derived by Walton for a big number of bodies like granular plant material permits only qualitative analysis of the phenomenon.

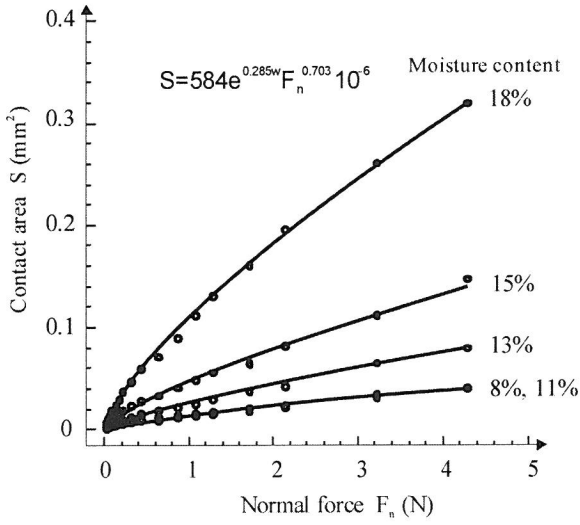

Fig. 14. Contact area of wheat grain with smooth surface as influenced by moisture content and normal load (Horabik and Molenda 2000)

Granular material volumetric elasticity has a very strong influence on the pressure transmitted by the granular material onto the structure of the container or silo (Łapko 1989, Łapko and Prusiel 2000). For the purpose of solving practical problems, an empirical value of modulus of elasticity of granular material in bulk is usually adopted, constant for a given range of pressure values (Prusiel and Nikitin 2000, Sawicki and Świdziński 1995). In the case of granular materials of plant origin, the value of the modulus is strongly related to moisture content. Stasiak and Molenda (2001) showed that the modulus of elasticity of wheat grain, determined under the conditions of oedometric compression at the vertical pressure of 100 kPa and grain moisture content of 10% was 22 MPa, and at grain moisture content of 20% decreased to 11 MPa, while Poisson constant ν did not depend on grain moisture and oscillated around 0.2. Modulus of elasticity of maize kernels in bulk determined by Frontczak and Metzger (1985) in oedometric compression test at vertical pressure within the range of 100-240 kPa decreased from 14 MPa to 6 MPa at moisture content increasing from 7% to 23.5%. The Eurocode 1 (2003) recommends that the value of modulus of elasticity of grain in bulk should be related to the size of the silo or, in other words, to the range of pressure values within the bulk of granular material. In the case of silos with diameters within the range of 6-9 m the Standard recommends the use the values of cereal grain bulk modulus of elasticity of 10 MPa for grain height of 15 m and 20 MPa for the height of 30 m, and to double the modulus values for silo diameters over 9 m.

The total vertical strain in granular materials under loading may be described as proposed by Sawicki and Świdziński (1995). The model equation is based on the elasto-plastic approach and assumes that during loading both reversible (elastic) and irreversible (plastic) strains develop in the sample. Plastic ε_z^p and elastic ε_z^e strains develop in the material during loading:

$$\varepsilon_z = \varepsilon_z^e + \varepsilon_z^p \tag{31}$$

$$\varepsilon_z = D_1 \ln\left(1 + D_2 \sigma_{z0}^{\alpha}\right) + \frac{\sigma_{z0}}{E}\left(1 - \frac{2\nu^{*2}}{1-\nu^*}\right) \tag{32}$$

where:
ε_z – total vertical strain,
ε_z^p – plastic vertical strain,
ε_z^e – elastic vertical strain,
σ_{z0}– mean vertical pressure on the top cover,
E– modulus of elasticity,
ν^*– equivalent of Poisson's ratio for loading $\nu^*=K_o/(1+K_o)$,
K_o– slope of straight line $\sigma_x=K_o\sigma_z$,
D_1, D_2, α– model parameters.

K_o, which is used to calculate the equivalent Poisson's ratio ν^* during loading, is the ratio of the horizontal stress σ_x and vertical stress σ_{z0} during consolidation of the sample. During this phase of compression the horizontal deformation which is the sum of plastic and elastic horizontal strains, is zero ($\varepsilon_x=\varepsilon_x^e+\varepsilon_x^p=0$). D_1 and D_2 are compaction coefficients. Originally Sawicki and Świdziński (1995) assumed the value of the exponent α to be equal to 3/2, but in our examination the value of α was treated as a variable to obtain a better fit of the experimental results to the model curve.

Two phases of the unloading can be observed (Fig. 15). The first phase is characterized by a purely elastic deformation and was used in the determination of elastic constants, the modulus of elasticity E and Poisson's ratio ν. The second stage of unloading is characterized by both elastic and plastic deformations. It was assumed that the material reversible response is governed by Hooke's law:

$$\varepsilon^e{}_x = \frac{1}{E}\left[(1-\nu)\sigma_x - \nu\sigma_{z0}\right] \tag{33}$$

$$\varepsilon^e{}_z = \frac{1}{E}\left[\sigma_{z0} - 2\nu\sigma_x\right] \tag{34}$$

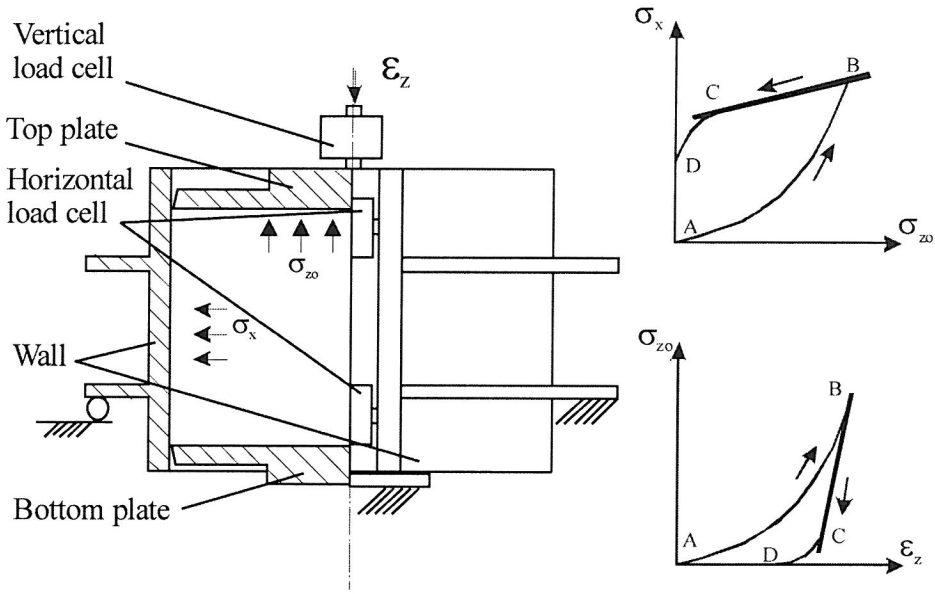

Fig. 15. Uniaxial compression test and determination of modulus of elasticity (Stasiak and Molenda 2001)

During the first phase of unloading (path AB) granular materials exhibit a linear relationship which is characteristic of elastic deformation. Assuming that $\varepsilon^e_x = 0$ from (eq. 33) $\sigma_x/\sigma_{z0} = (\nu/1-\nu)$ is obtained and applying the assumption that $\varepsilon_z = \varepsilon^e_z$ to equation 34, ε_z may be expressed as below:

$$\varepsilon_z = \frac{\sigma_{z0}}{E}\left(1 - \frac{2\nu^2}{1-\nu}\right) \tag{35}$$

Elastic constants were determined using experimental results measured during the linear phase of unloading. The ratio of horizontal stress σ_x to vertical stress σ_{z0} was assumed constant (elastic state of stress) and the slope of the straight portion of the curve defined by A, where $A = \sigma_x/\sigma_{z0} = \nu/(1-\nu)$ was determined. Values of A for different granular materials were estimated using linear regression procedure applied to experimental values of stresses (Fig. 15). Knowing A, values of Poisson's ratio ν were calculated as:

$$\nu = \frac{A}{1+A} \tag{36}$$

Values of modulus of elasticity E were estimated using relationship $\varepsilon_z(\sigma_{z0})$ (eq. 38) with experimental values of ε_z and σ_{z0}, and ν determined as described above.

The apparatus utilized was an oedometer whose walls were formed by two semicircular halves cut along the axis (Fig. 15). The two semicircular halves were connected with four load cells installed in pairs on the two connection lines, restoring cylindrical shape of the wall. Bottom and top plates of the chamber transmitted the vertical load through the load cells. The experimental setup allowed for the determination of mean lateral pressure σ_x, mean vertical pressure on the bottom σ_z, and the mean vertical pressure acting on the top plate σ_{z0}. The surface of the cylinder walls was smooth while the surfaces of the top and bottom plates were rough.

During testing the granular material was poured into the test chamber, without vibration or any other compacting action. The test sample was 80 mm high and 21 cm in diameter. The bedding was loaded in compression to the reference vertical stress, σ_{z0} of 100 kPa using a universal testing machine at a constant loading rate of 0.35 mm min^{-1}. The displacement of the sample was measured using an inductive transducer having an accuracy of 0.01 mm. Loading was followed by unloading which took place at the same speed of deformation until σ_{z0} of 0 kPa was reached.

5.3. Strength parameters

5.3.1. Methods and apparatus

Two test methods are recommended by Eurocode 1 (2003) for the estimation of strength parameters (angle of internal friction φ and cohesion c): direct shear test and triaxial compression test.

5.3.1.1. Direct shear test

For this test reference may be made to the ASTM D6128 (2000), but the parameters derived following that standard are not identical with those defined in Eurocode 1. The test apparatus is a cylindrical shear cell as shown in Figure 16. The diameter of the cylindrical shear cell should be at least 20 times of the maximum particle size and not less than 40 times the mean particle size. The height H of the sample should be between $0.3D$ and $0.4D$.

The up-to-date method of testing flow properties is based on the concept of Jenike, first published in 1961. The apparatus consists of the lower ring, the upper ring and the base. The chamber of the apparatus, comprised of the lower and upper ring, is filled with a sample of granular material. The lid is loaded with vertical force N and horizontal force is applied on a bracket attached to the lid. Shear tests performed with identically consolidated samples under different normal loads give maximum shear forces T for every normal force N. Ratios of forces N and T to the shear cell cross-section area give normal stress σ and shear stress τ. Characteristic of σ versus τ represents the maximum shear stress that

a sample can support under a certain normal stress and is called yield locus. Material bulk density ρ is the parameter of the yield locus. With an increase in normal consolidation stress, bulk density increases and the yield locus moves upwards. Each yield locus terminates at point E in the direction of increasing normal stress σ. The conditions of point E are called steady state flow, which is the flow with no change in bulk density and stresses.

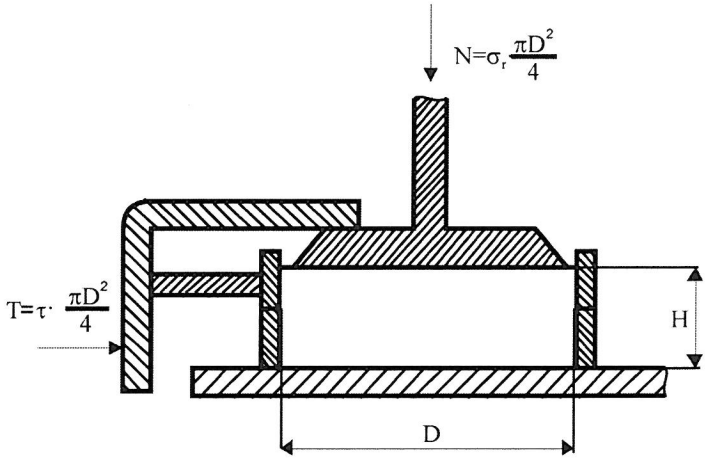

Fig. 16. Jenike shear cell

The original procedure of the shear test was as follows:

1. A prescribed mass of material was placed into the compartment of the apparatus;
2. Vertical consolidation reference pressure, σ_r, was applied for a prescribed period of time;
3. Sample was sheared until an asymptotic value of frictional force (steady flow) was approached, thus values of σ_r and τ_r stresses at the terminus of yield locus were determined;
4. Steps (1) and (2) were repeated;
5. Sample was sheared until 95% of an asymptotic value of frictional force was achieved;
6. Vertical consolidation reference pressure, σ_r, was released to zero;
7. Vertical pressure, σ_{z1}, was applied for a period of static holding;
8. Sample was sheared under pressure, σ_{z1}, until the end of the prescribed shear path;
9. Steps (4) to (8) were repeated for vertical pressures of σ_{z2} and σ_{z3}, and thus three points on the yield locus were obtained.

The Jenike method allows the determination of: cohesion c, angle of internal friction φ and effective angle of internal friction δ (Fig. 17).

Eurocode 1 (2003) recommends using a simplified Jenike method (including consolidation and shearing of the sample) for the determination of strength parameters (Fig. 17). The shear cell diameter D should be at last 20 times the maximum particle size and not less than 40 times the mean particle size. The height H should be between 0.3 and 0.4 D. The maximum particle size is limited to ensure that interaction of material with the cell wall will not influence the measured property. The sample should be poured into the test cell, without vibration or other compacting forces, and the consolidation stress σ_r applied. A top plate should be rotated clockwise and anticlockwise about the vertical axis several times through an angle of at least 10 degrees to consolidate the sample.

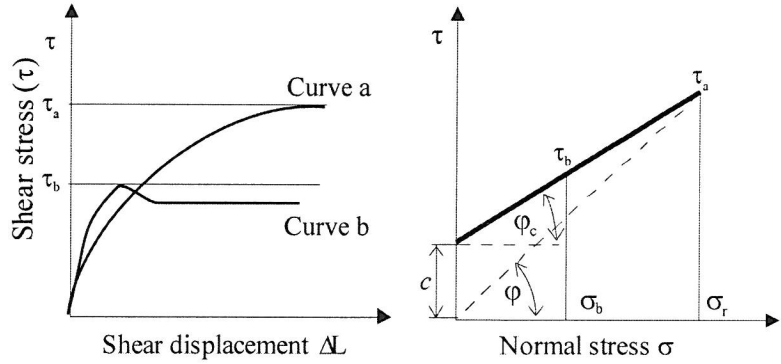

Fig. 17. Determination of shear strength parameters

The Eurocode 1 shearing procedure is as follows:

- The reference stress σ_r should be approximately equal to the vertical stress in the stored material.
- Shearing of the sample should be carried out at a constant rate of approximately 0.04 mm min^{-1}.
- To calculate strength parameters of granular material maximum shear strength τ should be used that developed at or before the horizontal displacement had reached the value of $\Delta L = 0.06D$.
- At least two tests should be carried out as defined in (5) and (6) below.
- The first sample should be sheared under a normal load causing the reference stress σ_r to obtain the failure shear stress τ_a.
- The second sample should first be preloaded under a normal load causing the stress σ_r and just brought to shear failure as for the first sample. Shearing should be stopped and the applied shear load reduced to zero. The

normal load on the second sample should than be reduced to a value causing approximately half the consolidation stress ($\sigma_b = \sigma_r/2$) and sheared again to obtain the failure shear stress τ_b.

Two parameters of the material – cohesion c and angle of internal friction φ should be used to define the effects of a stored solid's strength on silo pressures after the silo has been filled. The loading angle of internal friction φ_l for the stored solid should be calculated as:

$$\varphi_1 = \arctan\left(\frac{\tau_a}{\sigma_r}\right). \tag{37}$$

The cohesion c that develops in the stored solid under the reference stress σ_r should be calculated as:

$$c = \tau_a - \sigma_r \tan\varphi_c, \tag{38}$$

in which:

$$\varphi_c = \arctan\left(\frac{\tau_a - \tau_b}{\sigma_r - \sigma_b}\right). \tag{39}$$

where φ_c is the unloading internal friction angle for an over-consolidated material.

The value of cohesion c depends strongly on the consolidation stress, so cannot be regarded as a fixed property of the solid. For a cohesion-less material (where $c = 0$), frictional strength should be described only by the angle of internal friction φ_l that is equal to φ_c.

As an alternative to direct shear test, Eurocode 1 recommends triaxial compression test for the estimation of frictional strength parameters of granular material.

5.3.1.2. Triaxial compression test

Determination of strength parameters of wheat at five levels of moisture content of 10, 12.5, 15, 1.5 and 20% was performed using direct shear and triaxial compression tests. The parameters were determined following Eurocode 1 with a cylindrical shear box, 210 mm in diameter and with 80 mm bedding height. The sample was poured into the box without vibration and the reference stress of 100 kPa was applied. A top plate was rotated backwards and forwards three times through an angle of ten degrees to consolidate the sample. Following consolidation, the sample was sheared under normal stress equal to reference stress, at the rate of 10.8 mm min^{-1}. Second sub-test was performed for consolidation reference stress of 100 kPa and test load value of normal stress of 50 kPa. Three replications were performed. Triaxial compression tests with a sample 15 cm in diameter and 30 cm high were conducted on

wheat to compare results with the results of direct shear test. Comparison of angles of internal friction of wheat obtained in direct shear test and those obtained in triaxial compression test is shown in Figure 18.

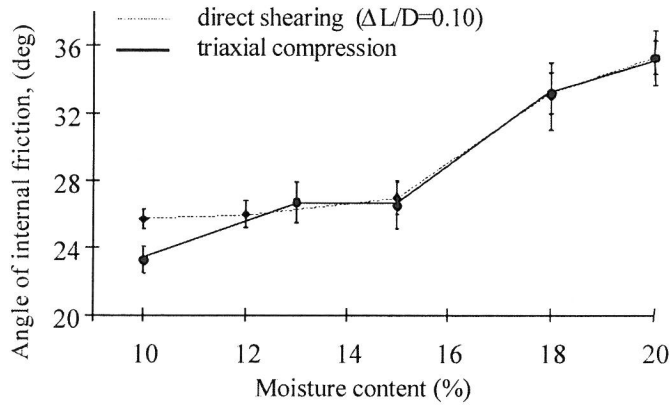

Fig. 18. Mean values and 95% confidence intervals of the angle of internal friction of wheat determined with the direct shear test and the triaxial compression test (Molenda and Horabik 2005)

Mean values for five levels of moisture content taken as one sample were not significantly different except the values for 10% of m.c. To obtain such an agreement of the results of two testing methods, the procedures had to be modified. In the case of direct shear test the shear deformation was extended up to 0.10 of sample diameter instead of 0.05 as recommended by Eurocode 1. In the case of triaxial compression test the sample was compacted by tapping during filling, up to a density equal to that of the sample in direct shear test. No clear explanation may be given for the discrepancy of results of direct shear test and triaxial compression test at 10% of grain moisture content. The probable reason is difference in the mechanism of deformation in the two tests combined with distinctly lower (than at higher levels of moisture content) grain-on-grain coefficient of friction.

5.3.2. Factors influencing angle of internal friction of cereals

5.3.2.1. Moisture content of the material

Grain moisture content has deep influence on the mechanical properties of grain in bulk (Horabik and Molenda 2002) as it modifies surface properties of seed-coat as well as the properties of kernel endosperm. Changing moisture content of grain influences shear stress-strain characteristics, and consequently

the determination of strength parameters: the angle of internal friction φ and the cohesion c. Figure 19 presents data obtained in direct shear test for wheat of moisture contents of 12, 20 and 22%.

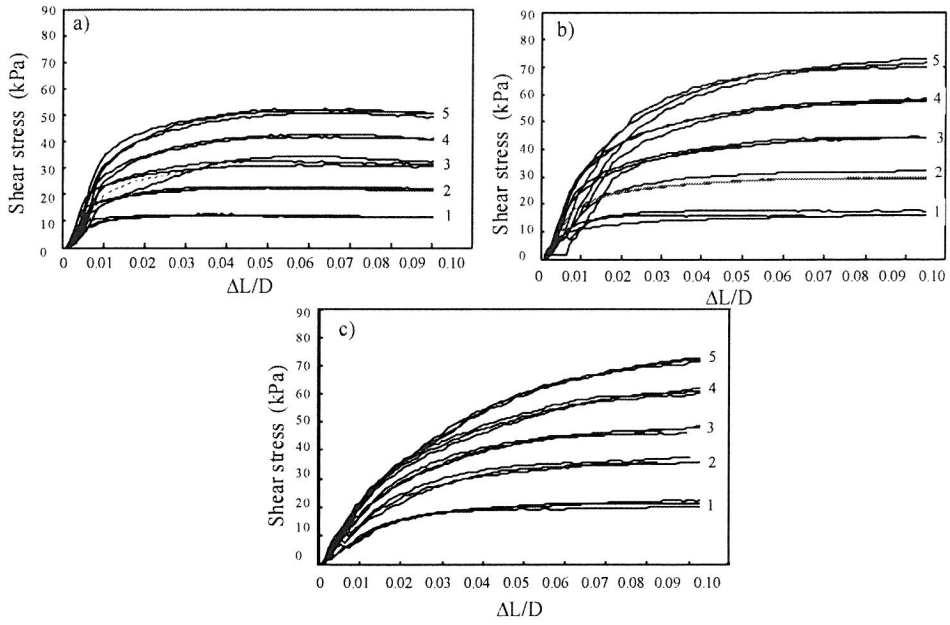

Fig. 19. Shear stress τ versus ratio of displacement to the sample diameter $\Delta L/D$ for wheat of moisture contents of: a) 12%, b) 20% and c) 22%, for normal stress σ_n of: 1-20 kPa, 2-40 kPa, 3-60 kPa, 4-80 kPa and 5-100 kPa (Molenda and Horabik 2005)

The results show that for wheat at 10% of m.c. (Fig. 19a) experimental curves stabilized or attained maximum below the 0.05 $\Delta L/D$ level of strain required by Eurocode 1. An increase in grain moisture content resulted in an increase in shear path to attain a stable level. In the case of grain of 20% moisture content (Fig. 19b) and 100 kPa of normal pressure the test curve stabilized at a stress level clearly above the 0.05 of the sample diameter. For grain moisture content of 22% (Fig. 19c) shear stress stabilized only for the two lowest levels of normal stress and for strain of approximately equal to 0.05 $\Delta L/D$ that precluded determination of the strength parameters. These results show that to determine strength parameters of wet grain an extension of shearing path up to 0.10 of sample diameter is necessary.

5.3.2.2. Bulk density

Stress-strain behaviour of granular material depends on the bulk density of the sample. Dense samples dilate during shear test while loose samples decrease in volume. In dense samples shear stress attains a peak value, and with continuing shear displacement it drops back to a lower ultimate value and remains at that constant level during further shear. In the loose state most granular materials tend to decrease in volume when subjected to shear under constant normal load. For such samples shear stress gradually increases until it reaches ultimate value. Thereafter, with increasing displacement it remains stable. The density at which material is sheared without change in volume is termed, after Cassagrande (1936), the critical density.

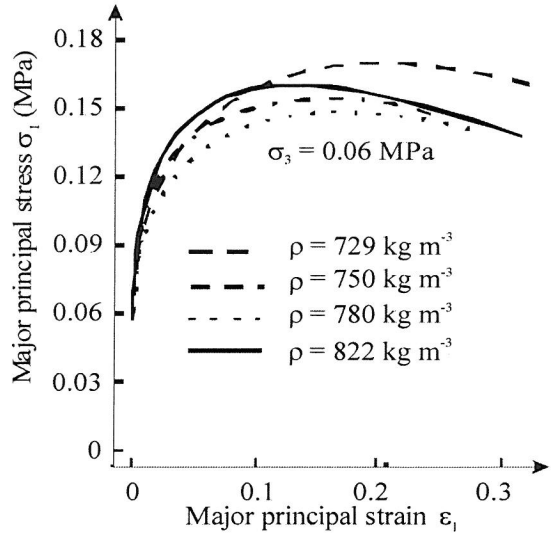

Fig. 20. Relationships of stress versus strain obtained in triaxial compression test for wheat grain of moisture content of 13% and four levels of bulk density (Molenda and Horabik 2005)

Figure 20 illustrates relationships between axial total stress and axial strain in triaxial compression of wheat grain of 13% in moisture content at four levels of bulk density (Łukaszuk and Horabik 2002). The graphs show that increase in density ρ resulted in a quantitative change in material properties. For denser samples higher were both the maximum value of σ_1 and the maximum value of axial strain ε_1. For the sample of bulk density of 822 kg m^{-3} the axial stress reached maximum value σ_{1max} for ε_1 of 0.1. For the sample of the lowest density (of 729 kg m^{-3}) the stress σ_{1max} was attained at ε_1 of 0.22, thus at the strain at least four times higher than ε_1 of 0.06 recommended by Eurocode 1.

5.3.2.3. Time of consolidation

The time of consolidation is one of the most important factors influencing mechanical properties of powders. For example, a long period of storage of powders in bags or in silo can lead to caking when the material becomes nearly solid, causing serious problems in handling. In the case of food powders moisture is the most severe factor causing caking. In order to determine the effects of time of consolidation, the sample has to be compressed for the prescribed period of time before the shear test is performed.

Figure 21 shows the results of determination of strength parameters of wheat meal following Eurocode 1 procedure. The sample was sheared immediately after consolidation by twists or remained under reference load for additional two hours. Time consolidation resulted in an increase of the angle of internal friction from 31°±4° to 43°± 2°. After the time consolidation, the sample usually returns to its original state if no chemical or physical changes have taken place. In such a case the material may be used for the measurement of the next point of the $\sigma(\tau)$ characteristic. This may be verified by running normal instantaneous test procedure. If any change in strength properties occurs after the time consolidation, this points out to chemical or other irreversible changes and a new sample should be taken for determination of the next point of the characteristic.

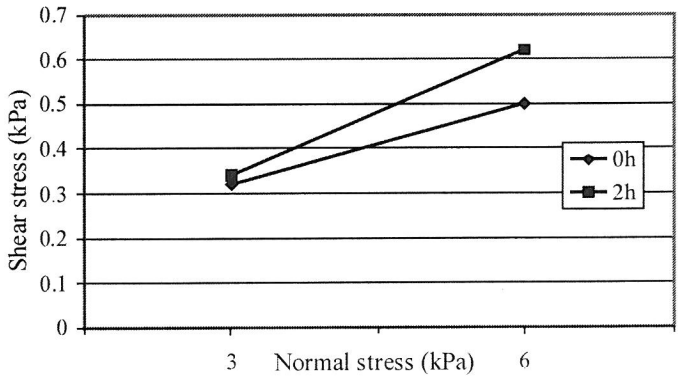

Fig. 21. Shear stress versus normal stress relationship from direct shear test for wheat meal without time consolidation and consolidated for two hours (Molenda and Horabik 2005)

5.3.2.4. Method of sample deposition. Anisotropy of packing

The angle of natural repose Φ and the phenomenon of grains lying nearly along the generatrix of the formed cone were used for producing the preferred grain orientation. Rye grains were poured through a funnel into the shear box inclined to horizontal at an angle β. The outlet of the funnel was placed near the box wall and lifted

along the wall generatrix so that the outlet was constantly approximately 20 mm above the surface of gathered grains. The grain was allowed to slide down the surface of natural repose to the front side of the box. Any change in the angle of inclination of the shear box to the horizontal resulted in a change of preferred inclination γ of long axes of grains to the bottom of the box.

Examination of an influence of the angle of preferred grain orientation on the shear stress-strain characteristic was performed under the normal pressure of 100 kPa. Samples were prepared so that the preferred orientation of grain formed angles, γ, of inclination to the shearing direction of: 0, 10, 20, 30 and 40 degrees. To preserve the packing structure of the bedding no additional consolidation was applied. The angle of preferred orientation of grains was found to influence strongly the stress-strain characteristics as shown in Figure 22. The strongest was the sample with γ of 40° showing maximum shear stress τ_{max} of approximately 50 kPa, while the lowest τ_{max} of approximately 30 kPa was found in the case of $\gamma = 0$ °. The probable reason for the observed difference of behaviour is the distribution of contact normals.

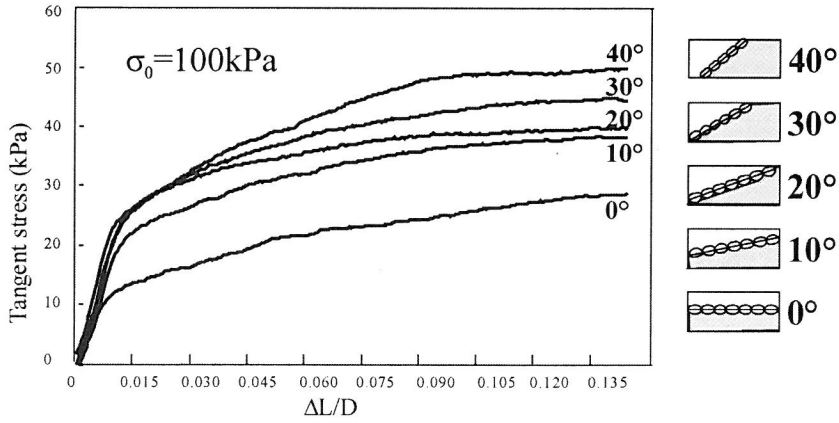

Fig. 22. Relationships of shear stress versus ratio of displacement to the sample diameter ΔL/D. Samples of rye with an angle of preferred inclination of kernels long axes to horizontal ranging from 0 to 40 degrees (Molenda and Horabik 2005)

Oda (1972) suggested that, for a two dimensional system, the distribution of contact normals may be approximated by an ellipse. The major axis of such an ellipse is initially oriented normal to the bedding plane. The preferred orientation of the long axes of the particles is parallel to the bedding plane. In the process of biaxial deformation the distribution of the contact normals changes so that a greater number of contact normals tend to orient themselves in the direction of contact force.

Testing with grain samples deposited in various ways and subsequently consolidated by twisting (as recommended by Eurocode 1 (2003)) did not show any differences in stress-strain characteristics, and consequently in obtained values of the angle of internal friction. This result shows that the consolidation procedure of Eurocode 1 erased all stress history similarly to pre-shearing to steady-state as recommended by Jenike (1961).

5.3.2.5. Surface properties of particles

The inter-particle friction is an obvious component of shear strength and in 1960's and 70's attempts were undertaken to find a relationship of the two effects. Rowe (1969) suggested that the primary task was to separate the strength component of particle structure from that of inter-particle friction. This author derived relationships of strength limits for loose and dense sands that gave "quite close" agreement over the range of the angle of inter-granular friction φ_μ from 17° to 39° for cohesion-less soils. Apart from φ_μ and density, Rowe considered measurement technique for the stress state of deformed sample and found that for dense sands triaxial compression and direct shear gave similar results. Feda (1977) summarized results of efforts undertaken up to 1975. No substantial progress in theoretical description of internal friction took place after that time. The structural component (or packing structure) of internal friction remains difficult to describe and monitor, but these days may be treated by DEM. Analysis of force distributions in three-dimensional granular assemblies performed by Blair *et al.* (2001) regarded the significance of inter-particle friction. The authors varied the coefficient of static friction between grains in such a way that for rough beads it was three times higher than for smooth ones. The resultant force distributions for rough beads were not significantly different from the distributions for the smooth beads. The tests have shown that particle deformation is the key factor for intergranular force distribution. Results of Blair *et al.* show that the phenomenon of internal friction still remains far from a conclusive description.

5.3.2.6. Formation of shear bands

Granular materials are deformed in many ways during processing. For a small strain the deformation is usually uniform. For a larger strain the deformation localises into a narrow region of shearing band. This region separates almost rigid blocks of a granular material. An effective rupture zone called a boundary layer or shear zone forms along the rough or corrugated wall in a silo with plug flow when friction between wall and grain is higher than internal friction of grain (Mühlhaus

and Vardoulakis 1987). There is always a shear zone of a width equal to a few particle diameters in which the velocity changes rapidly from that in the bulk to that at the wall. The thickness of the boundary layer was found to be dependent on the granular material. Zhang *et al.* (1994) examined shear zones in wheat sliding against corrugated steel surface. The lower boundary of the shear zone was estimated at 4.5 mm below corrugation peaks and the upper boundary was 18.5 mm above the corrugation peaks. The dilation in the boundary layer resulting from shearing during discharge gives rise to an overpressure. The overpressure is independent of silo scale causing a decrease in the relative overpressure with increased silo size.

The shear zone in granular material has recently become the object of wider interest of researchers. The determination of the thickness of the shear zone is important for the estimation of forces transferred from the granular material to the structure. The thickness of the shear zones depends on the wall roughness, the grain diameter, the specimen size and the boundary value problem considered (Tejchman and Wu 1995). The relation between shear band thickness and grain size has profound implications for investigations of progressive failures within granular solids. According to direct experimental observations of Roscoe (1970), the width of shear bands is about 10 times the average grain diameter. Investigations concerning the shear band formation are mainly based on computer simulations or theoretical modelling. The thickness of fully developed shear band was found to be approximately 16 times the mean grain diameter. Only a few researchers investigated experimentally the formation of the shear band in bulk of grain (Molenda *et al.* 1998, Nedderman and Laohakul 1980, Zhang *et al.* 1994).

Triaxial compression tests (Horabik *et al.* 2000) were performed to obtain information on the displacement distribution of particles inside the shear band. The sample was 30 cm high and 15 cm in diameter. The volume of the sample was divided into 30 cylindrical regions using two different colours of seeds: stained and not stained mustard seeds. Each region was 3 cm high and 3 cm thick. In the vertical direction the sample was divided into three cylindrical coaxial regions by inserting two cylindrical moulds of diameters of 3 cm and 9 cm into the sample mould. Layers of seed of 3 cm in height were poured into each of the three cylindrical regions of the sample. Ten layers of stained and not stained seed were poured into each column of the sample.

Vertical cross-section of the sample of triaxial compression at $\varepsilon_1 = 0.17$ with the initial and deformed meshes indicated is shown in Figure 23. Orientation angle of the shear zone α and its thickness were also indicated. The shear zone was oriented at an angle of:

$$\alpha = \frac{\pi}{4} + \frac{\varphi}{2} \tag{40}$$

with the horizontal axis (direction of the minor principal stress σ_3) as predicted by the Mohr-Coulomb theory where φ is the angle of internal friction.

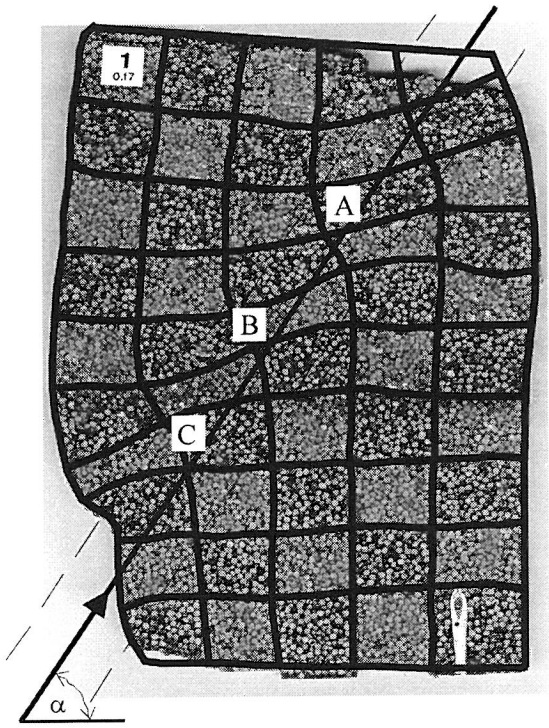

Fig. 23. Cross-section of mustard seeds sample deformed in triaxial compression test showing localization of deformation as shear band (Molenda and Horabik 2005)

Average value of the angle of internal friction for stained and not stained seed as 26°. Distributions of displacement across the shear band, at axial strain ε1 of 0.1 and 0.17, are shown in Figures 24 and 25. Vectors connecting the line of original and deformed mesh represent the distribution of displacement across the shear band. Vertical component of the vector represents the shear displacement, ΔL_s, and horizontal component represents the normal displacement, ΔL_n. The thickness of the shear band was determined from the width of the ramp in the η direction (Horabik *et al.* 2000). The thickness of the fully developed shear band was found to be 15 times the average grain diameter.

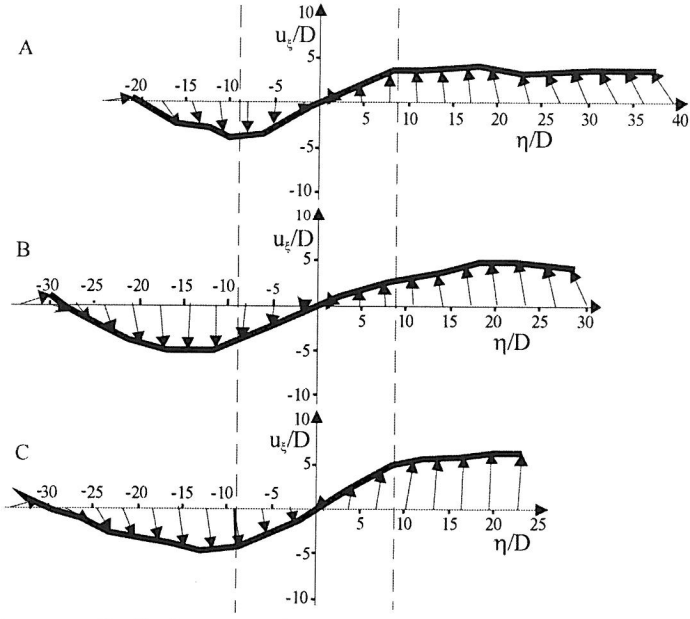

Fig. 24. Displacement distribution across shear band $\varepsilon_1 = 0.1$ (Horabik *et al.* 2000)

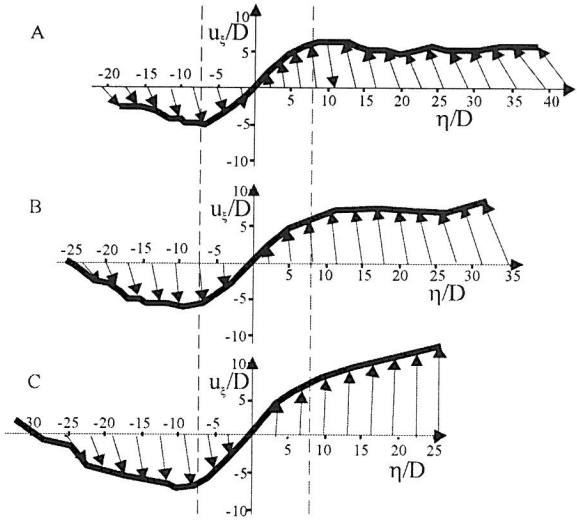

Fig. 25. Displacement distribution across shear band $\varepsilon_1 = 0.17$ (Horabik *et al.* 2000)

5.4. Coefficient of friction

5.4.1. Theories of dry friction

Friction is a set of phenomena taking place in the contact area between two bodies in relative displacement that cause resistance to motion. The measure of friction is the resultant tangential force acting during relative displacement of the two bodies. The earliest researchers of friction explained this effect by the necessity of rising of one of the bodies on the asperities of the other body (Perent 1704; Euler 1748 following Hebda and Wachal 1980). In this approach, the coefficient of friction was equal to the angle of inclination of individual asperity. The first wider examinations of friction were performed by Guillaume Amontons. In the publication of 1699 this author formulated two laws of friction that had been forgotten after being formulated by da Vinci in 15th century. The relationship $T = \mu N$, where N is normal force, T is tangential force, μ is coefficient of friction, is known as the Amontons low of friction and in some applications is used up till now (Buckley 1981). A different point of view was presented by Desaguliers in 1724. This author indicated that smooth surfaces of metals or other substances may be polished in such a way that friction would increase, and attributed the behaviour to adhesion acting in true contact areas. This statement initiated long lasting contradiction between adherents of mechanical and molecular theories of friction. In 1781 Coulomb published his "Theory of simple machines" where he acknowledged the influence of adhesion on friction. However he pointed out to the work that had to be done during relative sliding of rough surfaces as the main source of friction. Coulomb expressed the low of friction as follows:

$$T = \mu N + C, \tag{41}$$

where C was a constant dependent on the molecular interaction of surfaces in friction (cohesion).

Coulomb postulated that the value of C is constant for flat surfaces, and independent of the normal load. Leslie criticized Coulomb's theory in 1804 and indicated that it should contain the incorporate deformation of surface asperities as the necessary condition for energy losses to take place. This remark was supported by work of Bowden and Tabor (1908) who claimed that the character of interaction between bodies depended on the relation between their hardness, as well as on temperatures of melting of the substances and the temperature of the contact area. According to Bowden, friction force is composed of the force necessary to shear bonds between asperities and the force necessary to draw a groove in the weaker material. This author did not consider either molecular interaction of

surfaces or the influence of surface roughness, and assumed purely mechanical interaction of bodies in friction. Progress in technologies of surface treatment did not result in the elimination of friction, a fact that supported the point of view of followers of molecular theories of friction. In 1929 Tomlison (following Hebda and Wachal, 1980) proposed that friction was a result of adhesion of sliding surfaces. Dispersion of energy was a result of continual changes of pairs of interacting molecules and of the creation of new molecular bonds. Based on laboratory testing, Tomlison formulated an empirical relationship for coefficient of friction in the form of:

$$\mu = 0.18 \cdot 10^8 \left(A_k + A_p\right)^{2/3}, \tag{42}$$

where A_k and A_p – material parameters.

Another molecular theory of friction was proposed by Deriagin (following Kragelsky *et al.* 1977). This author proposed that friction depended on molecular roughness of the material that was interrelated with material structure. Deriagin's concept was valid in the case of ideal sliding, but did not consider frictional wear of sliding materials. In 1939 Kargelsky *et al.* (1977) published the principles of a molecular-mechanical theory of friction suggesting a "dual nature of friction". Later investigations by numerous researchers did not lead to any general theory of friction. Currently two types of coefficients of friction are used (Blau 2001), one that represents friction opposing the onset of relative motion, and one that represents friction opposing the continuance of relative motion once that motion has started. The former is called static coefficient of friction, and the latter – kinetic coefficient of friction. It is currently widely accepted that friction is not an intrinsic material property of the two contacting materials. The system approach has became a tool for the interpretation and use of friction data in modelling friction, developing friction mitigating materials, developing friction test methods, and designing machinery.

5.4.2. Experimental methods

Testing the friction of granular materials requires an apparatus in which relative motion of the material and a sample of construction material takes place. Relative motion may be rectilinear or rotary. In the case of rectilinear motion the sliding surface has the shape of a flat plate or band, while in the case of rotary motion it has the shape of a disc or cylinder. In Figure 26 apparatus used by various authors are presented as reported in literature (Balassy *et al.* 1989, Brubaker and Pos 1965, Bucklin *et al.* 1989, Drozdow *et al.* 1986, Fiala 1965, Kutzbach and Scherer 1977, Lobotka 1967, Moysey and Hiltz 1985, Raltchev and Barov 1970, Richter 1954, Schwedes 1975, Snyder *et al.* 1967, Thompson and Ross 1983).

The choice of a specific shape of sliding surface decides on important features of the measuring system. Apparatuses with the flat plate (Fig. 26 a, b) assure uniform distribution of sliding velocity, uniform distribution of normal pressure and easy interchange of sliding surface.

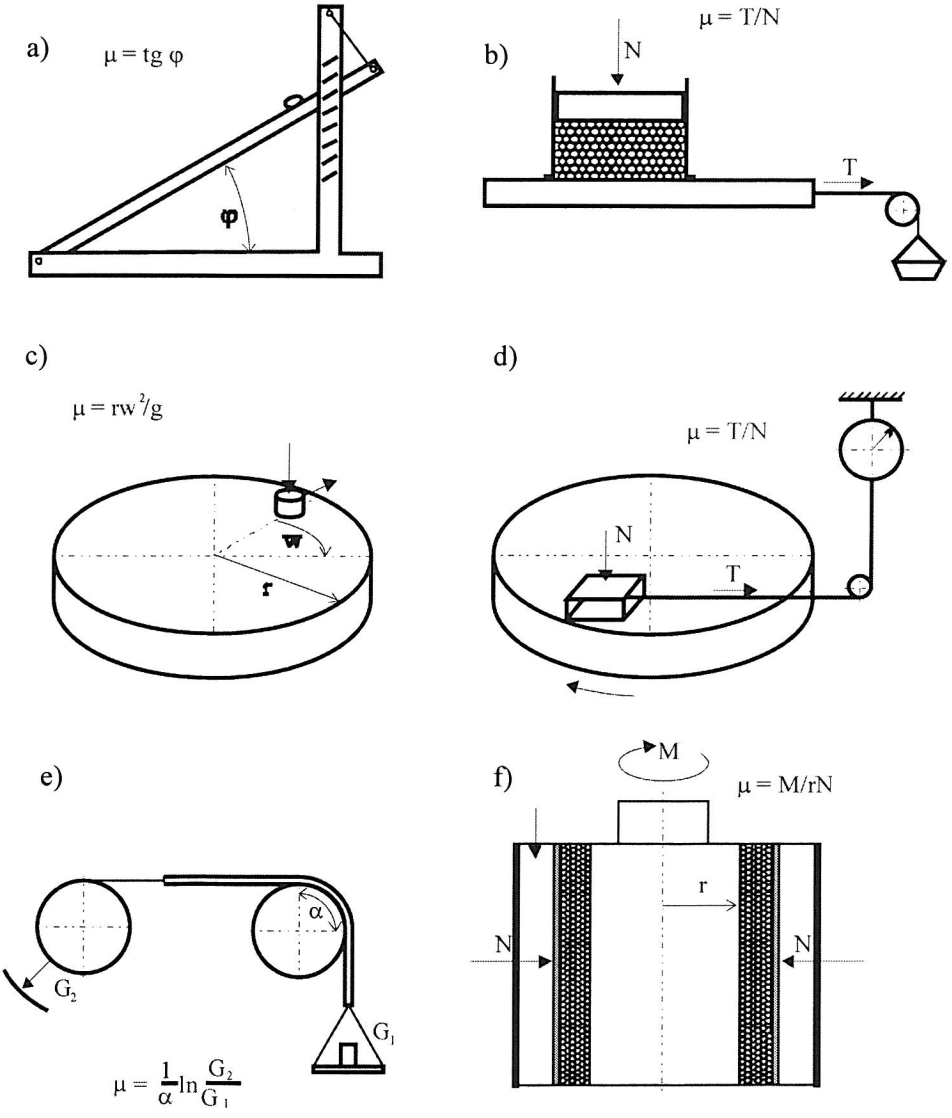

Fig. 26. Apparatuses used for determination of coefficient of friction of granular materials against construction material (Mohsenin 1978)

However, sliding velocity and sliding path are limited. Use of continuous band (Fig. 26 e) allows for uniform distribution of velocity and pressure with higher sliding speed and unlimited sliding path. However, frictional element in this shape is susceptible to vibration and may be produced only out of flexible materials. The shape of cylinder (Fig. 26 f) assures uniform distribution of sliding speed, but distribution of pressure is uneven, and obtaining interchangeable frictional surface poses a hard task to design and machine. Disc rotating around vertical axis (Fig. 26 c, d) allows for easy change of sliding surface, unlimited sliding path, high sliding velocity and uniform distribution of pressure. However, sliding velocity varies along the disc radius.

The coefficient of friction of granular materials of plant origin depends on numerous factors, among which the following are regarded as the most important: moisture content, normal pressure, sliding velocity, surface state and ambient conditions. The influence of these factors on the coefficient of friction will be shown below, taking wheat grain as an example.

5.4.3. Factors influencing the coefficient of friction

5.4.3.1. Moisture content

Already early investigations of grain friction pointed out to moisture content as one of the crucial factors influencing friction. According to Canadian Farm Building Code (1977), increase in moisture content of stored grain may result in a six-fold increase in pressure acting on silo wall. Richter (1954), based on his investigations on straw, hay and silage, reported an increase in the coefficient of friction with an increase in moisture content. Similar tendency was observed by Brubaker and Pos (1965) for friction of wheat against four types of construction materials. These authors suggested that after exceeding 13% of moisture content of grain a particularly fast increase in friction took place. Determination of wheat friction performed by Snyder *et al.* (1967) in a climatic chamber showed that increase in grain moisture content as well as increase of air relative humidity resulted in an increase of coefficient of friction. Hanzelik *et al.*(1968) did not observe any increase in coefficient of friction with an increase in moisture content. Probable reason for this disagreement with other authors was very low normal load applied in their equipment that was an inclined plate. Stewart *et al.* (1969), in their testing on sorgo, confirmed the tendency of faster increase in the coefficient of friction for moisture content above 13%. These authors found also that an increase in moisture content produced a particularly high increase in the coefficient of friction in the case of surfaces of low asperities. Thompson and Ross (1983) measured friction of wheat against galvanized steel and found the coefficient of

friction versus moisture content characteristic with a maximum for 20% of grain moisture content. These authors suggested that at moisture content from 16% to 20% kernels became soft and deformation around the asperity took place that generated stronger bonds than in the case of hard, dry grains. Further increase in moisture content caused a decrease in the coefficient of friction resulting, according to these authors, from the presence of liquid water in the contact area. Increase of coefficient of friction with an increase in moisture content was confirmed by results of Tsang-Mui-Chung *et al.* (1984), Balassy *et al.* (1989), Scherer and Kutzbach (1978). Lawton (1980) confirmed the above stated tendency; however for some materials he found a relationship with minimum coefficient of friction for moisture content of 15%. Molenda *et al.* (1995), for wheat sliding against steel surface, also found the relationship between friction force and moisture content with a minimum at approximately 15%, as shown in Figure 27.

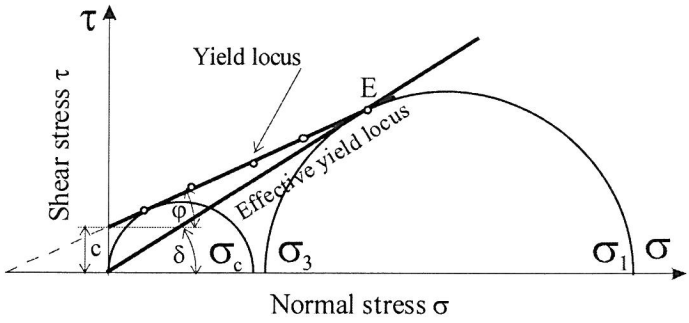

Fig. 27. Force of friction versus moisture content for wheat sliding on smooth steel surface. Experimental results and estimated curve (Molenda *et al.* 1995)

5.4.3.2. Surface roughness

Researchers were usually interested in friction of grain against materials that were commonly used in the construction of agricultural equipment and storage facilities. In earlier investigations wood, steel and rubber were tested, later investigations on galvanized steel, concrete, aluminium, polyethylene or teflon have been conducted. The state of the surface of investigated material was not precisely defined in a majority of published results because of the complexity of methods of determination of surface properties. Usually the commercial name of material was given, sometimes with a parameter of surface roughness added. As an example, Cyrus (1985) reported an increase in the coefficient of friction of wheat kernel against steel with an increase in parameter R_a in a range from 0.9 to 11 μm. A specific difficulty of investigation of friction is the changing state of surface with prolonging time of

measurements. Richter (1954) observed that the coefficient of friction decreased with increasing number of performed tests. He suggested polishing sliding surface till the moment of stabilization of frictional force. Thompson and Ross (1983) observed considerable variations of coefficient of friction between samples of galvanized steel received from different sources. These authors reported that coefficients of friction and their standard deviations decreased in subsequent measurements. Snyder *et al.* (1967), on the contrary, observed a decrease in the coefficient of friction with prolonged frictional contact. Washing the frictional surfaces with carbon tetrachloride reduced the coefficient to its original value. The substance found after evaporation of the solvent was determined to be cutin, a wax-like substance found on the surface of grain kernels. The effect of cutin on the friction coefficient was more noticeable after the metal surface was allowed to age for one or more days. Molenda *et al.* (1995) determined the friction coefficient of pairs of wheat grains on steel plates of different roughness. Results of these tests are presented in Figure 28.

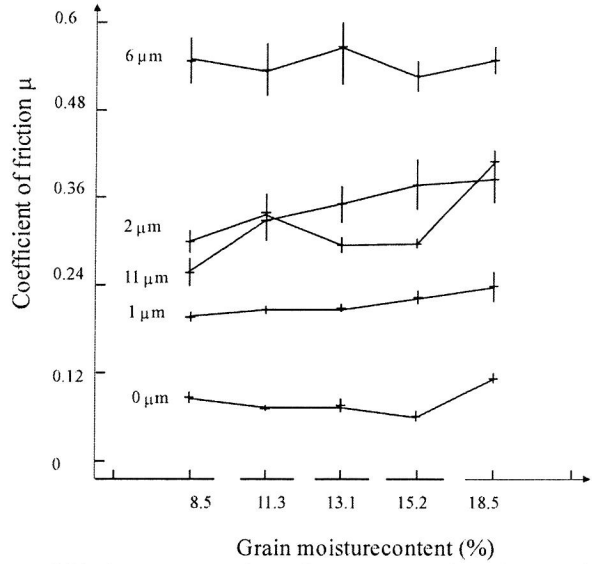

Fig. 28. Coefficient of friction versus grain moisture content for wheat grains sliding on steel plate of five levels of surface roughness (Molenda *et al.* 1995)

In the case of smooth surface, a minimum of μ of 0.6 was found at moisture content of 15.2%. For the plate of surface roughness R_t of 1 μm, the values of coefficient of friction consistently increased with increasing moisture content. For the remaining plates the coefficient of friction increased with increasing surface roughness, but no clear tendency with an increase in moisture content was observed. The apparent inconsistency of observed frictional behaviour is probably

a result of varied degree of contribution of basic phenomena in the resultant coefficient of friction. In the case of smooth surface the effect of adhesion prevailed. With increasing surface roughness the first deformation of surface asperities became relevant, while cutting of grain surface took place by asperities of plates of the highest levels of surface roughness.

5.4.3.3. Normal pressure

Normal pressure was shown to be another important factor influencing friction. Thompson and Ross (1983) applied normal pressure in a range from 7 to 172 kPa and observed a decrease in the coefficient of friction of wheat against steel with an increase in pressure. The authors suggest that with an increase in normal pressure contact stress increased less than proportionally. Hertz's theory (Mindlin 1949) postulated that with an increase in normal force N normal contact stress increases as $N^{1/3}$. This way, according to Thompson and Ross (1983), frictional forces in the contact area that are proportional to normal loads are weaker than proportional to normal stress. In such a way Hertz's theory would explain the decrease in the coefficient of friction with an increase in normal pressure.

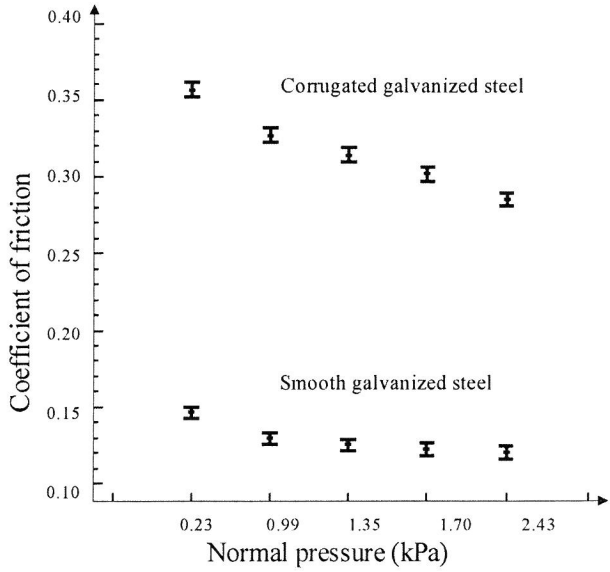

Fig. 29. Coefficient of friction of wheat on smooth and corrugated galvanized steel determined using tilting table method. Mean values and 95% confidence intervals for five levels of normal pressure (Molenda *et al.* 2000) normal pressure

A similar tendency was reported by Fiala (1965) for different agricultural materials, Lobotka (1967) in the case of corn and Zhang *et al.* (1988) for wheat. Moore *et al.* (1984) stated an opposite tendency, one of increase in the coefficient of friction with an increase in normal wall load in a silo made of corrugated steel. Typical results of friction of wheat against smooth and corrugated galvanized steel are shown in Figure 29 after Molenda *et al.* (2000). The tests were performed using the tilting table method and soft red winter wheat of 11.5% moisture content.

5.4.3.4. Velocity of sliding

Because friction on the contact area is a visco-elastic phenomenon, researchers were aware of the influence of velocity on grain to construction material friction. Usually sliding velocity was a parameter under control during testing. However, no in-depth interpretation of the influence of velocity on the coefficient of friction of granular materials of plant origin has been given. Generalizing the findings of numerous authors it may be stated that, in the range of low velocities, the coefficient of friction increases with an increase in sliding velocity. In a range of velocity around 1 m s^{-1} it reaches its maximum, and decreases after surpassing this value (Ducho *et al.* 1967, Fiala 1965, Kutzbach and Scherer 1977).

5.4.3.5. Wear in

Above mentioned changes in the coefficient of friction with prolonged frictional contact cause variations of frictional loads with the time of operation of equipment. Molenda *et al.* (1996) determined wall and floor loads in a smooth wall model silo as a function of fill and unload cycles. The authors found that repeated loading cycles resulted in a decrease of the coefficient of wall friction. During the first three discharges vibrations of wall load were observed, resulting from the stick-slip friction. Decrease of the coefficient of friction resulted in a decrease in vertical wall loads and an increase in floor loads. The vertical wall load-to-total grain load ratios decreased rapidly for the first several loading cycles. It was approximately 54% for the first loading cycle, 29% for the 9th, and 25% for 23rd LC.

5.4.3.6. Frictional vibrations. Slip-stick effect

Several investigators studying grain friction have observed the slip-stick behaviour. Bucklin *et al.* (1996) studied frictional behaviour of wheat by pulling test blades of galvanized steel through pressurized grain. The velocity at which the slip-stick behaviour ended and smooth behaviour begun was defined as the critical velocity. Pressure had no statistically significant influence on the critical velocity. However, a statistically significant relationship was found between the coefficient of friction and the logarithm of the critical velocity. Critical velocity was higher for

surfaces which had a high coefficient of friction. In experiments of Molenda *et al.* (2000) at lower sliding speeds, longer periods of motionless contact (sticking) were observed for all levels of normal pressure tested. Frictional forces of greater magnitude were also observed at these lower sliding speeds. Probably, longer "stick" time allowed for higher deformation of the system, and more elastic energy could be stored in grain. When the material slips, the energy is released. As the sliding speeds are increased, slippage occurs more often along with the release of the elastic energy.

5.5. Pressure ratio

The pressure ratio is one of the three most important physical properties of bulk solids, commonly used for calculation of pressure in a silo. Almost all design codes use a Janssen-type (Janssen 1985) pressure distribution to predict silo pressures (Wilms 1991). The well known Janssen formula uses the equilibrium of a horizontal slice of the granular material to estimate pressures in deep silos. The fundamental assumption of Janssen's method involves a relationship between the average stresses acting on the finite dimension of a slice, and stresses that act at the walls of a silo. Janssen assumed that the ratio between the average vertical stress σ_z and the stress normal to the wall, σ_x is a constant for a given bulk material stored in a silo:

$$\frac{\sigma_x}{\sigma_z} = k = const. \tag{43}$$

and k is to be determined from measurements. Other Janssen's assumptions are: fully mobilized friction at the interface of the bulk material and the walls of the silo, and constant bulk density (Drescher 1991).

Since the work of Janssen, several attempts aiming at an expression for k, based on postulating a mechanical model for bulk solids, have been proposed (Cowin 1977, Drescher 1991, Moysey 1979). A majority of the estimations are based on the assumption that the bulk material stored in or discharged from a silo is at a limiting state of stress. Another important assumption concerning the location of a region inside the slice of material where the yielding conditions occur involves relations between local stresses and the stresses averaged over the area or the perimeter of a slice (Drescher 1991).

In the case of a deep silo the following two stress cases are commonly considered: active for filling and storage mode, and passive for discharging mode. In the active case the vertical stress is higher than the lateral stress, while in the passive case the lateral stress is higher than the vertical one.

5.5.1. Yielding at the silo centre

Considering yielding at the silo centre, the stress ratio k can be easily obtained from Mohr's circle construction (Kezdi 1974, Moysey 1979) for the active case (Fig. 30a):

$$k = \frac{1 - \sin\varphi}{1 + \sin\varphi}, \tag{44}$$

and for the passive case (Fig. 30b):

$$k = \frac{1 + \sin\varphi}{1 - \sin\varphi}. \tag{45}$$

where φ is the angle of internal friction.

The commonly used assumption that the lateral stress is constant along the slice results in location of Mohr's circle for stresses at the wall outside the yield locus (Drescher 1991). This assumption does not adequately represent pressure distribution in granular material in a silo.

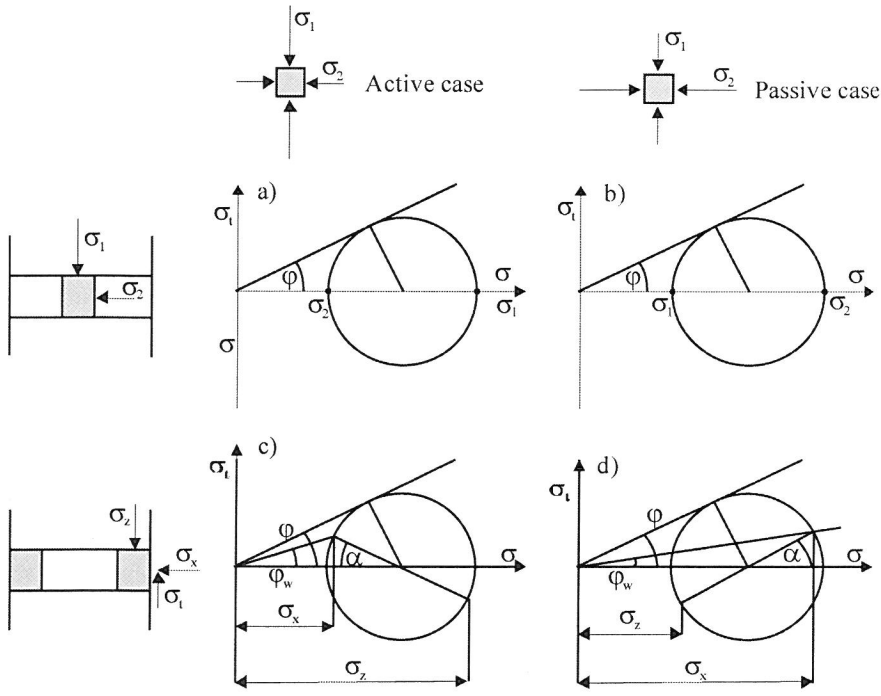

Fig. 30. Mohr's circles for active a), c) and passive b), (d) stress cases, a), b) – yielding at the centre, c), d) – yielding at the wall (Horabik and Molenda 2002)

5.5.2. Yielding at the silo wall

Considering the assumption that yielding occurs at the silo wall, the stress ratio k can be determined from the Mohr's circle construction as the function of the angle of internal friction and the angle of wall friction φ_w:

- for the active case (Fig. 30c):

$$k = \frac{1 - \sin\varphi\cos\alpha}{1 + \sin\varphi\cos\alpha}, \tag{46}$$

where:

$$\alpha = \arcsin\frac{\sin\varphi_w}{\sin\varphi} - \varphi_w, \tag{47}$$

- and for the passive case (Fig. 30d):

$$k = \frac{1 + \sin\varphi\cos\alpha}{1 - \sin\varphi\cos\alpha}, \tag{48}$$

where:

$$\alpha = \arcsin\frac{\sin\varphi_w}{\sin\varphi} + \varphi_w. \tag{49}$$

A plot of the pressure ratio for yielding at the silo wall and the active and the passive stress cases for typical range of values of the angle of internal friction and the angle of wall friction is shown in Figure 31. The pressure ratio observed in practice varies in a considerably smaller range (Kwade *et al.* 1994). A plot of the stress ratio calculated according to the following formula recommended by Eurocode 1 (2003):

$$k_\varphi = 1.1(1 - \sin\varphi), \tag{50}$$

is shown in Figure 31. The angle of internal friction φ used in this formula should be determined experimentally in the direct shear test or in the triaxial compression test. The plot of the pressure ratio obtained from formula (50) is located in the upper limit of theoretical values obtained for the active stress case and yielding at the wall (i.e. for the wall friction angle φ_w close to the internal friction angle φ).

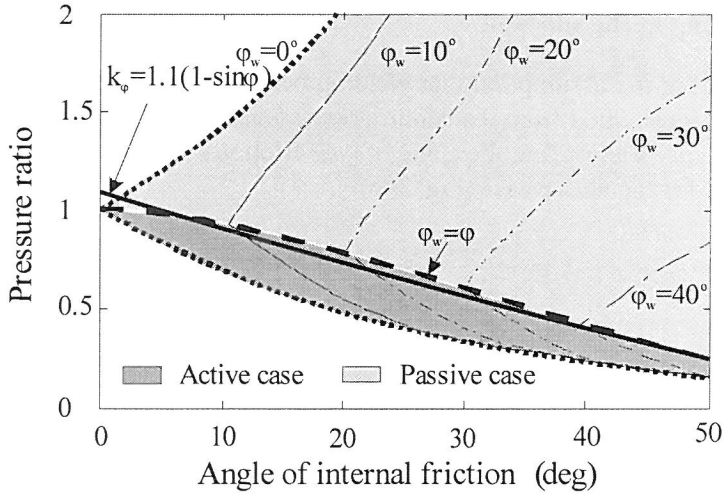

Fig. 31. Pressure ratio as a function of the angle of internal friction and the angle of wall friction for yielding at the wall in the active and passive cases (Horabik *et al.* 2000) — the pressure ratio according to Eurocode 1 (2003)

5.5.3. Experimental procedures

The most popular method of experimental determination of the lateral to vertical pressure ratio is the uniaxial compression test (Kwade *et al.* 1994, Molenda and Horabik 1998). An experimental set for the uniaxial compression (Fig. 32) was built according to the general guideline of the Eurocode 1 (2003) standard. The sample was poured into the chamber through centrally located spout, without vibration or other compacting actions. The specimen was loaded to the reference vertical stress of 100 kPa using a universal loading frame at the constant displacement rate 0.35 mm min^{-1}. The top plate was rotated backwards and forwards three times through an angle of 10 degrees to consolidate the sample. Next, the sample was reloaded to the reference vertical stress, and the slope of the lateral to the vertical pressure increase was determined. The pressure ratio k_s appropriate for filling and storing was determined as (Eurocode 1 2003, PN-B-03254-2002):

$$k_s = 1.1k_{s0}, \tag{51}$$

where

$$k_{s0} = \Delta\sigma_x/\Delta\sigma_{zm} \tag{52}$$

at the reference vertical stress σ_{zm}=100 kPa, σ_{zm}=(σ_z+ σ_{zo})/2.

Experiments were performed for samples of seeds of different size and shape and typical storage moisture content. Extended range of moisture content was applied for tests performed for cereal grain 10-20% and 6-15% for rapeseeds. The angle of internal friction of tested seeds was measured using Jenike shear tester of 210 mm in diameter according to the procedure recommended by Eurocode 1 (2003).

The second series of experiments was performed in the model silo 0.6 m in diameter and 0.6 m high. The experimental set-up allowed for determination of the mean lateral pressure σ_x, tangent wall stress, σ_t, and mean vertical pressure σ_z (Molenda and Horabik 1998). The coefficient of wall friction, μ^*, was determined as the ratio of mean vertical wall stress σ_t to mean lateral pressure σ_x. The average value of the stress ratio, k, was calculated utilizing a numerical solution of Janssen's equation for the mean vertical pressure on the bottom of the container. Layer of grain was loaded through flat, rigid top cover and a series of uniaxial compression tests were performed in the same way as in the uniaxial tester. The set-up was used to indicate the influence of filling method resulting in different structure of granular material on the pressure ratio.

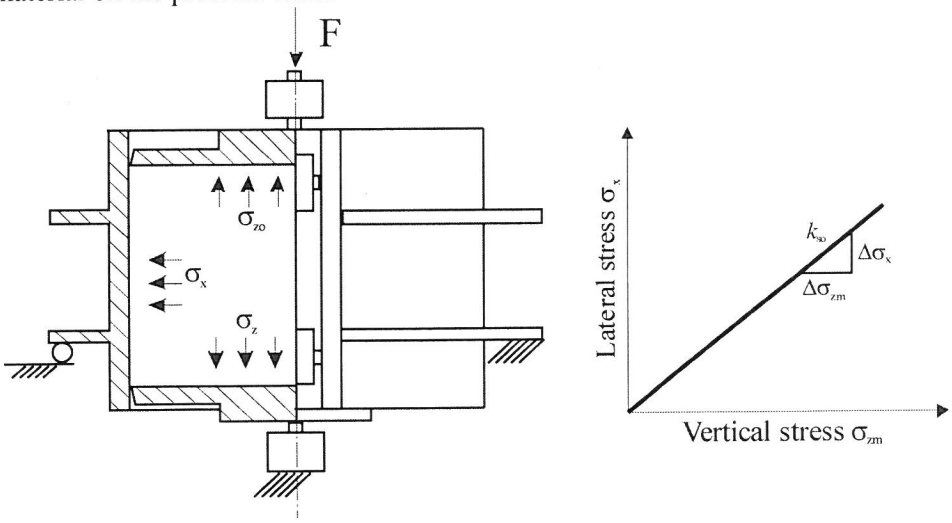

Fig. 32. Uniaxial compression tester: 1 – bottom plate, 2 – wall of the tester, 3 – top plate, 4 – load cells (vertical pressure), 5 – load cells (lateral pressure)

5.5.4. Factors influencing the pressure ratio

The recommended value of the lateral to vertical pressure ratio varies somewhat but the use of a value of approximately 0.4 is common. The pressure ratio

depends on the type of grain, moisture content, bulk density and bedding structure of grain formed during the filling process. The angle of internal friction and the angle of friction on the wall material increase with an increase in the moisture content of grain, while the bulk density decreases or increases depending on the pressure level (Łukaszuk *et al.* 2001, Molenda and Horabik 1994, Molenda *et al.* 1995, Thompson and Ross, 1983). The angle of friction at the interface of grain and the wall material depends strongly on the roughness of the wall surface. All those three properties of bulk of grain influence the pressure ratio.

5.5.4.1. Friction force mobilization

During monotonic uniaxial loading the pressure ratio generally increases to an asymptotic value characteristic for the material. For such a loading it can be assumed that the wall friction is fully mobilized but we cannot be sure of the same about the internal friction. Therefore the value of the pressure ratio characteristic for yielding at the wall in the active case (formula 50) should be treated as the lower boundary of the possible values of the pressure ratio.

Examples of plots of the pressure ratio and the wall friction coefficient versus normal pressure obtained during loading and unloading loops of rape seeds and wheat grain in the model silo are presented in Figure 33 (Horabik and Rusinek 2000).

During loading the pressure ratio increased to the asymptotic value typical for the given material while the wall friction coefficient decreased to the asymptotic value of the friction coefficient. On the contrary, during unloading the pressure ratio increased and the friction coefficient decreased. During each next loading-unloading cycle the course of the pressure ratio loops was similar to the first one while the friction coefficient loops were moved down with an almost constant rate.

During the first cycle of loading the experimental value of the pressure ratio is close to the predicted value for the active case and yielding at the silo centre or yielding in frictionless wall silo (pointed line, $\varphi_w = 0°$). It means that the principal stresses were close to the vertical and horizontal directions. The biggest part of the pressure ratio loop is located in the area of values predicted for the case of yielding at the wall in the active case. During unloading the pressure ratio loop goes beyond the value calculated according to Eurocode 1 recommendation (solid line) and arrives into the area of values typical for passive case (above dashed line). The pressure ratio loops result from superposition of elastic and plastic interactions between grains. Although the limit states of the model comprise only the plastic interactions, the predicted values of the pressure ratio correspond fairly well to the experimental ones.

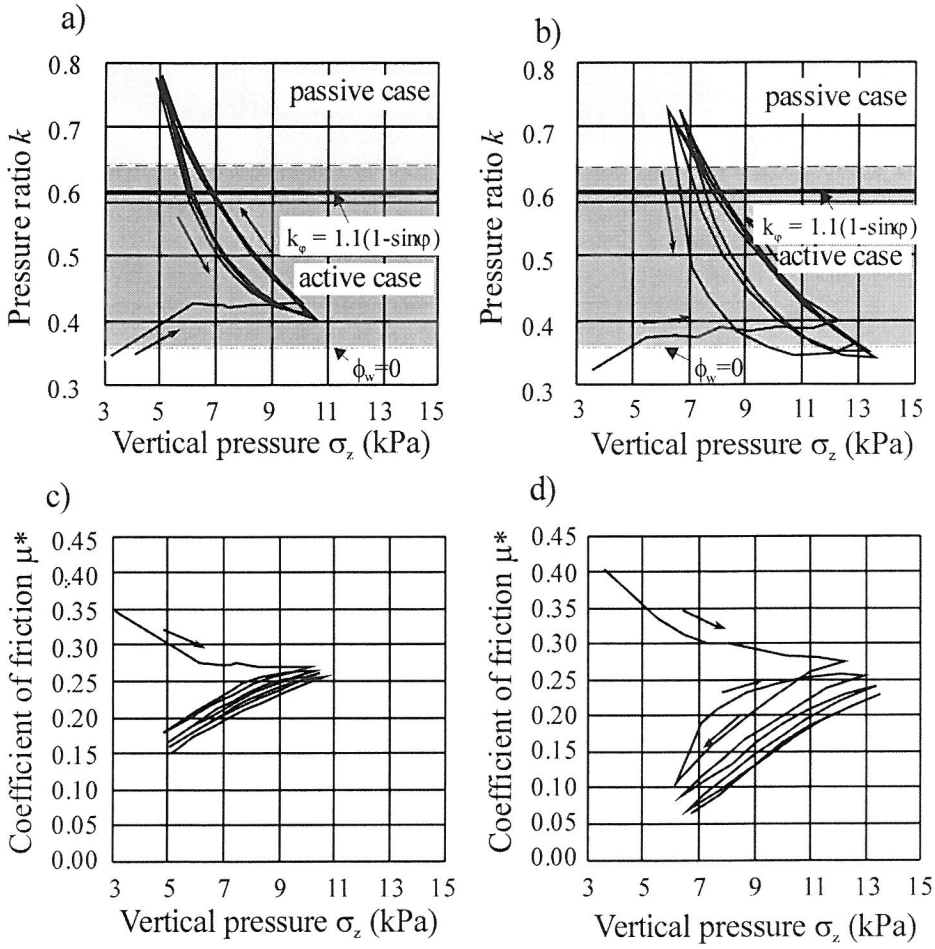

Fig. 33. Pressure ratio a) and wall friction coefficient of rape seeds c) and wheat grain b), d) during loading-unloading cycles (Horabik and Rusinek 2000)

5.5.4.2. Packing structure

The pressure ratio is influenced by the procedure of sample preparation (Kwade *et al.* 1994, Horabik and Rusinek 2000). Distributed filling produces higher density as compared to stream filling. This results in a higher angle of internal friction and a lower pressure ratio (Fig. 34). Filling procedure affects not only the bulk density but also the packing structure of granular material i.e. mutual orientation of particles and distribution of normal direction at contact points. In the case of distributed filling, inter-particle force chains are oriented

mainly vertically. Edometric compaction strengthens this structure and, as a consequence, the pressure ratio is relatively low. This type of structure results in funnel flow during discharge. On the contrary, concentrated (stream) filling results in looser structure. Particles sliding off along the surface of natural repose cone generate some preferences in particles orientation which additionally influences the stress transition. Finally, the pressure ratio is much higher than in the case of distributed filling and during discharge material tends to mass flow.

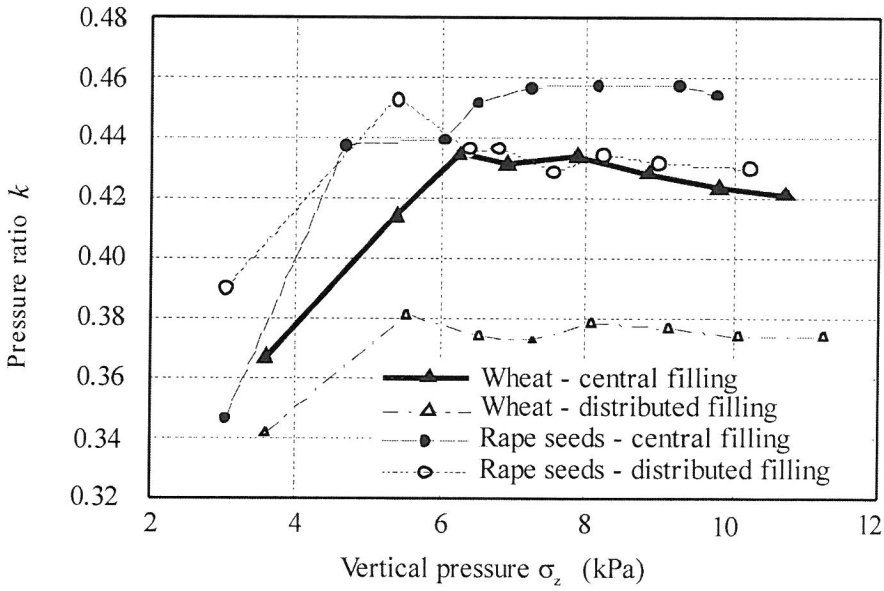

Fig. 34. Effect of the filling procedure on the pressure ratio determined on the model silo

5.5.4.3. Moisture content

With increasing moisture content, the friction force and the cohesion between grains increase. As a result a smaller part of the vertical loading is transmitted into the lateral direction. Consequently, the lateral to vertical pressure ratio should decrease with an increase in moisture content. Tests performed for cereals grain confirm this relationship (Fig. 35). Nearly a linear decrease of the pressure ratio with an increase in moisture content was obtained for corn, rye and rape seeds. Another course of changes was obtained for barley: the pressure ratio was almost constant in the range of moisture content up to 17.5% and then decreased. This indicates that the influence of some other factors still remains out of control.

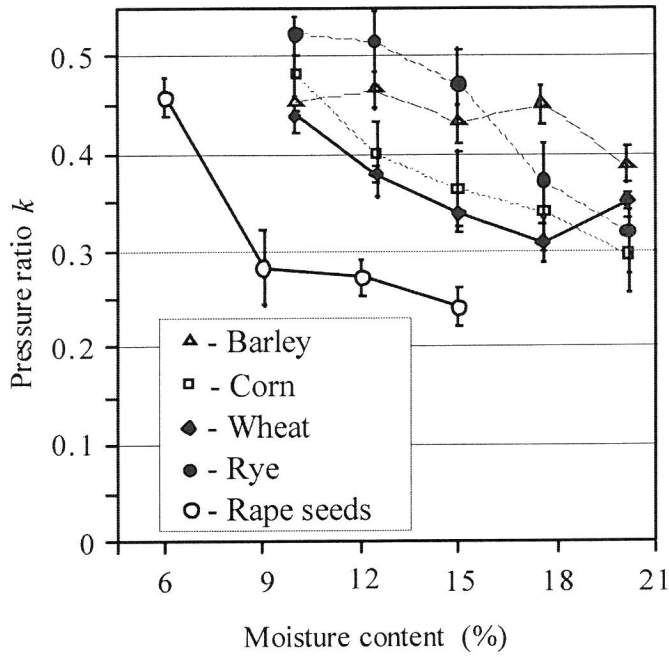

Fig. 35. Pressure ratio as influenced by moisture content of grain

5.5.4.4. Grain shape and surface roughness

The shape, size and roughness of seeds were found to influence the pressure ratio. The influence of surface roughness can be determined in an indirect way by considering its influence on the angle of internal friction. The more rough the surface the higher the angle of internal friction and consequently the lower the pressure ratio. In practice it is difficult to separate the influence of the shape and roughness of grain. It is much easier to observe the combined effect of both factors: the smoother the surface and the closer the shape to a sphere, the higher the pressure ratio. The pressure ratio of the material composed of elongated grains, like cereal grain, is generally lower than the pressure ratio of material composed of spherical grains. The spherical shape of soybeans as compared to the lenticular shape of lentil seeds results in different distribution of contact points in bedding of material. Almost vertical orientation of the shortest axis of lentil seeds obtained during filling the tester results in easier transmission of vertical load into the lateral direction than in the case of spherical (soybean) or corrugated seeds (pea).

6. INDICES OF STRENGTH AND FLOWABILITY USED BY PROCESS TECHNOLOGY

Some specialists (see Bell *et al.* 1994) consider the Jenike method of testing flowability to be much more complex and time consuming than less sophisticated measures. These authors state that the Jenike process takes at least 4 to 6 hours per sample, and the specific ramifications of the resulting flow function are understandable for only very few engineers practicing in the USA. Testing a bulk material with a Jenike cell takes more time and skill than the average producer or consumer of powders is willing to invest, unless there is a major financial stake such as the design of a new silo.

Current state of theory and technology of granular materials does not allow for wider standardization of material parameters and methods of their determination. However, industrial practice needs material parameters for design of processes, as well as measures of quality of products. Increasing number of consulting firms appear on the market and offer help in solutions of technological difficulties or determination of material parameters. High credibility is gained by firms led by specialists of respect established earlier in academia. Probably a good illustration of the demand from practice and proposed solutions are the offers of consulting groups founded by A. Jenike or by J.R. Johanson. These two specialists were earlier employees of academia. The establishment of Jenike addresses its offer to the following industries: chemical, environment protection, food, glass, metallurgy, mineral solids, paper, pharmaceuticals, mining, plastics and metal powders. Jenike and Johanson (2005) propose standard tests for determination of cohesion, coefficient of wall friction, angle of internal friction, compressibility, permeability and angle of chute inclination to allow for stable flow. Determination of material parameters may also be performed as a function of: consolidation time, normal pressure, ambient temperature and humidity. The apparatus applied is a direct shear box (Jenike method) equipped with consolidation bench. Ring shear apparatus is also available that apart of typical application of Jenike tester enables the estimation of wear of material due to attrition. For cases where determination of parameters does not give satisfying description of the process, consultants propose model investigations.

6.1. Quality determination

Quality control is an important task in the production and processing of granular materials because it allows for undisturbed flow of material and keeping constant composition of processed powder. Therefore, several new solutions of material testers have been proposed in recent decades that are currently verified. Quality control has to be carried out in such points along the production line

where product properties may change and result in damage of equipment or deterioration of product quality. Determination of quality of raw material is performed for protection against introducing portions of material of low value or undesired flowability. Variations in flowability may be the result of action of numerous factors. For complex processes many ingredients are used that are delivered from different producers. Constancy of properties of raw material depends on the method of production. Confirmation of the consistence of nominal properties of the material and its actual properties requires regular examination.

In numerous processes equipment is tuned during start up procedure when sometimes a large amount of by-product is produced. Examination of this start up product allows to decide if it may be reintroduced in the line. In typical process conditions maximum cohesion is determined to avoid flow problems in the system. In some cases, however, the value of end product is determined by minimum cohesive strength. For certain group of materials the best product is the most difficult to produce, and increase in quality above an acceptable level is very costly. In such cases quality control is particularly important.

Ploof and Carson (1994) summarized the quality requirements posted by the market for a powder quality tester. First of all the tester has to be easy to use, with minimum requirement for skills and training. Time needed for performing measurement and analysis of results should be possibly short. Moreover, results of measurements should be precise, repeatable and should deliver significant information about the material. And finally, the construction of the tester should be simple and compact, allowing for mobility. Such a kind of equipment may be easily placed in proper location on the production line instead of delivering material samples to the laboratory.

6.2. Peschl rotational split level shear tester

Peschl (1989a) presented a promising proposal of a rotational shear apparatus with associated method of determination of mechanical properties of powders (Peschl 1989b), and a method of quality control of powders for industrial application (Peschl 1989c). The author analysed existing equipment and found that some apparatuses overestimate the values of parameters as compared to values in a full-scale installation, while others underestimate those values. Peschl, based on his examinations of industrial powders, stated that rotational split level (RSL) shear testers give values similar to those encountered in practice. In the RSL apparatus, shearing of the samples takes place through the rotational movement of the lower part of the sample against the upper part of the sample. The horizontal cross-section area of the sample equals 30 cm^2 while its volume is 45 cm^3. With rotational movement, no limit on shear displacement exists, and the shear plane forms in the middle of sample height where the disturbances from horizontal borders of

the sample are the least. The author recommends choosing such experimental procedure that would most closely reflect the conditions of real process for which the material parameters are determined. Peschl preferred not to suggest any standard procedure, but offered the possibility of programming of shear conditions with automatic control of the apparatus. Procedure of data analysis allows for linear or exponential approximation of yield condition. For majority of easy flowing or low-cohesion materials, linear approximation is a sufficient solution. In such a case material parameters have a clear interpretation.

Some materials are characterized by strongly non-linear yield condition in a range of low normal pressures. For this group Peschl (1989c) suggested linear approximation in two intervals. Out of straight line estimated for the range of higher pressure the higher principal stress σ_1 should be determined, while cohesion c and unconfined yield stress σ_c should be determined out of the course of a straight line estimated for the lower range of normal pressure. If the mentioned above do not give satisfactory accuracy of description of the yield condition, a non-linear approximation using exponential function is necessary. The method of approximation cannot be settled at advance, but must be an outcome of consideration of particular case. Peschl claimed that his method gave the possibility of simulation of all conditions existing in practice, proper determination of parameters and, consequently, reliable operation of industrial installations. The author concluded that powder technology gained the level of engineering science and allowed for design of industrial installations without beforehand experimenting on equipment and installation.

Flowability is a material property of increasing importance. With passage of time, this property is more extensively used as a measure of material quality. Consumers expect constant flowability of washing powder, milk powder or sugar. For mixing, dosing and packing, stable flowability is a crucial parameter for reliable processing and stable values of end-product. Peschl verified his method testing products of pharmaceutical and coal industry (Peschl 1989c) and recommended its use for quality determination. The obtained parameters are: consolidation pressure (σ_1), angle of internal friction (φ) and unconfined compressive strength (σ_c). The only parameter of free flowing material is the angle of internal friction. To characterize a cohesive material two parameters are necessary – the angle of internal friction and cohesion. Consolidation pressure should be set close to the pressure that acts on the material under the conditions of technological process considered. The angle of internal friction is a function of stresses σ_1 and σ_c. As the non-dimensional parameter the author proposed "absolute flowability – *FLA*:

$$FLA = \frac{(\sigma_1 - \sigma_2) \cdot \rho}{\sigma_c \rho_w} \tag{53}$$

where:
ρ_w – density of water
ρ – density of bulk material.

Bell *et al.* (1994) examined a number of methods of quality determination of powders regarding their usefulness in industry including the method of Peschl. Two directions in simplification of powder quality assessment were explored: automation of the Jenike approach and elaboration of a new method. The Peschl method is an example of the first approach. Bell *et al.* admitted that the method gave repeatable results in the range of intermediate and low normal pressures. The possibility of performing several measurements on one sample of powder is an advantage of this method, however special care should be taken in the case of materials susceptible to damage in shearing. Automation applied in the tester results in its relatively high price that limits the number of units that can be placed along production lines. Moreover, the advantage of automation became dubious when determination of flowability with time consolidation is required. Such examination requires separate samples consolidated under different pressures and in controlled ambient conditions, thus the same sample cannot be examined without conditioning for every single test.

6.3. Johanson's apparatus and indices

J.R. Johanson separated from Jenike & Johanson in 1985 and before long proposed his own method of determination of mechanical properties of powders (Johanson 1992). The basic unit of this equipment is an indicizer test cell shown in Figure 36. The sample is consolidated in a cylindrical mould using a two-piece piston that measures the consolidation pressure directly on the inner piston while the inner and outer pistons move together. The outer piston receives all the drag effects on the cylinder wall and this way eliminates any drag effects that act on the inner piston when the compaction pressure is measured. The sample is consolidated up to a prescribed level of major principal stress. Once the consolidation is complete, the vertical load is removed. The lower piston drops to allow the sample to be unconfined. The outer, upper piston is then raised relative to the inner piston and the shear failure induced by the downward movement of the inner piston. This way the unconfined yield strength σ_c is directly measured. The author claims that his method gives more accurate results than the Jenike method while the procedure of determination requires less time, and states that it allows the researcher, expert, designer, engineer, purchasing agent or equipment vendor "to access solids flow properties with ease and confidence".

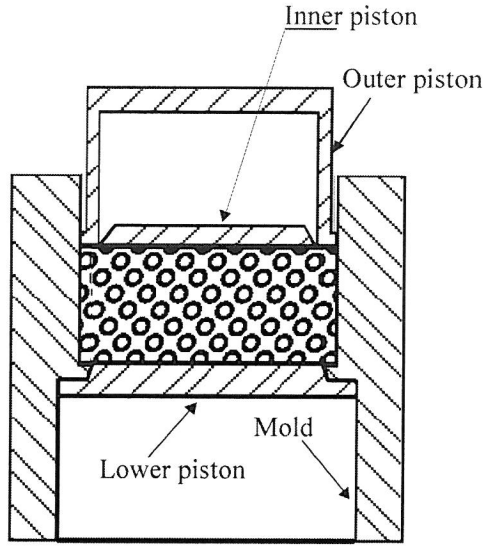

Fig. 36. Johanson indicizer test cell (Johanson 1992)

The Johanson indicizer was tested by specialists of DuPont (Bell *et al.* 1994). The authors point out to the importance of flowability determination and inform that in industrial practice the aim of 95% of examinations of powders is performed in regard to product design and quality, not for silo design. The authors state that they were very interested in Johanson's tester because it was the first unit to be fast in use, relatively simple and available at a moderate price. Examination of several common powders was performed and compared with results of the Jenike method. It was found that the equipment gave highly repeatable results for a relatively large group of materials. Performing measurement does not require long time or special skills of the technician. Calculation of unconfined yield strength σ_c using Johanson's test parameters showed that the indicizer gave lower values than the direct shear test. When the ratio of unconfined yield strength to powder density σ_c/γ was used as a measure of flowability, a low degree of consistence with the direct shear test was observed, particularly at low range of normal pressure. At higher levels of normal pressure, both the methods gave fairly close results. The authors (Bell *et al.* 1994) performed a ranking of a number of materials based on the Jenike and Johanson methods and found that the two methods gave results in a fairly good agreement. In summary, Johanson's indcizer was found to be a convenient and repeatable tool to use, but its predicted σ_c values and arching and rathole diameters did not correlate well with the results of the Jenike cell. For some materials good agreement of flowability ranking was obtained under certain circumstances, but the basis for these limiting circumstances could not be quantified.

JR Johanson Inc. proposed investigations of materials in a wide range of temperature and moisture content. Standard testing has been offered for determination of density, permeability, strength and angles of friction and adhesion. Testing of flowability using Johanson's indices is also offered. Values of parameters for determination of the indices are measured under pressures and for scale factors corresponding to the dimensions of equipment applied in the process under consideration. Some indices have physical dimensions expressed in US units, as for that market the equipment was meant.

The set of indices with their physical interpretation is shown in Figure 37 following Johanson (2000). Basic properties of materials are measured at specific consolidation pressures or a scale factor relative to the process equipment size. Indices cited below are given in U.S. units as a basis of the bin diameter D = 10 ft (3.05 m) and a hopper diameter D = 1 ft (0.305 m).

The Arching Index (AI), with a typical range of 0-4 ft (1.22 m), is the conical hopper outlet required for unaided gravity flow after dropping the solids into an empty hopper and ensuring arch collapse in a conical bin. The *AI* is related with material properties as follows: $AI = 2.2\sigma_c/\gamma$, where σ_c i γ are measured under normal consolidation pressure of: 3 γ *d*/2.

The *Ratholing Index (RI)* – typical range, 0-30 ft (0 to 9.15 m) – is the flow channel size in a hopper required for a solid to collapse into the hole above the outlet, if arching did not occur. *RI* also provides a good indication of lumping tendency. If, after a time at rest, the solids *RI* exceeds 10 ft (3.05 m) a lump breaker may be needed in the system. The *RI* is related with material properties as follows: $RI = 2{,}5\sigma_c/\gamma$ where σ_c and γ are measured at consolidation pressure of γd.

The *Hopper Index (HI)* is the minimum half-angle of a conical hopper, required to ensure flow along the hopper walls. Its value is $HI = 42 - \varphi'$, where $-\varphi'$ is the angle of kinetic friction measured at normal consolidation stress of γd, or if φ' increases with an increase in stress value of φ' determined at the stress level of γD.

The *Flow Rate Index (FRI)* – typical range 1-12000 lb min^{-1} (0.5 to 5400 kg min^{-1}) is the rate at which the solid will flow through a hopper outlet of diameter d when totally deaerated. Low value of *FRI* usually points out to fine, highly compressible powder. Particles of sizes in excess of 400 μm are usually incompressible, very permeable, and have a high *FRI*. Variation in the value of the index may be a signal of segregation or change in composition of powder mixture during processing.

The *Feed Density Index (FDI)* and *Bin Density Index (BDI)* are values of bulk specific weight expected at a conical hopper's discharge outlet or bulk specific weight expected in a container full of solids or in a mixer after agitation stops. The *FDI* is measured at a pressure of γd, while *BDI* is determined at a pressure level of γD.

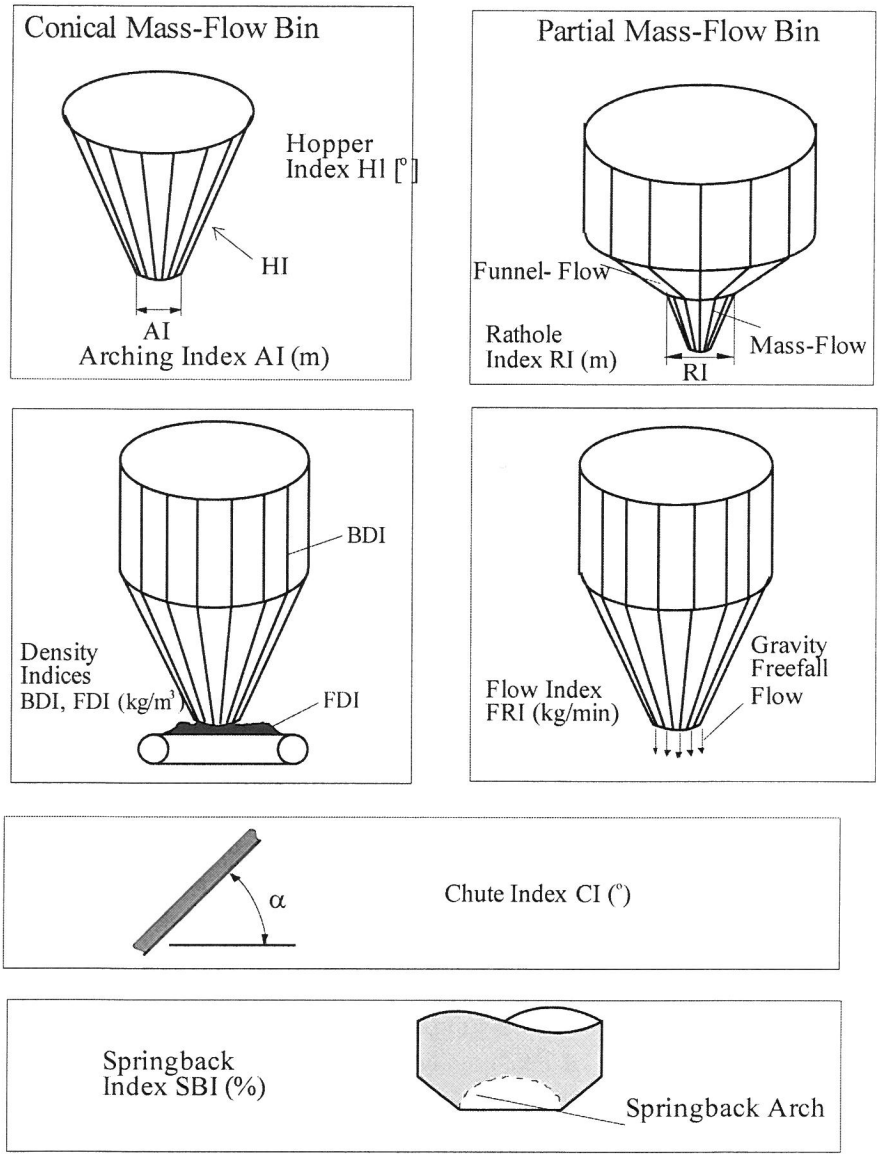

Fig. 37. Johanson indices (Jenike 1964)

The *Chute Index (CI)* is recommended chute angle to eliminate solids build up on a chute at impact points. The index takes value of $CI = ASC + 10°$, where *ASC* is an angle of slipping friction along the flat surface of the bulk solid sample compressed with the pressure of 4700 N m^{-2} and unloaded prior to determination of *ASC*.

The *Springback Index (SBI)* is the percentage of elastic springback after consolidation, and indicates when springy solids (as straw, wood, polymer foam) may arch. *SBI* is measured by compressing the solid to a pressure of $D \times BDI$, and then noting the percentage change in the sample height when the load is released.

Knowledge of material characteristics expressed as values of indices allows for design of technological process as anticipated. Johanson (2000) presented an example of use of the indices in design of the process of blending without segregation of components.

6.4. Jenike & Johanson powder quality tester

Tester of Jenike & Johanson (Ploof and Carson, 1994) consists of two units: the body containing the sample holder, and the control unit (Fig. 38). Sample of the volume of one US gallon (3.785 dm^3), has a cylindrical upper part while its lower part is conical. The upper lip of the holder may be closed with a tight cover housing a connector for supply of compressed air and fixing of the manometer. Outlet of the conical part of the sample holder can be closed with a sliding perforated plate with aperture diameter lower than the dimension of finest particles of tested material. The procedure requires a period of shaking to aerate the sample.

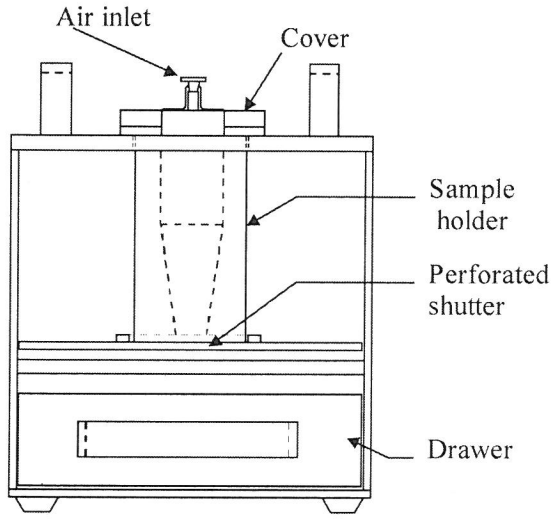

Fig. 38. Jenike & Johanson quality control tester (Ploof and Carson 1994)

The sample holder proper for particular tested material is placed in the body of the apparatus and thoroughly filled. The holder is closed with the cover and prescribed air pressure is applied that is adjusted with the valve and kept constant

for 30 seconds. Then the pressure is decreased to zero and the perforated plate removed to open the outlet. The pressure gauge is turned on, and pressure in the sample holder increased till the moment of collapse of an arch when material flow commences. The measurement cycle from consolidation to outflow is repeated four times (at least) for one level of consolidation pressure. Results obtained with the tester were compared with results of the Jenike method for limestone powder and baking soda. Part of the tests showed fairly good agreement of results of the two methods, while another part was in disagreement. The authors concluded that the tester may be successfully applied for comparison of different lots of the same material (Ploof and Carson 1994).

6.5. Uniaxial tester of POSTEC

Led by premises similar to those reported by other designers of powder testers, researchers of the Norwegian institution POSTEC proposed their own solution. The tester is a type of indirect shear apparatus, namely uniaxial, and its description here is quoted after Maltby and Enstad (1993). In uniaxial compression test a compressive failure strength similar to the unconfined yield strength σ_c may be determined directly as a function of the consolidation stress σ_1. The measurement is taken in a fraction of time required by other testers. Due to the consolidation procedure used, the tester does not measure the flow function, and therefore should not be used for silo design unless a correction factor is introduced. The procedure used assures the scatter of the results is minimal, which together with the rapidity with which such measurements can be made, makes the test perfectly suitable for quality control purposes. In the POSTEC tester (Fig. 39) the sample is confined in a slightly conical die and consolidated by the piston moving vertically down. The flexible membrane is stretched between the outer surface of the piston and inner surface of the lower part of the die. A layer of lubricant is spread between the flexible membrane and the die wall. The die is filled upside down and closed with a tight cover, turned upside down again and placed into the guiding device of the tester. The sample is consolidated by moving the piston until the predetermined value of σ_1 is reached, corresponding to a strain ε_1. After a predetermined time of sample stabilization the die is raised up and compressive failure strength is measured with the piston moving down. The maximum value σ_c is reached before the sample falls apart.

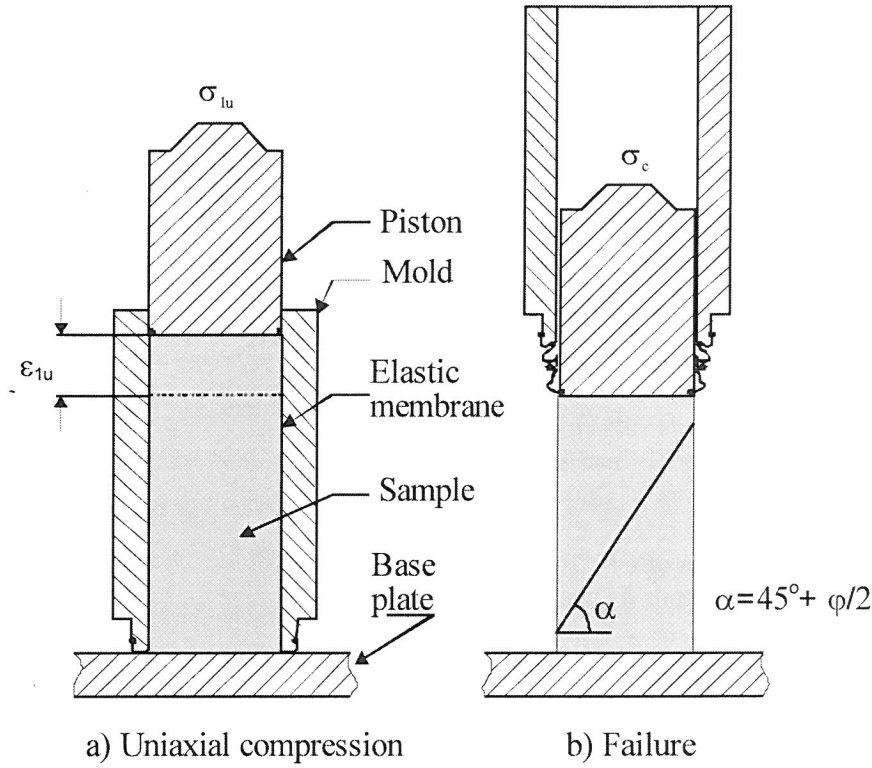

Fig. 39. POSTEC uniaxial tester (Maltby and Enstad 1993)

The apparatus allows for direct observation of the forming of failure surface that theoretically forms an angle of $\alpha = 45° + \varphi/2$ with the horizontal plane. More complicated shape of failure surface points indicates that the sample was not tall enough. Using precise procedure for examination of BCR-limestone, Maltby and Enstad obtained the maximum deviation of the strength σ_c not higher than ± 0,13 kPa, not dependent on the level of consolidation pressure. These authors have reported good repeatability of results with deviation not higher than 5%. According to the authors, the reproducibility of the tester, together with operator independence and fairly rapid test procedure make the equipment a suitable tool for quality control of powders. Accuracy of the method allows for flow property deviations from batch to batch in batch production operations. The equipment may be also used for investigations of the compaction properties of slightly compacted samples, determination of the modulus of elasticity, or examinations of stress relaxation and creep phenomena of powders.

6.6. Carr indices

Chemical industry and, particularly, pharmaceutical industry need characterization of fine powders. Flowability determines operations of transport, mixing, dosing, storage granulation or forming tablets. Carr Indices are willingly used by practitioners of those industries, and were standardized by the American Society for Testing Materials. The method can be applied to free flowing and moderately cohesive powders and granular materials up to 2mm in size. Materials must be able to pour through a 7.0 ± 1.0 mm diameter funnel outlet when in aerated state. The method consists of eight measurements and two calculations to provide ten tests for Carr Indices. These ten tests are as follows:

A. Measurement of Carr Angle of Repose
B. Measurement of Carr Angle of Fall
C. Calculation of Carr Angle of Difference
D. Measurement of Carr Loose Bulk Density
E. Measurement of Carr Packed Bulk Density
F. Calculation of Carr Compressibility
G. Measurement of Carr Cohesion
H. Measurement of Carr Uniformity
I. Measurement of Carr Angle of Spatula
J. Measurement of Carr Dispersibility.

In practice the Carr Index *CI* is also popular, that is defined (ASTM-D 6128 2000) as:

$$CI(\%) = \frac{100 \times (\rho_t - \rho_l)}{\rho_t}, \tag{54}$$

where:
ρ_t – tapped bulk density,
ρ_b – loose bulk density.

This parameter is determined, after compaction of material by tapping, in a cylindrical container of a volume from 10 to 1000 ml, with user-defined number of taps (from 10 to 500). Out of the same measurement another popular parameter, the Hausner Ratio, may be calculated as:

$$R_h = \frac{\rho_t}{\rho_l}. \tag{55}$$

In industrial practice it is assumed that the powder is easy flowing having *CI* in range from 5 to 15%, while durable tablets may produced of powder having R_h not higher than 1.6.

6.7. In-line control of structure of granular products

For contemporary highly automated mass production in-line methods of characterization of materials are in the highest demand. In the first approach in-line methods of measurement of particle size distribution were elaborated. Knowledge of particle size distribution allows for efficient process control and control of product quality. Process output continuously increases and delay between laboratory measurement and process correction may be unacceptable. Currently pneumatic conveying is extensively used in industry because it enables efficient flow control using optical methods. Harvill *et al.* (1995) described one of such devices, based on laser diffraction of light and used in a large range of laboratory and industrial applications. Measuring unit consists of an optical head, interface, pc and software. Stream of particles flows through the cylindrical channel across the laser light beam. Velocity of the stream does not influence the result of the measurement. Scattered light passes through the receiver lens and is focused on the log-scaled annular ring detector. The detector is scanned by the interface with high speed and levels of signal on the separate rings are recorded. Each ring of the detector measures the total signal intensity. Each particle scatters light on all rings of the detector, therefore the measured signal is the summation of all the light scattered from all particles. After acquiring a significant number of scans, relative particle concentration is calculated by the software. The instrument allows for efficient determination of both particle size distribution and particle concentration directly and in real time. It has been successfully used in production of pharmaceuticals for optimization of the mill. The instrument provides continuous feedback control to compensate for mill-setting drift, wear, operator errors, variations in raw material etc.

Like in pharmaceutical industry, in-line process control may increase efficiency of food industry. The basic factor in food product quality is its structure. Bijnen *et al.* (2002) analysed current trends in development of process sensors in food industry. Market requirements enforce precise process control. The development of these new process regimes requires better understanding of the structure-process-equipment relationships. Precise in-line measurements become necessary. Basic attributes of product microstructure are: overall product composition, properties and state of all phases, distribution properties of dispersed phases and spatial organization of dispersed entities. The authors reviewed methods that might be applied for in-line measurements and pointed out their limitations.

- Sensors for the determination of product composition (the content of: water, fat/oil, carbohydrates, and proteins) currently achieve a relative accuracy of 0.1 to 1%. These are often sufficient, but the calibration procedures (if any) in a rapid changing product portfolio should be minimal.

- Sensors for monitoring the state of phase will be mainly applied for understanding the basic phenomena underlying the process, for development of new processes and process control. The use of laser-based acoustic pulse sensors and detectors seems promising for monitoring the properties of phase state because of the flexibility due to remote sensing. In-line quality assessment will remain often difficult because in many food products the final state of phase (rate of crystallization or gelation) is formed after the filling operation and during storage.
- Current solutions of in-line particle size detection allow mainly for quantification in relation to droplet size empirically calibrated. For a rapid changing product portfolio and variable ingredients, these abilities may prove insufficient.
- Some options for absolute in-line particle size quantifications are present, but current solution are able only to determine qualitative relation to droplet size calibrated empirically. For a rapid changing product portfolio and variable ingredients, these abilities may prove insufficient. In-line imaging and image analysis may deliver quantitative information necessary for process control in flexible factory conditions. Close monitoring of this information may allow for process control and quality assessment at the same time.
- The area of characterization of particles arrangement inside a product matrix remains still in too early a stage of exploration for having significant implications on the process measurement instrumentation.

6.8. Tendencies in development of applications

Last two decades of 20th century observed an increase in interest in particulate materials. Industry has been using more and more raw products, and produced increasing amounts of products in granular form. Global competition enforced increase in the scale of production that required automatic process control. Market demands stable quality of products delivered under the same trade mark. Material in granular form is much easier for storage, processing, mixing dosing, packing and distribution. Requirements of practice stimulated development of knowledge about granular materials, particularly in three areas:

- theoretical investigations seeking constitutive model of material,
- methods of determination of material characteristics for use in design of processes and equipment, and
- elaboration of methods of quality assessment and indices to measure quality.

Beginning in the 80-ties of the previous century, an unprecedented increase in calculation power of computers commonly accessible took place that enabled

new possibilities of theoretical investigations. New theoretical approaches appeared, two of them gained matured form: numerical modeling including interactions in contact areas between individual particles, and the application of earlier known theories that required extensive calculations.

Regarding modeling behavior of the bedding of material based on interactions in contact points between particles, the DEM method that originates from work of Cundall and Strack (1979) remains promising. Good examples of a new approach to known methods are the applications of the theory of non-symmetric elasticity of Cosserats by Mühlhaus and Vardoulakis (1987) or by Chang and Ma (1990).

In the field of experimental investigations, new measurement methods have been elaborated and known methods have been improved to interpret unclear phenomena or to facilitate strenuous and time consuming measurement procedures. Regarding determination of strength parameters of granular materials, Jenike (1961) has been widely accepted and standardized in many national design codes as well as in international Eurocode 1 (2003). From among numerous earlier elaborated instruments, the ring shear tester will probably gain the position of recognized measurement technique. It is particularly useful in investigations of food products and granular plant materials. Because of high deformability of particles these materials require long shearing path to reach steady flow, and deformation in the ring shear apparatus is unlimited. The second significant advantage of the ring shear apparatus is the possibility of examinations under low level of normal load. Vertical loading force related to the relatively large surface of lateral section of the channel of the apparatus gives low values of normal pressure. Description of mechanical behaviour of granular materials under low normal load (in thin layer) is currently in particular interest of industrial practice. The two advantages of the ring shear tester open new fields of its application as well as promise the possibility of interpretation of some phenomena that still remain unclear.

Two other old methods for the measurement of angle of repose and of angle of friction with inclined table will probably remain as standards for the determination of mechanical properties of granular material thanks to their simplicity.

Search for methods of examination of product quality and for quality indices has been a symptomatic trend of technology of granular materials in the last several years. Quality assessment in the sense of granular mechanics means the determination of material flowability. Within the approach of Jenike (1961) that is recently widely accepted the measure of flowability is the flow function $ff = \sigma_c(\sigma_1)$, i.e. the relationship between unconfined compression strength and major consolidation pressure. The direct shear tester or the Jenike method has, however, some disadvantages pointed out by practitioners. Testing is tedious and time consuming, while elaboration and interpretation of results require significant knowledge. In-

dustrial practitioners demand a quick and simple method with an unmistakable and intelligible quality index. Academic laboratories and consulting firms put their propositions on the market one after the other, but none of them gained wide acceptation till now. Probably, for process engineering the set of Johanson's indices has been accepted, while in the pharmaceutical industry Carr indices are commonly used.

7. DISCRETE ELEMENT METHOD

The Discrete Element Method (DEM), based on the microstructural approach, provides an opportunity for more detailed investigation of granular systems.

Cundall and Strack proposed the method in 1979 to simulate interactions occurring between rigid rock blocks and, next, to study ground mechanics. The method was used to model processes in 2D and 3D systems composed of circular and spherical shaped elements. The method initiated the development of computational techniques based on the micromechanical approach. The technique allows for establishment of positions and velocities of particles through time integration of equations of Newton's second law for each particle. The application of force-displacement laws allows for calculation of contact forces and moments of force acting between particles. The method uses the Coulomb friction law to describe the friction occurring in the contact areas.

The deformations of particles are very small in comparison to the deformation of a particulate assembly. Particles are assumed to be elastic objects whose normal, tangential and rotational displacements are taken into account. Interactions between particles are modelled using model contacts. Static balance is achieved by a system through dispersion of energy which is a consequence of friction and damping.

The discrete element method uses the force-displacement laws and theories of the contact mechanics and the impact mechanics. The issues of the contact mechanics and the impact mechanics which are the most crucial for DEM are presented in chapters 7.1 and 7.2.

7.1. Contact mechanics

The contact mechanics aims to study the stresses and deformations which arise when contact between the surfaces of two solid bodies occurs.

The subject of the contact mechanics was initiated in the 19th century when the classic paper of Heinrich Hertz *On the contact of elastic bodies* (Hertz, 1882) was published. The Hertz theory refers to frictionless surfaces and perfectly elastic bodies, which significantly limits its application. Progress in the contact mechanics in the second half of the 20th century resulted in discarding these restric-

tions and extension of the elastic theory to both sliding and rolling contact through proper treatment of friction at the interface of bodies in contact. The simultaneous development of the theories of plasticity and linear viscoelasticity provided possibility for non-elastic bodies to be examined.

Two following kinds of contacts are considered:

- Conforming contact - the one in which the two bodies touch at multiple points without deformation;
- Non-conforming contact - the one in which the profiles of the bodies are dissimilar and the bodies brought into contact without deformation only touch at a point (or possibly along a line). The contact area is small compared to the sizes of the objects and the stresses are highly concentrated in this area.

7.1.1. Motion and forces at contact point

The surfaces of bodies remaining in contact may undergo the following types of relative motions:

- sliding, in which a relative velocity between two surfaces at contact point is linear,
- rolling, in which a relative angular velocity acts between the two bodies about an axis lying in the common tangent plane that passes through the coincident contact points,
- spin, which is a relative angular velocity about the common normal that passes through the contact point.

Any motion of contacting surfaces can be regarded as a combination of the motions defined above.

The resultant force exerted by one surface on the another one at a contact point is a sum of normal force F acting along the common normal and tangential force T in tangent plane sustained by friction. The relationship between F and T can be expressed using the Coulomb friction law which says that sliding in contact point occurs when the tangential force is higher than the friction force:

$$\begin{aligned} T &< \mu F && \text{no sliding} \\ T &\geq \mu F && \text{sliding} \end{aligned} \qquad (56)$$

where μ is the coefficient of friction.

7.1.2. Normal contact of elastic solids; Hertz theory

The first analysis of the stresses at the contact point between two solid bodies was conducted by Hertz (1882). He adopted the hypothesis that the contact area is elliptical and introduced the simplification that each body can be regarded as an elastic half-space loaded over a small elliptical region of its plane surface. Due to this simplification the highly concentrated contact stresses are treated separately from the general distribution of stress in the bodies which arises from their shape and the way in which they are supported. The smooth surfaces are assumed to ensure transmission of normal pressure between them only.

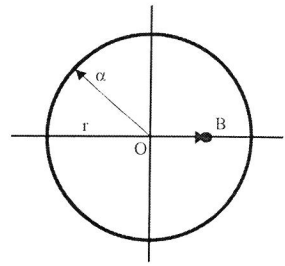

Fig. 40. Pressure applied to a circular region; displacement at a point B (Johnson 2004)

Assuming contact area to be circular with a radius a (Fig. 40), the distribution of pressure exerted between two frictionless elastic solid bodies in contact area, proposed by Hertz theory, can be written as (Johnson 2004):

$$p = p_0(a^2 - r^2)^{\frac{1}{2}}/a, \tag{57}$$

where p_0 is the maximum normal pressure, a is the radius of contact area and r is the distance between the center of contact area and the point where the pressure is exerted.

That distribution of pressure gives rise to normal displacement expressed as follows:

$$x = \frac{1-\nu^2}{E}\frac{\pi p_0}{4a}(2a^2 - r^2), \tag{58}$$

where ν is the Poisson ratio and E is the Young modulus.

The radius of contact circle a and mutual approach of distant points in the two solids δ is given by equations (59) and (60):

$$a = \left(\frac{3PR}{4E^*}\right)^{\frac{1}{3}}, \tag{59}$$

$$\delta = \frac{a^2}{R} = \left(\frac{9P^2}{16RE^{*2}}\right)^{\frac{1}{3}}, \tag{60}$$

where P ishe a total load compressing the solid.

A relative radius of curvature R is related to the significant radii of bodies in contact (R_1, R_2) by

$$\frac{1}{R} = \frac{1}{R_1} + \frac{1}{R_2}, \tag{61}$$

and

$$\frac{1}{E^*} = \frac{1-\nu_1^2}{E_1} + \frac{1-\nu_2^2}{E_2}, \tag{62}$$

where E_1, E_2 and re ν_1, ν_2 are the Young's moduli and Poisson's ratios of the bodies.

The maximum pressure p_0 can be expressed as follows:

$$p_0 = \frac{3P}{2\pi a^2} = \left(\frac{6PE^{*2}}{\pi^3 R^2}\right)^{\frac{1}{3}}. \tag{63}$$

Aanalogous considerations for an elliptical contact area are presented by Johnson (2004).

The elastic deformation of solid bodies in contact area can be calculated on the basis of the Hertz theory after an elasticity, isotropy and heterogeneity of the material of solids are assumed. If the material of the solids is anisotropic or inhomogeneous, or their thickness is small in comparison to the size of contact area, their deformation under contact pressure will differ from the one assumed in the classical theory.

Willis (1966) showed that the contact area between two non-confirming anisotropic bodies of general shape is still elliptical in shape and that the pressure distribution is the same as the one obtained for isotropic solids. Willis found that the directions of axes of the ellipse of contact are determined by the geometry of the surface profiles, however, they also depend on the elastic constants.

Inhomogeneous materials are of interest in soil mechanics. Calladine and Greenwood (1978) showed that the stress fields produced by a concentrated line load or a concentrated point load are the same as those found in a homogeneous half-space, however the displacements in these materials are different.

7.1.3. Normal contact models

The contacting solids may be composed of both, elastic and inelastic (e.g. elastic-plastic and viscoplastic) materials which generate large contact forces during the impact resulting in local deformations near the contact point or global deformations of the entire body.

7.1.3.1. Elastic contact model

When the contact between two particles is assumed to be elastic, it is governed by the Hertz formula and the normal contact force is expressed by

$$F = Kx^{\eta}. \tag{64}$$

The K in above equation is the spring constant related to the elastic modulus E_1 and E_2, Poisson ratio v_1 and v_2, and radius R_1 and R_2 through the following expression:

$$K = \frac{4}{3}E^{*}R^{1/2}, \tag{65}$$

where the relative radius of curvature R and the relative elastic modulus are expressed by equations 61 and 62.

The x is a particle displacement and η is the index dependent on the contact interaction laws between the particles.

Linear and non-linear contact models of different relationships between contact force F and displacement x are distinguished. In the simple linear contact model the contact force is a linear relationship of displacement ($\eta = 1$). Thus, the equations (64) take the following form:

$$F = Kx, \tag{66}$$

The linear contact model has found a wide application in the modelling of material discharge (Ji and Shen 2004, Campbell 2002). Physical studies and analytical analysis showed more complex relationship between contact force and displacement of particle. In the non-linear elastic contact model, Hertz assumed the elastic index η to be of 3/2.

7.1.3.2. Elasto-plastic contact model

If the contact pressure during loading of contacting particles is less than the limiting contact pressure p_y, the contact is treated as elastic and is governed by the Hertz formula. Otherwise the elastic-perfectly plastic contact takes place and the yield occurs at displacement

$$x_y = \left(\frac{\pi p_y}{2E^{*}}\right)^2 R^{*}. \tag{67}$$

Figure 41 shows the force-displacement relationship for a loading-unloading loop for the contact area of elastic-perfectly plastic solids. After the yield occurs, the resulting contact force is the sum of the equivalent elastic force for the fraction of the contact area for which pressure is below the limiting contact pressure and the plastic component for the fraction of the contact area at which yield occurred. It is assumed that the force-displacement behavior is elastic during unloading and it follows the Hertz formula until the contact force reaches zero. The repulsive force during unloading results from the normal force acting on the elastic fraction of the contact area. After the contact force reaches zero, the permanent deformation occurs. The residual deformation $x_{residual}$ due to plastic deformation caused by the maximum normal force F_{max} corresponds to the maximum overlap x_{max} as follows:

$$x_{residual} = x_{max} - \left(\frac{3F_{max}}{4E^{*1/2}}\right)^{2/3}. \tag{68}$$

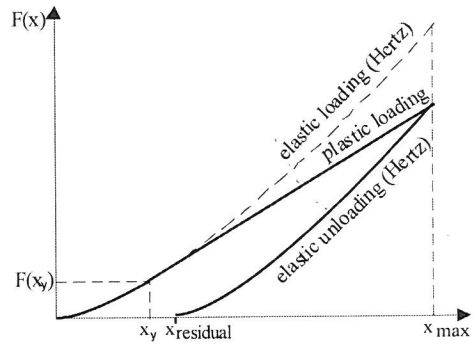

Fig. 41. Force-displacement relationship for elastic-perfectly plastic contact between spheres (Thorton and Ning 1998)

The following four stages may be distinguished during the contact between elastic-perfectly plastic solids:

- elastic loading

$$F = Kx^{3/2} \qquad x < x_y, \tag{69}$$

- perfectly plastic loading

$$F = Kx^{3/2} + \pi p_y R^*(x - x_y) \qquad x \geq x_y, \tag{70}$$

- elastic unloading

$$F = K(x - x_{residual})^{3/2}, \qquad x \geq x_{residual}, \tag{71}$$

- residual deformation

$$F = 0 \qquad x < x_{residual}. \qquad (72)$$

Figure 42 shows the evolution of contact force during impact of elastic-plastic solids, steel (a) and lead (b) spheres, with a steel bar at speed of 2.3 m s^{-1}. At this impact velocity both spheres suffer plastic deformation. The lead sphere has a smaller yield stress resulting in decrease in maximum force and prolongation of contact period in comparison with the steel sphere.

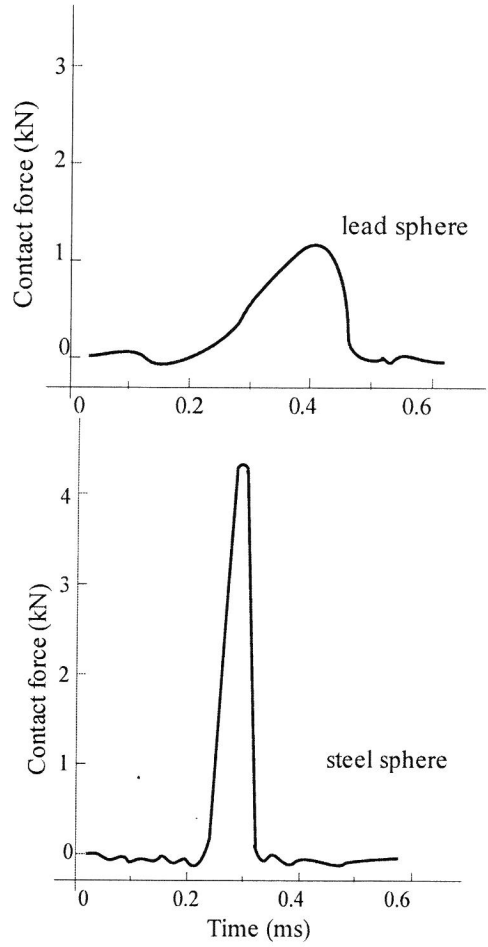

Fig. 42. Evolution of contact force during impact of steel (a) and lead (b) sphere with the steel bar at speed of 2.3 m s^{-1} (Johnson 2004)

When the plastic strains in solid are large compared to elastic strains and the elastic deformation may be neglected, the material may be considered as arigid-perfectly-plastic solid which flows plastically at a constant stress, in tension or in compression. In a body of a rigid-perfectly-plastic material under load the regions in which plastic flow occurs and the ones where no deformation occurs are distinguished. In the simplified perfectly plastic behaviour mode, the resulting normal contact force is the sum of the elastic and plastic forces acting on the elastic and plastic fractions of the contact area, respectively.

7.1.3.3. Viscoelastic contact model

The materials which exhibit time-dependent behavior in the relationship between force and displacement are termed a viscoelastic materials.

The viscoelastic contact between solids may be presented by the set composed by an elastic spring and a viscous damper. When the elements are serially connected, the Maxwell model is considered (Fig. 43) (Stronge 2000).

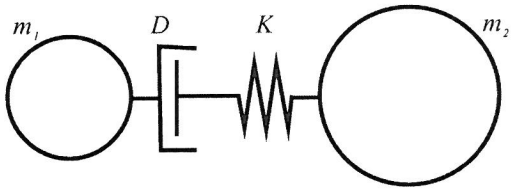

Fig. 43. Collinear collision bodies separated by a Maxwell viscoelastic element

The normal force between two contacting bodies may be expressed by the force acting in the spring or equivalent force which acts in the dashpot

$$F = Kx, \tag{73}$$

where K is a spring constant, x is the displacement of bodies due to the compression of the spring.

The equation of relative motion of solids is given by

$$m^*\ddot{x} + Kx = 0, \tag{74}$$

where the effective mass $m^* = (m_1^{-1} + m_2^{-1})^{-1}$.

For the linear viscoelastic Maxwell model the coefficient of restitution, expressing the energy dissipation occurring during impact of two bodies (described

in chapter 7.2.2), is independent on the normal impact speed. Experimental measurements showed a decrease in the coefficient of restitution with an increase in relative velocity, thus the non-linear viscoelastic model was proposed to achieve this velocity dependence. In that model, based on the Kelvin model (Sitkei 1986), the linear spring is connected in parallel to the non-linear damper (Fig. 44). The dashpot provides a force dependent on the relative velocity and the displacement. The normal force which depends on the normal relative displacement x and the relative velocity $\dot{x}$ is given by

$$F = Dx^{\varepsilon}\dot{x} + Kx^{\eta}, \tag{75}$$

where ε and η are indexes dependent on the contact interaction laws between the particles. The equation of relative motion for two contacting viscoelastic solids takes the following form

$$m^{*}\ddot{x} + Dx^{\varepsilon}\dot{x} + Kx^{\eta} = 0. \tag{76}$$

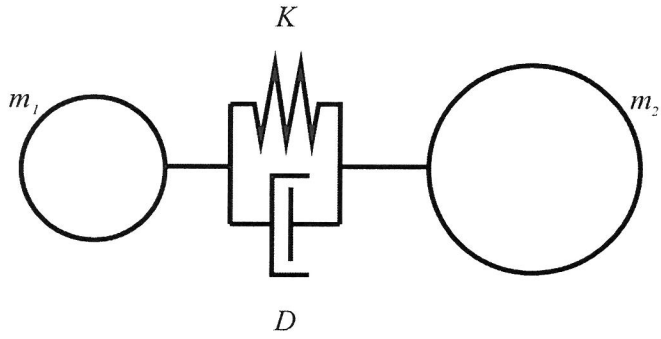

Fig. 44. Collinear collision bodies separated by a Kelvin viscoelastic element

Based on experimental and numerical data, the viscoelastic contact model has been proved through the application of damping index values of 1/2 (Kuwabara and Kono 1987), 1/4 (Falcon 1998) and 4/5 and 8/5 (Mishra and Murty 2001) for different material properties.

For nonlinear viscoelastic contact, Tsuji (1993) suggested ε=1/4. The equation of relative motion may be, thus, expressed as

$$m^{*}\ddot{x} + Dx^{1/4}\dot{x} + Kx^{3/2} = 0. \tag{77}$$

Damping coefficient

$$D = 2\sqrt{\frac{5}{4}}\beta\sqrt{Km^*}$$

is a function of an effective mass and damping ratio related to the coefficient of restitution e by

$$\beta = -\frac{\ln e}{\sqrt{(\ln e)^2+\pi^2}}$$

and the Hertz spring constant is expressed by equation 65.

Figure 45 shows the force-displacement relationship for a loading–unloading loop for the contact area of viscoelastic solids.

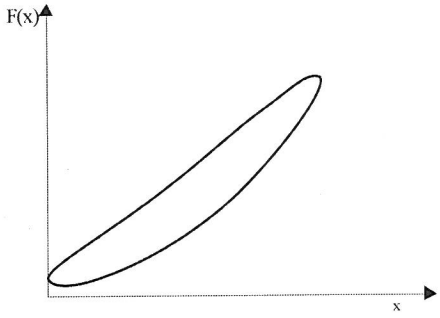

Fig. 45. Force-displacement relationship for viscoelastic contact between spheres

The relationship between the strain in a specimen of viscoelastic material under the action of constant stress σ_0 applied for a period t_1 is shown in figure 46. The strain shows an initial elastic response (OA) to the applied stress. A further delayed elastic strain (AB) is acquired in time. If the material is capable of flow or creep it will also acquire a steadily increasing creep strain (BC). When the stress is removed there is an immediate elastic response (CD = –OA) and a delayed elastic response DE. The specimen is left with a permanent strain at E which it acquired through the action of creep.

When impact between viscoelastic bodies takes place, during loading, the elastic and viscous components of the contact force act in the same direction. During unloading, the velocity vector is oriented in the opposite direction to that of the overlap, so the two components of the contact force act in opposite directions. The force during unloading is lower than that during loading and changes sign in the final stage of rebounding when the viscous component is greater than the elastic

one. As a consequence, unloading lasts longer than loading during collision. This is contrary to the elastoplastic contact model, in which, as a result of elastoplastic hysteresis, the duration of loading is longer than that of unloading.

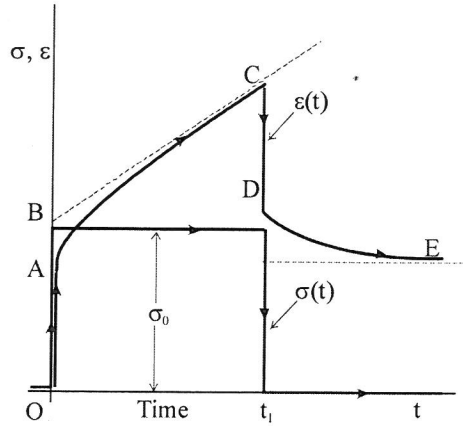

Fig. 46. Relationship between the strain in a specimen of viscoelastic material under the action of constant stress σ_0 (Johnson 2004)

7.1.4. Tangential loading and sliding contact

The relative linear velocity between two surfaces in contact is termed sliding. When the frictionless contact between a sphere sliding over a plane surface takes place the Hertz theory may be applied to calculate the size of the circular contact area (eq. 59) and the pressure distribution (eq. 57). In a frictionless contact, sliding motion does not affect the contact stresses.

However, frictionless contact is an idealisation which does not take place in reality. When real rough surfaces are in contact, the sliding occurs resulting in tangential force of friction, acting on each surface in the direction opposed to the direction of motion. When two solids of the same elastic constants are in contact, the tangential pressure transmitted between them results in equal and opposite normal displacements of any point on the interface. The shape and size of the contact area are determined by the profiles of the contacting surfaces and the normal force and they are not affected by the tangential force.

The tangential pressure influences the normal pressure and the contact area when contact between solids of different elastic properties takes place, however, that influence is small, particularly when the coefficient of friction is less than unity.

The relationship between normal force F and tangential force T in sliding contact may be expressed as follows:

$$\mu = \frac{|T|}{F}, \tag{78}$$

where μ is a coefficient of kinetic friction. The value of the coefficient of friction is a property of material determined by the physical conditions of the interface.

The tangential pressure transmitted between a sphere sliding over a plane surface, derived on the basis of Amontons' law of friction, is expressed by

$$q = \frac{3\mu F}{2\pi a^3}(a^2 - r^2)^{\frac{1}{2}}. \tag{79}$$

7.1.5. Variation of normal and tangential forces

The final state of stress in contact area between two contacting solids depends on both, the history of loading and the final values of normal and tangential forces.

The influence of various combinations of incremental change in normal and tangential forces on surface pressures and deformations arising between two solids was studied by Mindlin and Deresiewicz (1953).

Let us now consider two spheres, pressed initially by a normal force F_0 and afterwards compressed by an increasing obliqu force F_{ob} inclined at an angle α to the common normal (Fig. 47). This loading is equivalent to increasing the tangential load T and the normal load F by increments in the constant proportion tan α. The normal and tangential forces are related to the normal and tangential pressures (p, q) acting over the area of contact S by the expressions:

$$F = \int_S p\, dS, \tag{80}$$

$$T = \int_S q\, dS. \tag{81}$$

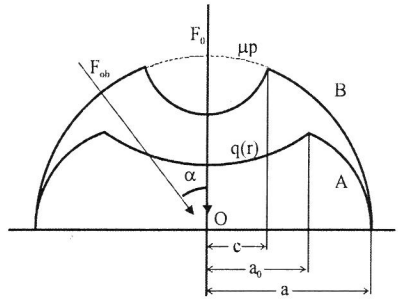

Fig. 47. Circular contact subjected to a steady normal load F_0 and an oblique force F_{ob}. A – no micro-slip; B – slip in annulus $c \leq r \leq a$ (Johnson 2004)

The contact radius may be expressed by equation (59) based on the Hertz theory

$$a = (KF)^{\frac{1}{3}}, \tag{82}$$

which for initial normal force F_0 may be written as follows

$$a_0 = (KF_0)^{\frac{1}{3}}. \tag{83}$$

The application of the oblique force results in an increase in tangential and normal forces in contact area. The tangential pressure may be expressed by:

$$q(r) = \frac{12E^* \tan\alpha}{6\pi R}\left\{(a^2 - r^2)^{\frac{1}{2}} - (a_0^2 - r^2)^{\frac{1}{2}}\right\} \quad , 0 \leq r \leq a_0 \tag{84}$$

and

$$q(r) = \frac{12E^* \tan\alpha}{6\pi R}(a^2 - r^2)^{\frac{1}{2}} \quad , a_0 \leq r \leq a \tag{85}$$

The normal pressure, given by the Hertz theory is expressed as follows:

$$p(r) = \frac{12E^*}{6\pi R}(a^2 - r^2)^{\frac{1}{2}} \tag{86}$$

The above equations were derived assuming the absence of slip. The condition is fulfilled for $\frac{q(r)}{p(r)} = \tan\alpha \leq \mu$.

When the constant normal force is applied, an applied tangential force results in a small relative motion (slip) over part of contact area. Over the remaining area, where no relative moton occurs, the surfaces stick. Slip takes place in the circumference of the contact area of radius $c \leq r \leq a$ (Fig. 47) and an annular area of slip develops radially inwards with tangential pressure increasing. The annular area increases until tangential pressure reaches its limiting value of $q(r) = \mu p(r)$, when the sticking area of contact is zero and rigid body sliding occurs. On the remainder of the contact area of the radius of c the tangential component of the displacement is constant. The relation between the inner radius of the annulus of slip and the applied tangential force may be expressed as follows

$$c = a(1 - \frac{T}{\mu N})^{1/3}. \tag{87}$$

The distribution of tangential traction during initial tangential loading for micro-slip is presented in Figure 47 by curve B. If the tangential force is reduced, then slip in the opposite direction spreads radially inwards from the perimeter of the contact area.

7.1.6. Rolling frition

The rolling is a relative angular velocity which acts between the two bodies about an axis lying in the common tangent plane that passes through the coincident contact points. The rolling may occur with the sliding or spin. The former one takes place when the tangential velocities of contacting bodies are unequal, while the latter one occurs when the angular velocities of the bodies are dissimilar. When rolling occurs without sliding or spin, a free rolling takes place.

Ideally rolling contact should occur without resistance to motion, but in reality energy is dissipated in various ways providing rolling friction. The sources of energy dissipation in rolling may arise through micro-slip and friction at contact interface or may be due to inelastic properties of the material or the roughness of the rolling surfaces (Johnson 2003). The micro-slip occurs at the interface when the rolling bodies have dissimilar elastic constants or curvatures. When the rolling resistance is due to the inelastic deformation of one or both bodies, the energy is dissipated within the solids, at a depth corresponding to the maximum shear component of the contact stresses, rather than at the interface. The roughness of the rolling surfaces influences the rolling friction in two ways. Firstly it intensifies the real contact pressure so that some local plastic deformation will occur even if the bulk stress level is within the elastic limit. In the second way, which refers to hard rough surfaces at light loads, the resistance is influenced by roughness through the energy expended in surmounting the irregularities.

The phenomenon of rolling friction, which has been of high interest to scientists for a long time, has been studied intensively by engineers and physicists, however, hitherto little is known about its basic mechanisms. There is still no first-principle expression for the rolling friction coefficient dependent only on the material constants of the rolling body. The availiable expressions still contain empirical parameters.

In the discrete element method proposed by Cundall and Strack, the contact model did not take into account the rolling motion of contacting particles and it assumed that contact occured in the contact points. The contact model between two particles was presented by the set of normal and shear springs, normal and shear dampers, normal and shear no-tension joints and a shear slider. However, real particles, showing rough surface texture, are in contact with neighbouring particles through contact surfaces, so that rolling resistance can play a higher role in the contact behaviour. When the rolling friction in the viscoelastic contact between solids is in-

cluded the contact model may be presented by an additional set of elements composed of an elastic spring, a viscous damper, a no-tension joint and a slider (Fig. 48), as proposed by Iwashita and Oda (2000). Both, the elastic spring and the dashpot work as resistance sources against relative rotation arising from rolling. That contact model provides the modified version of the discrete element method (MDEM) which is capable of dealing with the rolling resistance at contact points.

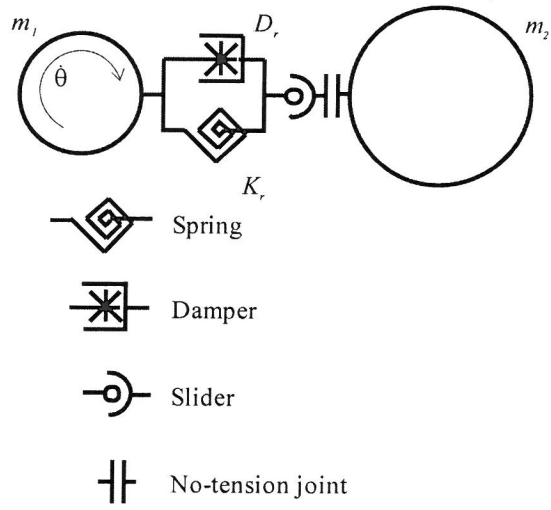

Fig. 48. Viscoelastic contact model with rolling friction (Iwashita and Oda 2000)

The sum of the resistances which stem from above mentioned sources must be in the equilibrium with the moment of force M

$$M = K_r\theta + D_r\dot{\theta}, \tag{88}$$

where θ is an angle of rotation and K_r and D_r are spring and damping constants. The slider starts working if the moment M satisfies the following condition:

$$|M| \geq \eta F, \tag{89}$$

where F is a normal force. The physical meaning of the coefficient η is similar to the interparticle friction coefficient μ. It has a dimension of length and it is a quotient of half of interparticle contact width B and a non-dimensional parameter α. The relationship between the moment of force and relative rotation of contacting spheres is presented in Figure 49.

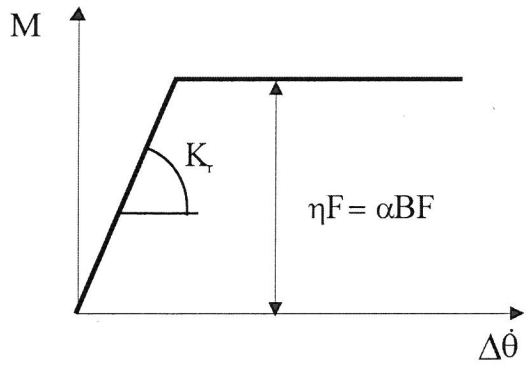

Fig. 49. Relationship between moment of force and relative rotation of contacting viscoelastic spheres (Iwashita and Oda 2000)

The equation of rolling motion of viscoelastic sphere without rolling friction may be expressed as follows

$$I\ddot{\theta} + K_r\theta R^2 + D_r\dot{\theta}R^2 = 0, \tag{90}$$

where I is a moment of inertia of particle, φ is an angle of rotation, R is a particle radius and $K_r$and D_r are spring and damping constants.

The inclusion of the rolling friction gives another rolling friction model. The equation of rolling motion with rolling friction, proposed by Zhou *et al.* (1999), takes the following form

$$I\ddot{\theta} + K_r\theta R^2 + D_r\dot{\theta}R^2 + \mu_r mg = 0, \tag{91}$$

where μ_r is a rolling friction coefficient, m is a mass of particle and g is a gravitational acceleration. The last term of the equation 91 is called the rolling friction torque M_r. Zhu and Yu (2006) proposed the rolling friction torque dependent on the angular acceleration of contacting particles $\dot{\theta}$, which is expressed as

$$M_r = -\min\{k_r|\dot{\theta}|, \mu_r mg\}\dot{\theta}, \tag{92}$$

where $-\min\{k_r|\dot{\theta}|, \mu_r mg\} = \frac{k_r|\dot{\theta}|+\mu_r mg-|k_r|\dot{\theta}|-\mu_r mg|}{2}$, k_r is the rotational stiffness dependent on the material constants of the rolling body (Zhu and Yu 2006).

The numerical investigation of the equilibrium, stability and free rolling problems of a sphere moving on a flat plane with reference to contact model with and without rolling friction, conducted by Zhu and Yu (2006), showed that, when the model

without rolling friction was applied the set of the equilibrium states of the system was not asymptotically stable, which disagreed with the fact that the sphere with small initial tangential velocity, angular velocity and tangential displacement should eventually stop. It was found that without rolling friction the sphere could roll on the plane without sliding only when both, the tangential force and torque acting on the sphere were zero, which was not reasonable for a viscoelastic sphere moving on a hard plane. On the other hand, the model with rolling friction could not describe the free rolling motion of the sphere with any material properties.

The rolling friction which generally stems from the asymmetry of the normal pressure distribution on the contact area of the contacting bodies is highly affected through adhesion and elecrtostatic interactions (Brilliantov and Pöschel 1998, Kondic 1999). Based on different considerations, other models of rolling friction torque have also been proposed, however, their insufficient effectiveness in modelling the real behaviour of particulate systems requires further investigations.

7.2. Impact mechanics

The impact of two bodies is a complex phenomenon occurring in the short period of time and generating high contact forces. The collision of bodies may be described through the *rigid body impact theory*, in which instantaneous change in velocity and the negligible displacement of bodies are assumed. The rigid body impact theory is an effective one for analyzing the response of hard bodies however for soft and deformable bodies more complex descriptions are required.

7.2.1. Compression and restitution phases of collision

The contact area remains small in comparison with particle dimension when rigid bodies impact. A rapid decrease in stresses generated in contact area takes place when the distance between the centres of bodies increases. The displacements of bodies are negligible due to the instantaneous period of contact, which depends on the normal compliance of the contact region and the effective mass of colliding objects.

When the elastic collision between two bodies occurs the attractive and repulsive forces are reversible, which is in contrary to non-elastic collision where the loss of kinetic energy occurs as a result of the cycle of compression (loading) and restitution (unloading) that take place in the contact region. During compression, kinetic energy is transformed into internal energy of deformation by the contact force and afterwards, during the phase of restitution, the elastic part of the internal energy is released. The bodies move apart from each other during restitution due to the forces generated by elastic strain energy stored during the compression phase. The compliance of deforming region during loading is higher than that during unloading, so a residual compression of the deformable particle remains after the collision.

The energy loss during two-body impact can be a result of, inter alia, irreversible elastic-plastic material behaviour, rate-dependent material behaviour or elastic waves trapped in the separating bodies.

7.2.2. Coefficient of restitution

Energy dissipation occurring during impact of two bodies of masses m_1 and m_2 results in an inelastic and irreversible relation between the normal component of contact force and the compression.

Energy loss can be expressed by means of energetic coefficient of restitution which is defined as the ratio of the elastic strain energy released during unloading (W_r) to the internal energy of deformation absorbed during compression (W_c):

$$e^2 = -\frac{W_r}{W_c}, \tag{93}$$

where:

$$W_c = -\frac{1}{2}mv_0^2, \tag{94}$$

$$W_r = \frac{mv_0^2}{2}\left(1 - \frac{p_f}{pc}\right)^2, \tag{95}$$

m is an effective mass $m = \frac{m_1 m_2}{m_1 + m_2}$, v_0 is an initial velocity, p_f is a final impulse at separation and p_c is an impulse applied during loading.

The coefficient of restitution has values in the range from 0 to 1, where 0 implies a perfectly plastic collision and 1 implies a perfectly elastic collision. When the values of final and initial velocities (v_f and v_0) of colliding bodies are known, the energy loss can be expressed as kinematic coefficient of restitution:

$$e = -\frac{v_f}{v_0}. \tag{96}$$

Above parameter was defined by Newton on the basis of measurements of energy loss in collision between identical balls.

The loss of energy during impact can be also expressed as the relationship between the normal impulse for restitution and that for compression (p_f and p_c) which is termed the kinetic coefficient of restitution:

$$e = \frac{p_f - p_c}{p_c}. \tag{97}$$

The coefficients of restitution defined above are equivalent unless the bodies are rough, the configuration is eccentric and the direction of slip varies during the collision.

The coefficient of restitution is not a material property. It depends on impact angle, impact speed and temperature of colliding bodies. Figure 50 (Stronge 2004) shows the relationship between the coefficient of restitution and relative speed of colliding nonlinear viscoelastic bodies.

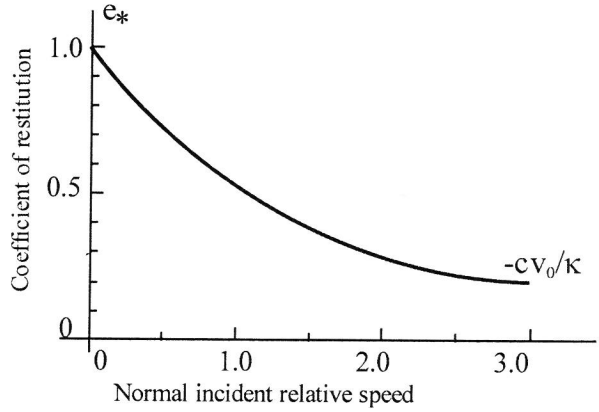

Fig. 50. Relationship between the coefficient of restitution and relative speed of colliding nonlinear viscoelastic bodies (Johnson 2004)

7.3. DEM calculation cycle

Let us consider a particle which is in contact with neighbouring particles in a particluate assembly. After the total contact force (F_{tot}) and moment (M) acting on the considered particle are calculated from the force-displacement laws, presented in the chapters 7.1.3 and 7.1.6, the Newton second law may be applied to express the equations of translational and rotational motions as follows:

$$m(\ddot{x})_N = (F_{tot})_N \,, \tag{98}$$

$$I(\ddot{\theta})_N = (M)_N \,, \tag{99}$$

where m is a mass of particle, I is a moment of inertia, $\ddot{x}$ and $\ddot{\theta}$ are accelerations of translational and rotational motions. The $(F_{tot})_N$ and $(M)_N$ are the sums of normal and tangential forces and moments of forces acting on an object at the beginning of elementary time step t_N. The resultant force and moment are assumed to act on a particle during the elementary time step Δt from $t_{N-1/2}$ to $t_{N+1/2}$. It is assumed that accelerations are constant during the interval Δt.

The time integration of the above equations provides the following equations which define particle velocities:

$$(\dot{x})_{N+\frac{1}{2}} = (\dot{x})_{N-\frac{1}{2}} + \frac{(F_{tot})_N \Delta t}{m}, \tag{100}$$

$$(\dot{\theta})_{N+\frac{1}{2}} = (\dot{\theta})_{N-\frac{1}{2}} + \frac{(M)_N \Delta t}{I}. \tag{101}$$

The time reintegration of these equations provides formulas which allow for establishing of the particle positions at the end of time step t_{N+1}:

$$(x)_{N+1} = (x)_{N+\frac{1}{2}} + (\dot{x})_{N+\frac{1}{2}} \Delta t, \tag{102}$$

$$(\theta)_{N+1} = (\theta)_{N+\frac{1}{2}} + (\dot{\theta})_{N+\frac{1}{2}} \Delta t. \tag{103}$$

The reiteration of calculation cycle, presented in Figure 51, allows for describing the motion of particle during modelling process. The iteration cycle is repeated for each particle in a particulate assembly during DEM simulation which requires high computational power.

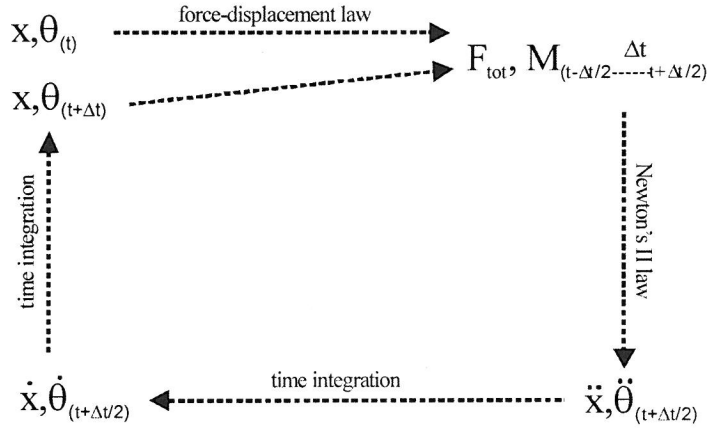

Fig. 51. Scheme of calculation cycle in DEM

7.4. Elementary time step

Elementary time step is one of the most important parameters of numerical methods. The selection of its value determines the stability of simulation and reduces the time of calculation. The numerical scheme is stable only if the elemen-

tary time step is less than the critical time step which is defined below.

The forces acting between particles in a granular system are transmitted through Rayleigh's waves propagating on surfaces of objects (Timoshenko and Goodier 1934, Johnson 2004). The time of contact force transmission between a particle and its neighbours is called the critical time step Δt_c. Its value can be found using the following formula:

$$\Delta t_c = 2\sqrt{\frac{m_{\min}}{K}}, \tag{104}$$

where K is a spring coefficient and m_{min} is the mass of the smallest particle in the system.

The formula proposed by Itasca (1998):

$$\Delta t_c^{Itasca} = \sqrt{\frac{m}{K}}, \tag{105}$$

allows for calculation of the critical time step of system composed of an infinite number of objects of mass m connected with springs.

Conducting a series of numerical tests for 2D and 3D systems, O'Sullivan and Bray (2004) revealed a dependence of Δt_c on packing structure and coordination number in a grain sphere assembly. According to the authors, stability of 2D and 3D systems composed of uniform particles can be reached at

$\Delta t_c \le 0{,}3\sqrt{\frac{m}{K}}$ and $\Delta t_c \le 0{,}17\sqrt{\frac{m}{K}}$, respectively.

Hassampour *et al.* 2008 used the following formula for critical time step in DEM code version TRUBAL:

$$\Delta t_c = \frac{\pi R_{\min}}{\xi}\sqrt{\frac{\rho}{E}}, \tag{106}$$

where R_{min} is the radius of the smallest particle in system, ρ and E are density and modulus of stiffness, and ξ is a coefficient dependent on Poisson's ratio

$\xi = 0.1631v + 0.8766$.

The above formula can be used for monodispersive systems. In the case of polydispersive systems, the critical time step should be calculated for the smallest particle.

The choice of elementary time step, which is related to the critical time step by

$$\Delta t = \chi \Delta t_c, \tag{107}$$

where $\chi < 1$, depends on conditions set in numerical tests. O'Sullivan *et al.* (2002) set $\chi = 0.3$ for modelling a biaxial compression test in 2D system. Zhang and Whiten (2001) proposed a method for automatic establishment of time step, which took into account the conditions of test.

7.5. Contact detection

As a consequence of particle displacements in a model system, contacts between objects disappear or the new ones are created. All these contacts need to be calculated during simulation.

The choice of contact detection method is of high importance. There are many papers which address that issue (Tijskens *et al.* 2003, Liu and Lemos 2001). Improvement of contact detection methods is necessary to increase the quality of methods based on the discrete approach.

The discrete element method treats particles as rigid elements deformable in contact points. If the distance between particles' centers is lower than the sum of their radii, contact exists between considered particles. The analysis of contact detection includes also nonspherical particles (polygons (Liu and Lemos 2001), ellipses (Lin and Ng 1997) and non-uniformly shaped clusters (Vu-Qouc *et al.* 2000)).

Contact detection becomes more complex in the case of ellipsoidal-shaped objects (Lin and Ng 1997).

High interest in a method in which the system is divided into many cells containing particles in contact can be observed (Tijskens *et al.* 2003). The application of that method in DEM code allows for fast and precise detection of contacts in a granular assembly.

7.6. DEM limitations

The microstructural approach of DEM which makes the method a useful tool in investigation of granular matter is also a source of its limitations and disadvantages.

The method, which treats granular assembly as a system of particles of characteristic mechanical and geometrical properties, precludes modelling of processes in systems of unlimited size. The technique requires machines of high computational power which are still unavailiable. That results in limitation of the number of particles in a system to 200 000 (Gröger and Katterfeld 2007).

The mentioned limitation can be surpassed by using periodic boundaries (Thornton 2000, Landry *et al.* 2003, Gröger and Katterfeld 2007). A particle in the neighbourhood of the wall of a model construction goes through the wall until the centre of weight of the particle is outside of the construction. The particle is

then moved to the neighbourhood of the opposite wall. Application of periodic boundaries allows for modelling processes in a representative volume (Masson and Martinez 2000) which is a part of a much more numerous system.

Comparison of results obtained from simulations of a chosen process conducted by different research teams revealed significant differences between the results (Mark *et al.* 1999). These discrepancies resulted from various DEM codes, contact models, contact detection methods etc. used by the researchers.

Investigation of granular materials by means of numerical techniques requires experimental verification of the methods (Gröger and Katterfeld 2007, O'Sullivan *et al.* 2002, Langston *et al.* 1995, Chung and Ooi 2005). Comparison between numerical and experimental results is a way of improving DEM, but the number of such research is still not large enough.

Originally, the method proposed by Cundall and Strack was used to model circular particles in 2D systems. Development of DEM resulted in the application of the method to simulate effects in 3D systems composed of nonspherical particles. However, nonspherical shapes and the third dimension provide new limitations and extend significantly the computational time.

There are few methods which allow for a reduction of computational time, for example: parallelisation technique (Sawley and Cleary 1999, Morris *et al.* 2001) or density scaling (O'Sullivan *et al.* 2002, Chung 2006, Zhang 2003). Depending on the objective of research and the kind of modelled process, a few-fold increase in density of the material influences only slightly the results while highly decreasing the simulation time (Chung 2006).

Chung and Ooi (2005) modelled the uniaxial compression test at a large scale of shear moduli ($G = 0.01G_0$, $0{,}001G_0$ oraz $0.0001G_0$). The authors pointed out a lack of influence of the parameter on force transmission in a particulate system. Decrease in G value resulted in a few-fold decrease in computational time.

The discrete element method can be used to investigate both, mineral and biological granular materials (Raji and Favier 2004, Tijskens *et al.* 2003). Specific properties of the latter one force to apply the contact models which take into account the effects occurring in grain beddings.

The limitations and possibilities of DEM presented in this chapter show that further improvement of the method and a reduction of the discrepancies between processes occurring in real and model systems are possible.

8. DISCRETE ELEMENT MODELLING OF MECHANICAL BEHAVIOR OF GRAINS AND SEEDS

Experience in laboratory testing of granular materials as well as review of literature led us to undertake numerical examination of properties of grain bedding. The two-dimensional simulations of shear test and granular flow and three-dimensional simulations of impact phenomena and uniaxial compression tests were conducted at the Institute of Agrophysics in Lublin using the discrete element method.

The experimental verification of computational technique was made by comparison between results obtained from numerical and physical experiments which provide new scientific insight into the behaviour of grain in bulk. The results from the investigations at the Institute of Agrophysics may contribute to more rapid adoption of the DEM computational technique for agriculture and food industry applications.

Granular plant materials of high significance in agricultural processing and a wide range of applications in industry were examined. The mechanical parameters of seeds of pea, bean, wheat and rapeseeds were applied to numerical tests as input parameters. Grains of various shapes and mechanical properties were selected. Due to the high influence of moisture content on the mechanical parameters of grains the investigation was carried out for various moisture contents of seed.

8.1. 2D DEM simulations

8.1.1. Direct shear test

2D DEM simulations were performed to analyse the distributions of velocity and force in Jenike's shear box filled with 500 spheres (Fig. 52).

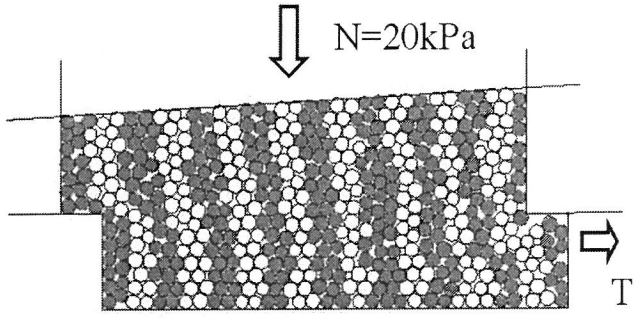

Fig. 52. Jenike's shear box with load consolidation of 20 kPa

The grains were generated and placed randomly in the shear box. Bedding was shared under externally applied load of 20 kPa. Shearing was generated by moving the lower part of the box horizontally with velocity of 0.4 mm s^{-1}.

The distribution of contact forces in bedding is shown in Figure 53, where the forces are represented by lines connecting the centres of interacting particles. It is visible that the force pattern is not uniform. The initially irregular contact force pattern (Fig. 53a) becomes more regular with shearing (Fig. 53b). Force chains run mostly from the left lower corner, where the shear forces act, to the right upper corner of the box, where the resisting forces act. Disintegration of forces and cutting contacts between particles in some regions of bedding can be also observed at certain moments of shearing.

Figure 54 shows that the distribution of velocity vectors changes during shearing. Few vectors lie along parallel lines running from the left lower corner to the right upper corner of the box. An increase in disturbance of velocities pattern in the upper box and regularity of vectors arrangement in the lower box are visible.

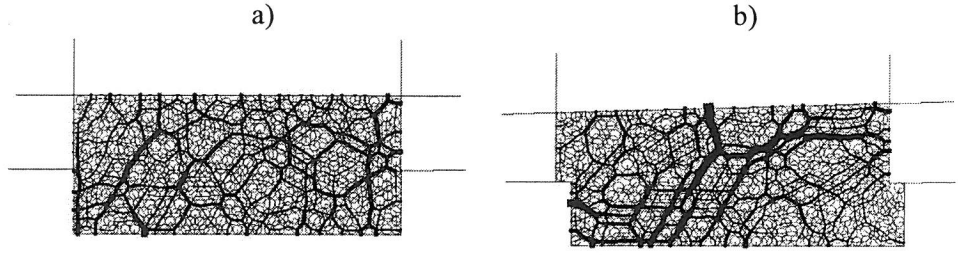

Fig. 53. Distribution of contact forces in bedding under externally applied load at shear displacement of 0.0 mm a) and 2.5 mm b)

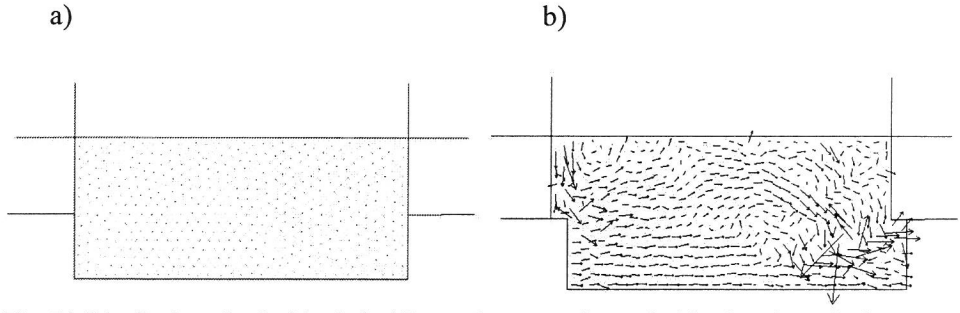

Fig. 54. Distribution of velocities in bedding under externally applied load at shear displacement of 0.0 mm a) and 2.5 mm b)

Changes of contact forces with progressing shearing are connected with changes of volume of particles. Figure 55 shows that increase in relative volume, i.e. the ratio of volume increment to the initial volume of particles, is followed by decrease in the sum of contact forces.

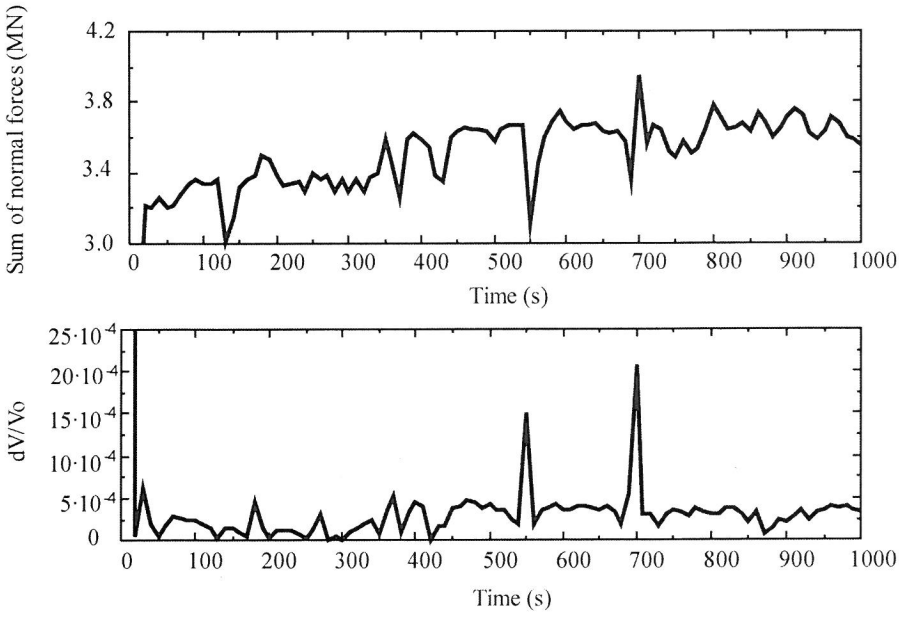

Fig. 55. Sum of contact forces (upper Figure) and relative volume (lower Figure) with time of shearing

Analogous simulations were performed for 6000 circular particles to examine the influence of rolling friction on the ratio of the tangential to normal forces acting on the shear box wall (*T/N*) in a particulate system under shear load. Two models were used: without rolling resistance ($\alpha = 0$) and with fully mobilised rolling resistance ($\alpha = 1$). Figure 56 shows the relationship between the ratio of tangential and normal forces acting on the wall and the shear strain. The simulations were conducted for interparticle and particle-to-wall friction coefficients of 0.3. Figure 56 shows that *T/N* value varied in the range from 0.3 to 0.4 when the rolling friction was neglected. When the rolling friction was involved, a significant increase in *T/N* value was observed. In the first part of shearing, when the shear strain was less than 0.04, the *T/N* value varied in the range from 0.5 to 0.6. Further shearing resulted in an increase in the *T/N* value but it was still higher than the *T/N* value obtained in the case when the rolling friction was excluded.

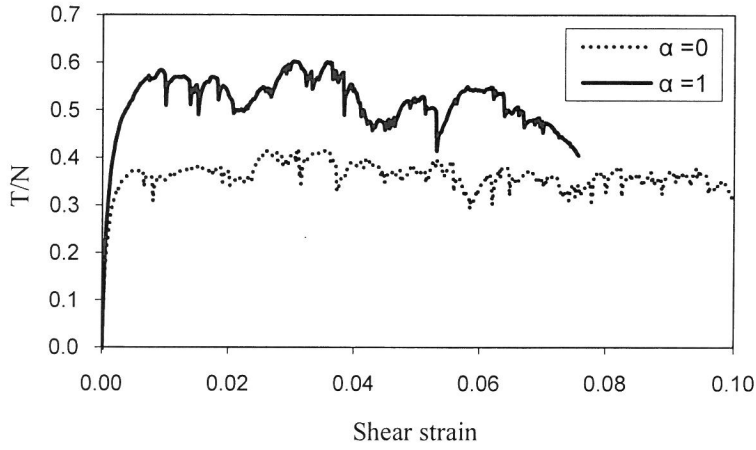

Fig. 56. Relationship between *T/N* value and shear strain for the particulate assembly composed of 6000 circular particles

8.1.2. Silo filling and discharge

The filling and discharge of a two-dimensional wedged-bottom silo holding circular objects was modelled to examine the distribution of contact forces acting between grains, as dependent on friction (interparticle μ_p and particle-to-wall μ_w) and packing structure of the particulate assembly (Sykut *et al.* 2008). Circular elements with diameters uniformly distributed between 1.8 and 2.2mm and density of 2500 kg·m^{-3} were modelled. The set of the material parameters applied in the simulations included the normal particle–particle and particle-wall spring constants ($k_{n,pp}$, $k_{n,pw}$), tangential spring constants ($k_{t,pp}$, $k_{t,pw}$), normal particle–particle and particle–wall damping coefficients ($\beta_{n,pp}$, $\beta_{n,pw}$) and simulation time step (Δt_{sim}). Spring constants k were adopted to represent relatively soft particles like cereal grains or rapeseeds. Damping constant β adopted in the simulations resulted in a relatively high coefficient of restitution of 0.96, characteristic for nearly elastic impacts of dry grains. Interparticle friction coefficients of 0.1 and 0.7 represented the maximum and minimum reported for the modelled materials. Initially, the elements were generated randomly in a specified region of the upper silo. Particles free to rotate and move dropped down onto the bottom of the silo under gravitational force. Discharge of the silo into the lower silo of identical geometry was performed through a central orifice placed in the bottom of the wedge-shaped hopper silo. The simulations were performed with 6000 particles contained in a silo 120 mm wide and 210 mm high.

Figure 57 shows the distribution of interparticle forces after filling the silo. In the case of smooth particles and walls (Fig. 57a), a concentration of the highest

forces was found in the lower part of the silo, while for rough elements (Fig. 57b) high intergranular forces appeared also in the upper regions of the assembly. Coefficient of friction considerably influenced the distribution of normal forces in contact points between grains. Its increase results from an extension of the region of higher forces.

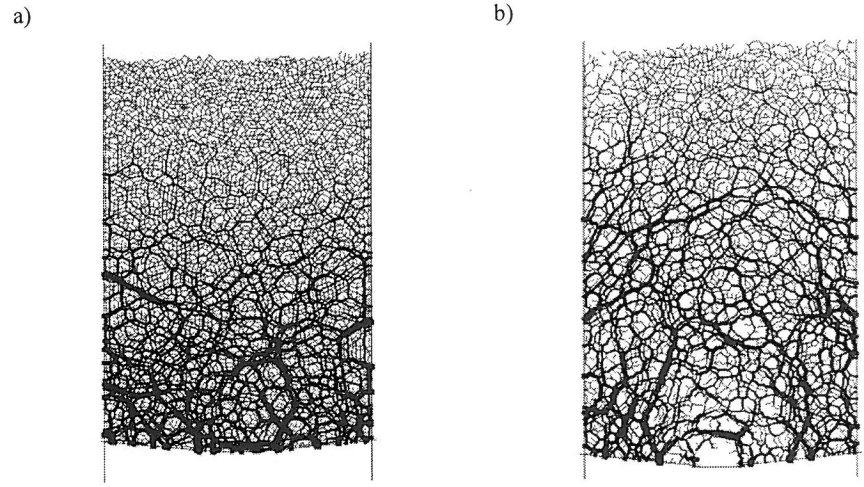

Fig. 57. Contact force transmission after filling the silo for: smooth ($\mu_p = \mu_w = 0.1$) a) and rough particles and walls ($\mu_p = \mu_w = 0.7$) b)

The averaged horizontal forces acting on both vertical walls in static assemblies, with interparticle and particle-wall friction coefficients of 0.1 and 0.7, are presented in Figure 58. Analysis of distribution of static force normal to the wall averaged for 10 particle–wall contacts indicated linear increase in values of forces with increase in particle bedding depth. The increase was considerably higher in the case of the smooth particles and walls. The results of DEM simulations did not show any distinct differences in the distributions of forces along the silo bottom (Fig. 59), which was probably due to too low a number of particles in the system. Increase in wall roughness from 0.1 to 0.7 resulted in a decrease in the averaged vertical force on the silo floor from $8.78 \cdot 10^{-4}$ to $7.32 \cdot 10^{-4}$ N, respectively, indicating qualitative agreement with experimental data obtained by Molenda *et al.* (1996). The values of static horizontal and vertical loads predicted in DEM simulations were compared with the loads estimated by Janssen's formula (Janssen 1895) with pressure ratio of 0.4 and friction coefficient of 0.1 and 0.7 (Figs 58 and 59). Both, the horizontal and vertical loads estimated using Janssen's equation were higher for friction coefficient of 0.1, which was in agreement with the DEM simulations.

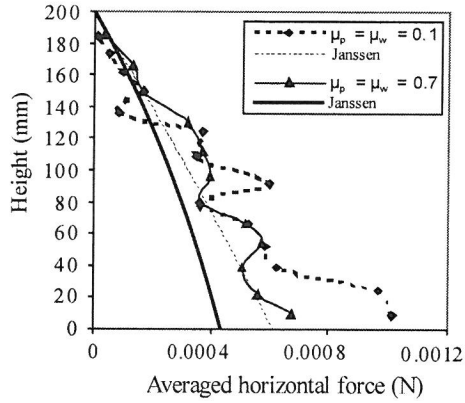

Fig. 58. Wall horizontal forces distribution with depth for smooth ($\mu_p = \mu_w = 0.1$) and rough particles and walls ($\mu_p = \mu_w = 0.7$)

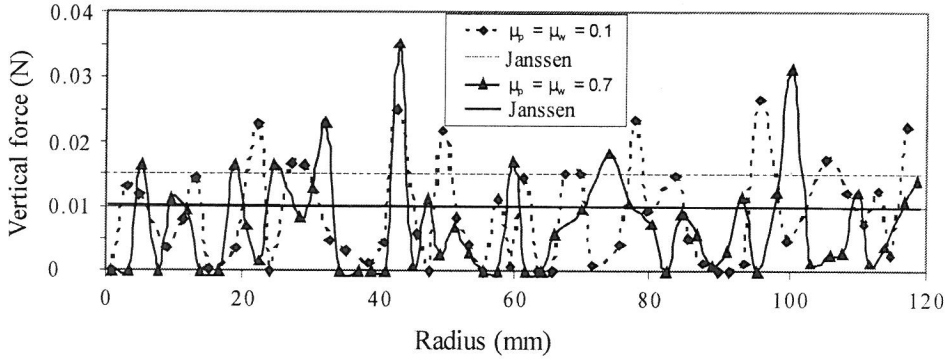

Fig. 59. Vertical force distribution on the silo bottom for smooth ($\mu_p = \mu_w = 0.1$) and rough particles and walls ($\mu_p = \mu_w = 0.7$)

8.2. 3D DEM simulations

8.2.1. Rapeseed impact against a flat surface

The mechanical properties of seeds are strongly influenced by the moisture content (w). Addition of water changes both the surface and bulk properties of seeds by softening the seed structure and filling internal air pores.

The w and impact velocity determine the mode of reaction of seed to impact and influence its susceptibility to impact damage. Rapeseed with high w behaves like rubber because of its soft structure and internal pores filled with capillary water. The water content strongly influences the mechanical properties of rapeseed. Wet seeds exhibit viscoelastic behavior. Various models can adequately

describe the impact behavior of spheres made of different materials under various experimental conditions (Kruggel-Emden *et al.* 2007). There are still doubts about which contact model should be adopted for DEM simulations of bulk rapeseed to describe precisely the physics of particle interactions. Efficient DEM simulations require possibly simple models of interactions.

Based on experimental data, two efficient contact models for DEM applications: the elastic-perfectly plastic contact model of Thornton and Ning (1998) for relatively dry rapeseed and the viscoelastic contact model of Kuwabara and Kono (1987) for wet rapeseed were used by Wojtkowski *et al.* (2010). Simulations of the free fall of rapeseed of various moisture coefficients onto a surface in the shape of a sphere and elastic were conducted. The evolution of contact force in time obtained from DEM simulations for the rapeseed are presented in Figure 60. Fairly good agreement between physical and numerical values of the ratio of fall time to rise time was obtained for the applied contact models. The results point to the suitability of the elastoplastic model for dry seeds, whereas for wet seeds the viscoelastic model gave a better fit.

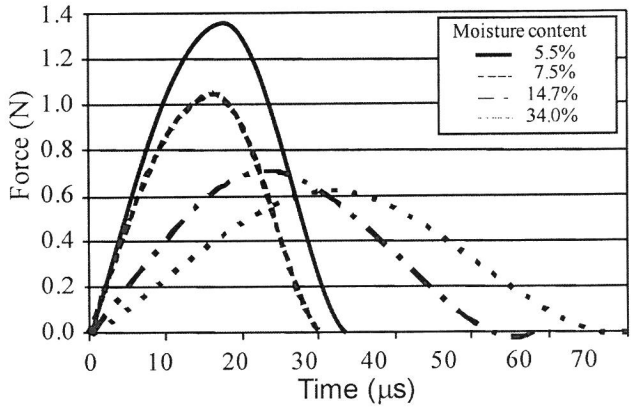

Fig. 60. Impact force vs. contact time relationships obtained in DEM simulation for rapeseed with four levels of moisture content

Figure 61 shows the relationships between force and normal displacement obtained in DEM simulations. For seed with moisture content of 5.5% (Fig. 61a) both the maximum force and displacement are greater than for seed with moisture content of 7.5% (Fig. 61b). For the elastoplastic model (Fig. 61a,b) the overlap on yield initiation was 3.7 and 3.4 μm for seeds with w of 5.5% and 7.5%, respectively. For the viscoelastic model (Fig. 61c,d) the contact force during the final stage of rebounding decreased to less than zero.

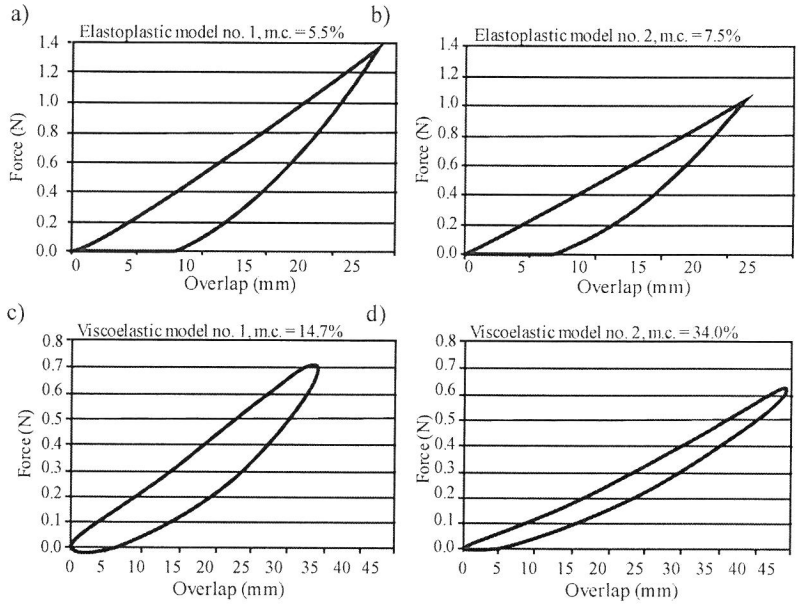

Fig. 61. Force-displacement relationship obtained from DEM simulations for elastoplastic and viscoelastic models

The comparison between the physical and numerical results showed that an elastoplastic model is efficient for simulation of the behavior of dry rapeseed, whereas a viscoelastic model gave closer estimates of experimental force–time relationships for wet seeds.

8.2.2. Uniaxial compression test

The uniaxial confined compression test is a common method to determine the mechanical properties of granular materials which are of interest to technological process designers. Both, physical (e.g. Rusinek *et al.* 2007, Sawicki 1994) and numerical (e.g. Thornton 2000, Azadi *et al.* 2008) modelling of compression of granular solid may provide valuable knowledge necessary for efficient design and useful scientific insight.

The uniaxial compression test provides the stress-strain characteristics of granular solid and material parameters (e.g. lateral-to-vertical pressure ratio k, effective elastic modulus E_e or Poisson's ratio v) which are strongly determined by the fabric of a granular assembly. The dependence of mechanical properties of grain bedding under compression test on particle shape, interparticle friction, variability of particle dimension, spatial orientation of grains and dimension of deposit will be discussed in detail in the next chapters.

8.2.2.1. Particle shape

The food and agricultural products constitute an important group of granular materials. The variety of shapes of grains and seeds results in different mechanical responses when subjected to processes occurring in silos and other technological devices.

Discrete element simulations of uniaxial compression test were conducted for monosized assemblies composed of particles of different aspect ratios (λ), which is a ratio of its longer to the shorter dimension. The agricultural grains were modelled either as a spherical element or 2 to 3 overlapping spheres of the same volume to form particles of different aspect ratios. The change of particle shape from spherical to non-spherical results in a decrease in porosity and increase in stiffness of the specimen when particle aspect ratio increases from unity to 1.6. Further increase in particle aspect ratio results in a decrease in bulk density, which shows little tendency of change of bulk stiffness.

The particle aspect ratio was found to have a significant effect on the pressure ratio, defined as the ratio of horizontal stress and vertical stress in grain assembly. Figure 62 shows that the change of particle shape from spherical to non-spherical results in a significant decrease in the lateral-to-vertical pressure ratio, which is caused by oblong particles exhibiting higher internal friction than spheres, resulting in lower pressure ratio. Further increase in particle aspect ratio beyond 1.6 only produced negligible changes in the pressure ratio. The initial porosity predicted for each simulation (S) is also indicated in the figure. Lateral-to-vertical pressure ratio appears to be more influenced by elongation of particles than by porosity.

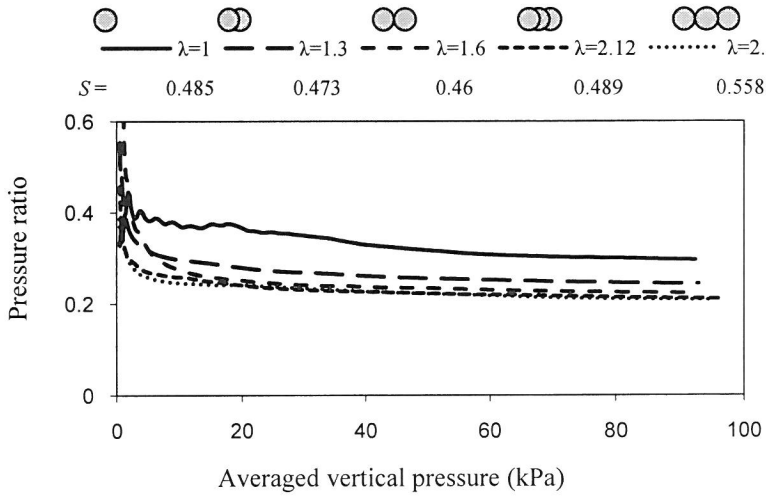

Fig. 62. Pressure ratio-vertical pressure curves for spherical and oblong seeds

Numerical simulations of uniaxial compression test conducted for monosized assemblies composed of particles of different aspect ratios showed that the packing density and the mechanical response were strongly influenced by the particle aspect ratio.

Figure 63 shows the evolution of volumetric effective elastic modulus E (Eurocode 1 2003):

$$E_e = H\frac{\Delta\sigma_z}{\Delta v}\left(1-\frac{2k^2}{1+k^2}\right) \tag{108}$$

where H is the height of a consolidated sample, $\Delta\sigma_z$ is the change in vertical pressure during each time step, Δv is the change in vertical displacement and k is the lateral-to-vertical pressure ratio, predicted for specimens composed of particles of various aspect ratios under confined compression. The change of particle shape from spherical to non-spherical results in an increase in stiffness of the specimen when $\lambda \leq 2.12$. There is no evidence of the tendency of change of stiffness with aspect ratio increasing. The significantly lower stiffness of specimen composed of the most elongated particles resulted from nearly 20% higher porosity of that specimen.

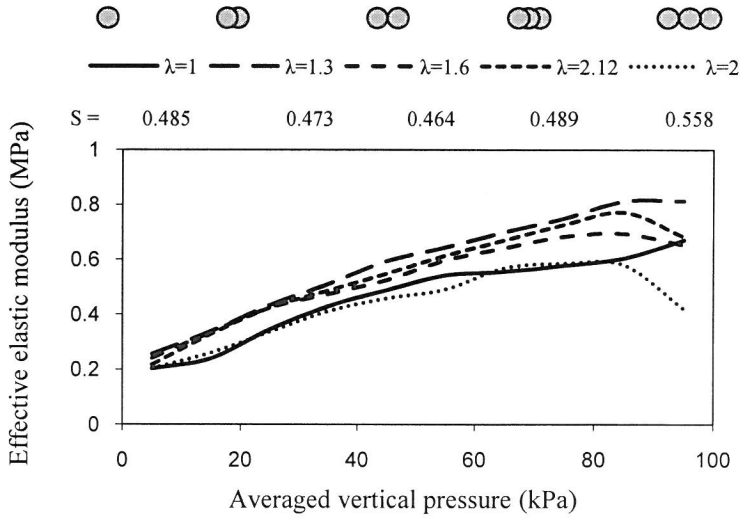

Fig. 63. Effective elastic modulus - vertical pressure curves for spherical and oblong particles

Particle shape determines the coordination number of particle CN which is shown in Figure 64. The change of particle representation resulted in 47% and 73% increase in the coordination number. The mean CN equalled 7.84 and 9.21 in specimens composed of two and three overlapping spheres, respectively. The

same coordination number was obtained for clusters of different aspect ratios created by the same number of spheres. The representation of non-spherical particle shape in DEM and the number of elementary spheres in a cluster determines, therefore, the coordination number.

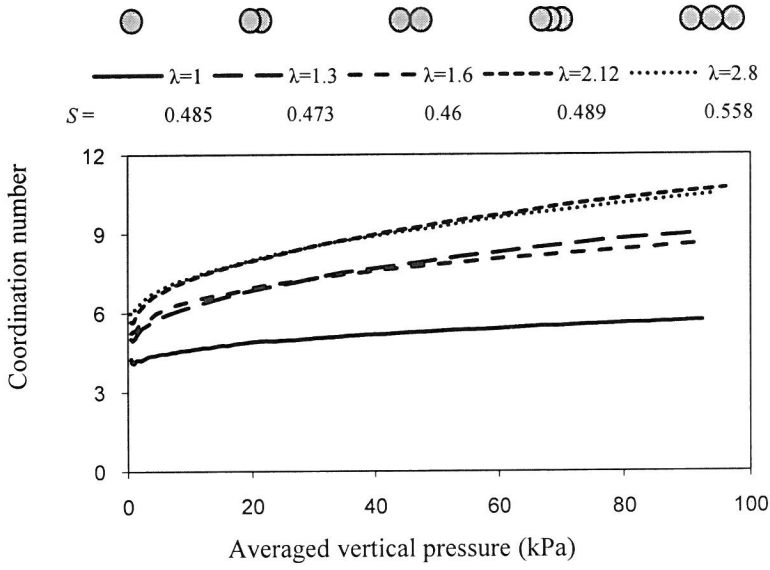

Fig. 64. The coordination numbers in specimens composed of particles of different aspect ratios under uniaxial compression

The DEM predictions are compared with the experimental results in Figures 65 and 66. The results are plotted using the mean values with the error bar indicating ± one standard deviation. The evolutions of effective elastic modulus and pressure ratio of numerical and physical samples under uniaxial compression load were compared, which are of interest to granular processes designers.

As shown in Figure 65a, DEM using spherical particles predicted a higher effective elastic modulus than the response observed for peas. This may be due to the real pea specimen having a larger porosity resulting in a softer response. The naturally non-ideally spherical shapes of real pea grains or the particle stiffness adopted used in the DEM computation may also play a role. Uniform spheres can get into crystalline formation and rotate excessively which is much reduced in real systems due to natural grain size variation and surface unevenness.

In the case of oblong particles DEM predicted significantly lower bulk stiffness at lower vertical pressures (Fig. 65b). The predicted stiffness exceeds experimental values when pressures are higher than 60 kPa. These discrepancies probably result

from the way of representing of bean grains as the clusters, which influences the contact stiffness significantly.

Figure 66 shows the lateral-to-vertical pressure ratio k_y, defined as the ratio of horizontal stress in y direction to the vertical stress in a specimen, as a function of vertical pressure in numerical and physical samples. The DEM prediction was in excellent agreement with the experimental results for the bean grains but over-predicted the pressure ratio for pea grains by 14%.

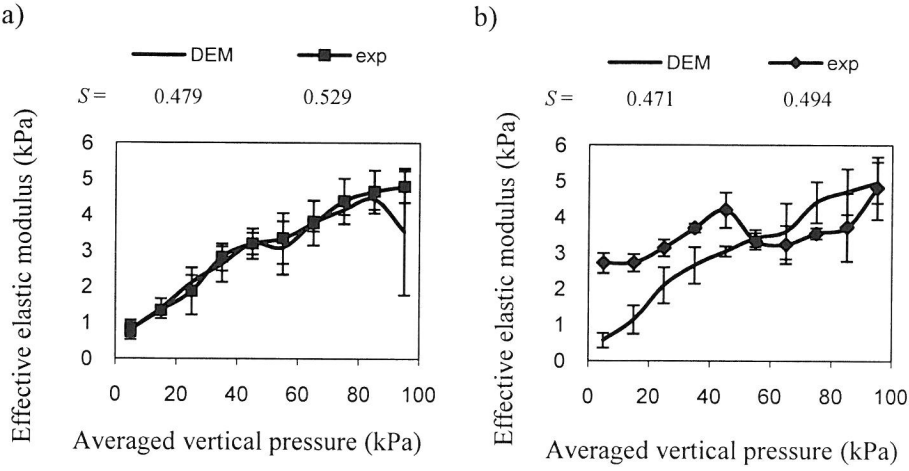

Fig. 65. Effective elastic modulus-vertical lid pressure curves for pea a) and bean b) obtained from numerical and physical experiments

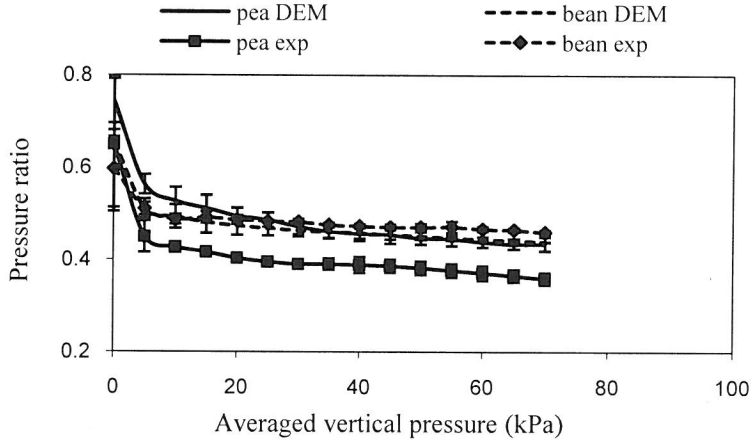

Fig. 66. Pressure ratio-vertical pressure curves for spherical and non-spherical seeds obtained from numerical and physical experiments

8.2.2.2. Interparticle friction

Contact condition is a fundamental aspect in the mechanics of granular materials which is still insufficiently solved. The crucial issue of the presence of limiting friction at a contact point and its influence on the shear strength of the particulate assembly has been of interest to scientists and engineers for many years.

The pressure ratios in spherical assemblies uniaxially compressed as a function of interparticle friction at vertical pressure of 50kPa are presented in Figure 67. Increase in the coefficient of friction from 0.1 to 0.3 results in lower horizontal forces in the specimen, providing 24% lower lateral-to-vertical pressure ratio. Further increase in μ_{pp} to 0.6 and 0.9 resulted in 41% and 50% decrease in the k_y value as compared to k_y at μ_{pp} of 0.1. The higher inter-particle friction results in higher internal friction angle (φ) and lower pressure ratio whose relationship may be determined from following equation (Eurocode 1 2003):

$$k = 1.1(1 - \sin\varphi). \tag{109}$$

Whilst equation 100 indicates a nearly linear relationship, the non-linear dependence of pressure ratio on the coefficient of friction predicted in Figure 67 is due to increasingly less mobilised friction in a system of higher interparticle friction.

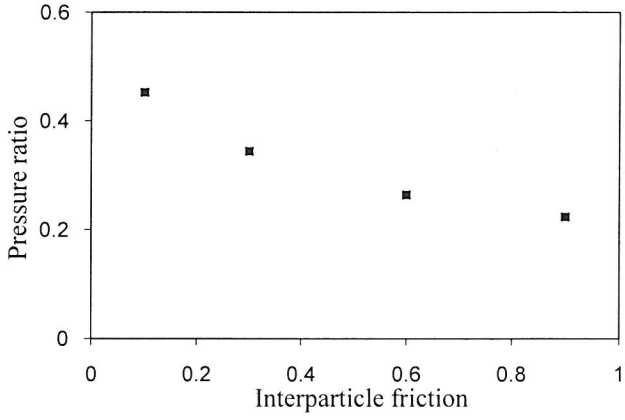

Fig. 67. Pressure ratio-interparticle friction relationship

8.2.2.3. Particle size heterogeneity

The majority of granular systems are composed of particles of heterogeneous size, which strongly determines their mechanical properties. DEM simulations for grain assemblies composed of both, spherical and non-spherical particles of size

variation of 0%, 20% and 40% showed a high influence of the orientation fabric in granular matter on its mechanical properties.

The analysis of evolution of effective elastic modulus E_e predicted for specimens composed of spheres and elongated particles of various size variations indicated no tendency of change of stiffness with increasing particle size variation (Fig. 68).

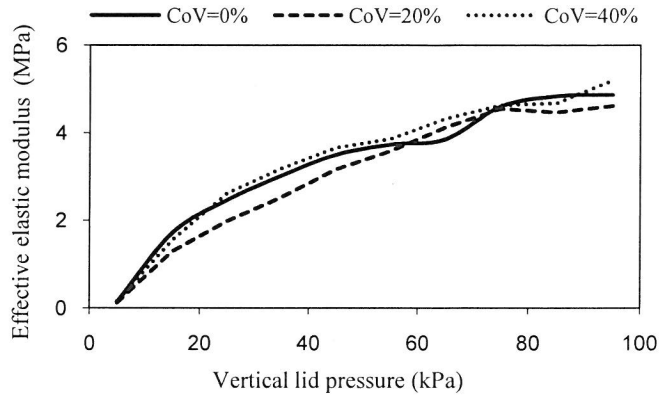

Fig. 68. The effective elastic modulus-vertical lid pressure relationships for sphere size variations of 0%, 20% and 40%

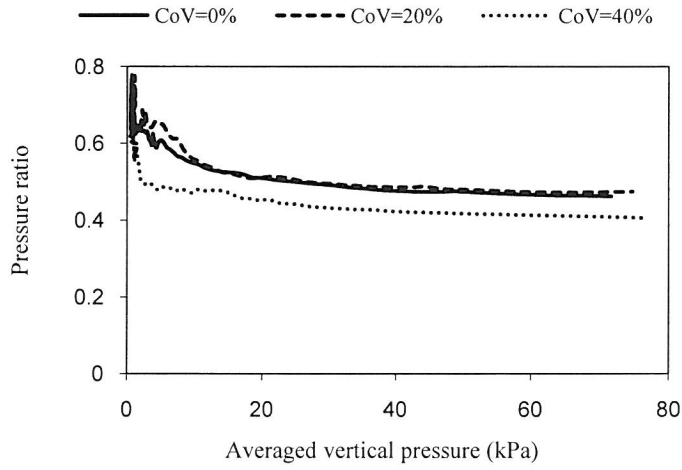

Fig. 69. The pressure ratio of specimen versus vertical pressure for sphere size variations of 0%, 20% and 40%

Figure 69 shows no influence of particle size variation on pressure ratio in sphere bedding when the coefficient of particle size variation increases from 0% to 20%. Further increase in the coefficient of particle size variation to 40% resulted in above 20% decrease in pressure ratio.

8.2.2.4. Spatial orientation of particles

Three-dimensional DEM simulations for grain assemblies composed of non-spherical particles modelled as 3 overlapping spheres of various initial spatial orientations showed a high influence of the orientation fabric in granular matter on its mechanical properties.

The initial configurations of specimens are presented in Figure 70.

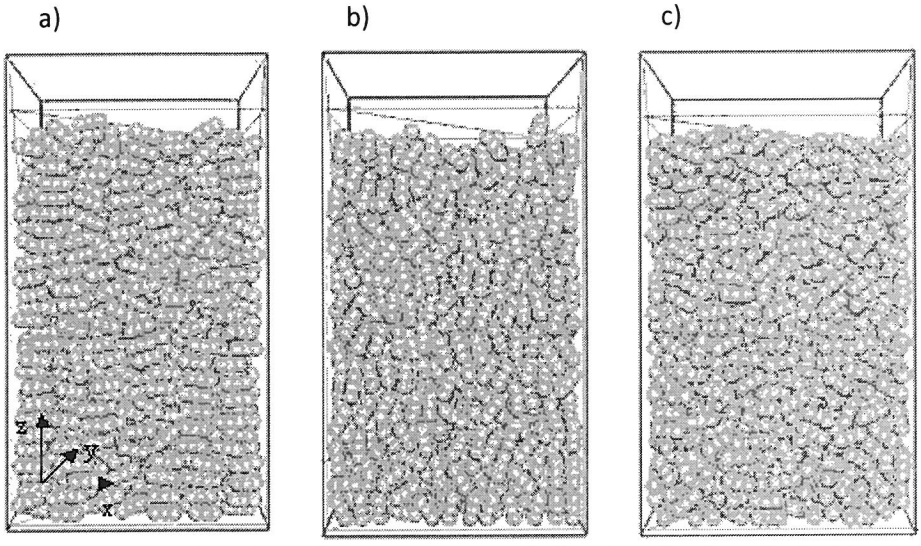

Fig. 70. Initial conFigurations of specimens composed of horizontally a), vertically b) and randomly oriented particles c)

Figure 71 presents the vertical pressure versus displacement characteristic. The mean values with the error bar indicating ± one standard deviation are plotted. The effective elastic modulus of numerical samples was calculated on the basis of the pressure versus displacement characteristic following the recommendations of Eurocode 1 (2003). The effective elastic moduli were calculated as 433.12 kPa, 440.97 kPa and 465.36 kPa for samples composed of horizontally, randomly and vertically oriented particles, respectively. The 7% lower elastic modulus of the sample composed of horizontally oriented particles as compared

to the one composed of vertically oriented granules was probably due to higher mobility of particles in the sample under loading resulting from lower interlocking friction. The interparticle friction which is a sum of adhesive and interlocking friction determines the mechanical response of granular media under compression. The interlocking friction plays a significantly high role in the case of granules of irregular shapes, as the ones modelled in the described project.

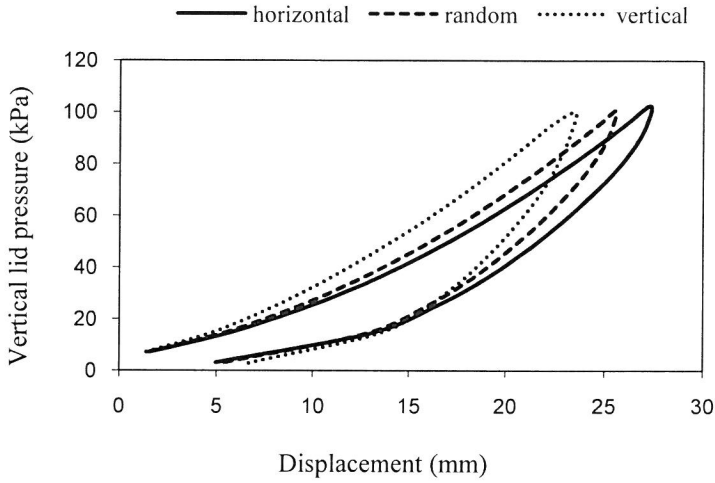

Fig. 71. Vertical pressure – displacement relationships for specimens of various initial orientation fabric

The change in initial particle orientation from horizontal to vertical resulted in a 16% decrease in the coordination number *CN*, defined as the number of contacts per one particle, at vertical pressure of 50 kPa (Fig. 72). The values of the coordination number in a granular assembly composed of randomly oriented particles lie between *CN* values estimated for vertical and horizontal particle orientations in the whole range of vertical pressure.

The study of the transmission of pressure in granular media was conducted. The comparison between pressure ratios in the specimens showed 14% and 27% increase in k value in specimens of randomly and vertically oriented particles, respectively, as compared to the one composed of horizontally oriented particles. The pressure ratios were calculated at vertical pressure of 50 kPa. So high differences in k values pointed to a high dependence of force transmission in a granular system on its orientation fabric.

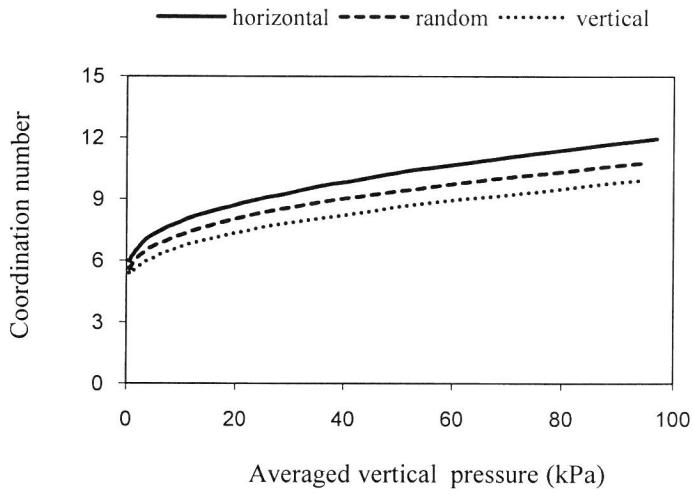

Fig. 72. Evolution of coordination number for specimens of various initial orientation fabric

8.2.2.5. Sample size effect

The study showed that the mechanical response of a granular assembly subjected to uniaxial compression is significantly affected by the dimensions of the system. Numerical tests revealed differences in stress transmission in spherical assemblies of thickness lower than five times the size of the particle. The findings pointed out that the specimen of a dimension not lower than five times the size of the particle should be used as a representative elementary volume (REV) for uniaxial compression testing.

Figure 73 (a to d) illustrates the evolution of the effective elastic modulus E_e with vertical pressure σ_z for test samples 1, 3, 5 and 7 particle diameters thick, i.e. from 8 to 44 mm. The results are plotted using the mean values for three simulations, with the error bar indicating ± one standard deviation.

The porosity for 1 diameter thick sample was found to be 0.53, which is distinctly higher than those for thicker samples - all at approximately 0.48. Modulus E_e was found to increase with σ_z increasing from 0 to 100 kPa with some fluctuations that were increasingly larger for thinner samples. No clear difference in the overall $E_e(\sigma_z)$ characteristics for various thicknesses of the sample was found. Increase in thickness T resulted in decreasing standard deviation due to the lower scatter resulting from averaging over a higher number of particles and weaker influence of walls.

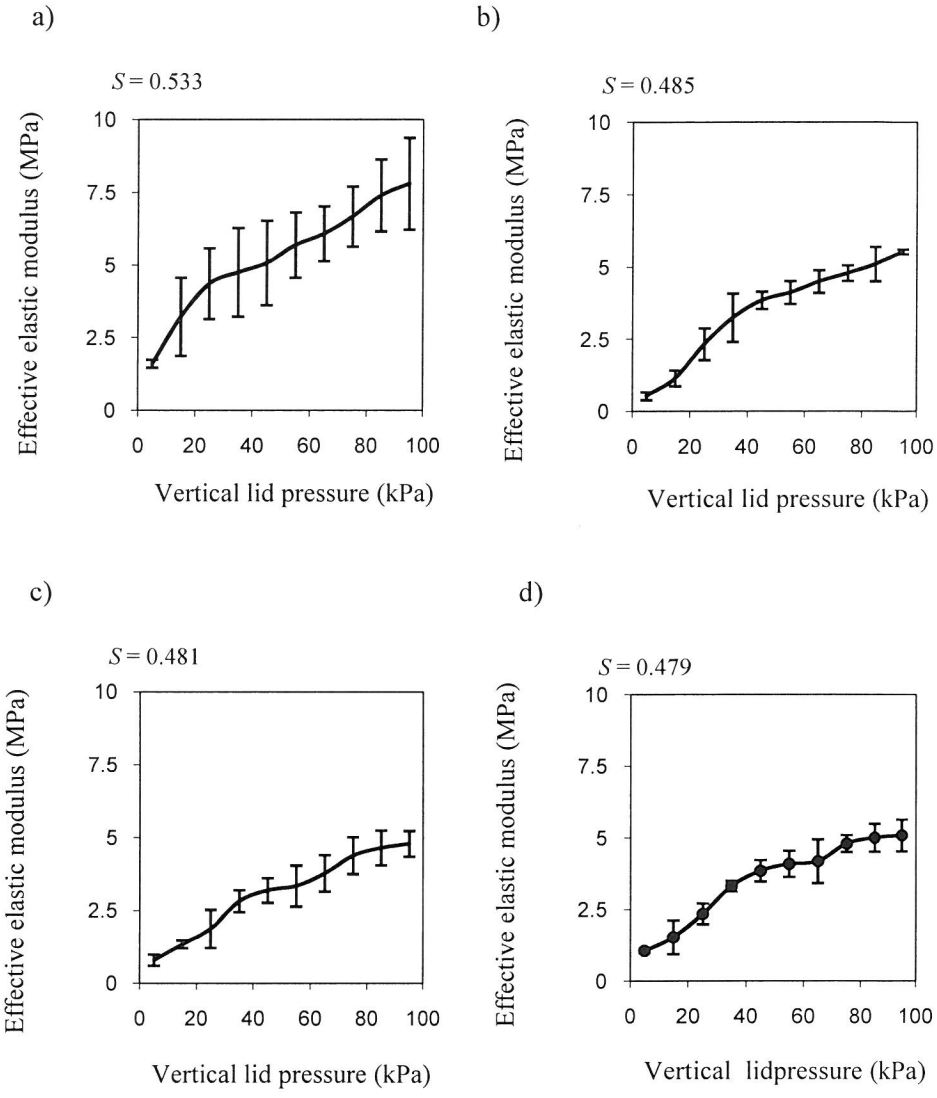

Fig. 73. Effective elastic modulus - vertical pressure relationships for numerical samples of various thickness: a) – T = 8 mm, b) – T = 21 mm, c) – T = 33 mm, d) –T = 44 mm

Figure 74 shows the lateral-to-vertical pressure ratio during the compression of specimens. The error bars are also indicated in the Figures.

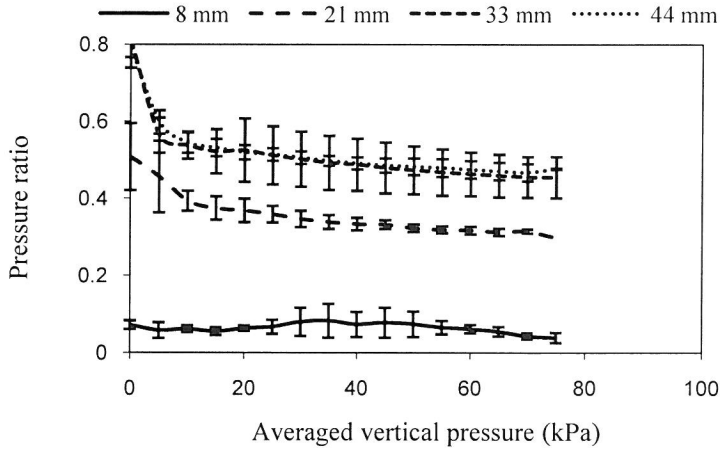

Fig. 74. Lateral-to-vertical pressure ratio in numerical samples of various thickness

The pressures transmitted in grain assemblies of various thicknesses varied strongly with sample width and so varied k. Here, each step of increase in sample width from 1 to 5 seed diameters resulted in an increase in the number of contact points. In the case of 1 diameter thick sample only several contact points existed at the 120 mm height of the sample, causing very uneven and unrepeatable distribution of contact points between seeds and with the wall. As a result, approximately six-fold increase in k (from 0.074 to 0.473 at 50 kPa of normal pressure) was observed with an increase of thickness of sample from 1 to 5 seed diameters. Further increase of thickness from 5 to 7 seed diameters did not bring any noticeable increase in k. Probably the sample width of 5 diameters was close to a threshold after which a set of contact forces acting on the wall might be treated as pressure. Following this result, sample width equal to five particle diameters may be recommended as the minimum sample width to obtain repeatable values of pressure ratio.

The DEM predictions are compared with experimental results in Figure 75. The results are plotted using the mean values with the error bars indicating ± one standard deviation. The porosities, effective elastic modulus, lateral-to-vertical pressure ratios and load-displacement responses of numerical and physical samples under compression load were compared which are of high interest to process designers.

The porosity of larger (thicker than one particle diameter) numerical samples was found approximately equal to 0.48, while that of larger physical specimens composed of non-perfect spheres was of approximately 0.53 or 10% higher. Contrary to multisized pea grains, uniform spheres can get into closer formation providing lower porosity.

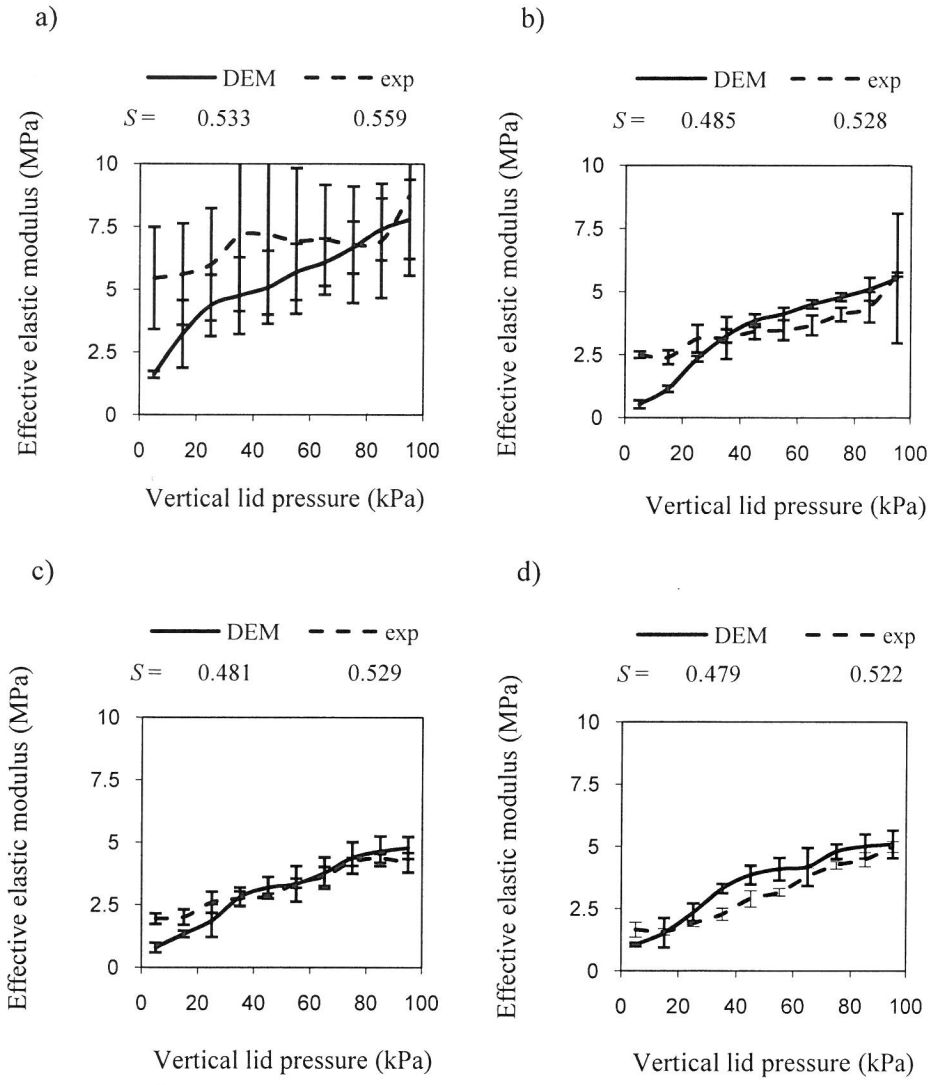

Fig. 75. Effective elastic modulus – vertical pressure relationships for numerical and physical samples of various thickness: a) – T = 8 mm, b) – T = 21 mm, c) – T = 33 mm, d) – T = 44 mm

As shown in Figure 75, the DEM simulations predicted lower effective elastic modulus than the experiments, particularly for the thinnest sample. That may be attributed to a number of factors including the non-spherical shapes of real pea grains, the denser initial packing (lower porosity) of the numerical samples and the higher

particle stiffness used in the DEM computation. Perfect spheres can form a denser packing (than non-spherical particles) and rotate more easily than in a real system where natural grain size variation, non-perfect shape and variability of surface friction exist. The differences between stiffness of numerical and physical samples decreased significantly for specimens of thickness from 3 to 7 times the particle size. For those samples, the differences between the numerical and experimental E_e values lie within the range of scatter. This is probably a result of combination of the abovementioned imperfections of real granular material and amplified by imperfections of the experimental apparatus as compared to the configuration of the numerical experiment. Imperfections of real apparatus include, among others: limited accuracy of its dimensions, non-perfectly rigid walls and their supports, imperfect plane surfaces or uneven distribution of frictional properties. These effects had a weaker influence in larger samples. The behaviour of larger samples of real material thus became closer to that of ideal material used in the numerical experiments.

The study showed that the mechanical response of a granular assembly subjected to uniaxial compression is significantly affected by the dimensions of the system. Both numerical and physical tests revealed differences in stress transmission in spherical or nearly spherical assemblies of thickness lower than five times the size of particle. The findings suggest that a specimen of dimension not lower than five times the size of the particle should be used as a representative elementary volume (REV) for uniaxial compression testing.

8.2.2.6. Moisture content of grain

Observation of the behaviour of specimens composed of spheres with parameters of rapeseed grains at different moisture contents under uniaxial compression was carried out.

The comparison of stress-strain relationships, which are plotted in Figure 76, showed various stiffnesses of the specimens.

The lowest strain of a specimen, $\varepsilon_z = 2.5\%$, at maximum vertical lid pressure was obtained at moisture content of 7.5%. Increase in moisture content to 9% resulted in 36% increase in strain. The lowest stiffness characterised a sphere assembly at $w = 12\%$, whose maximum strain equalled 3.8%.

Figure 77 shows relationships between pressure ratio and vertical pressure in specimens during the loading-unloading cycle. In both phases, higher horizontal stresses were generated in model assembly of rapeseed grain of 7.5% moisture content. Pressure ratio calculated for that specimen at vertical pressure of 50 kPa equaled to 0.376. The pressure ratio decreases as moisture content increases. The 12% decrease in k_y value was obtained for higher moisture contents. The 5% differences between k_y values calculated at $w = 9\%$ and $w = 12\%$ lied in the range of numerical scatter.

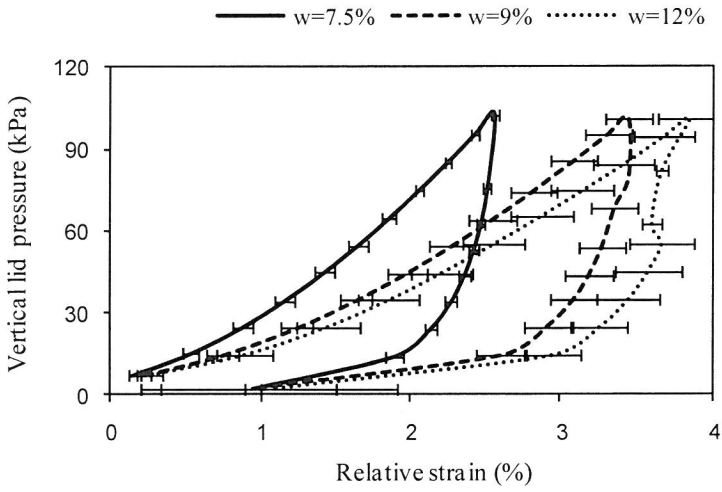

Fig. 76. The stress-strain curves for model rapeseed specimens at various moisture content

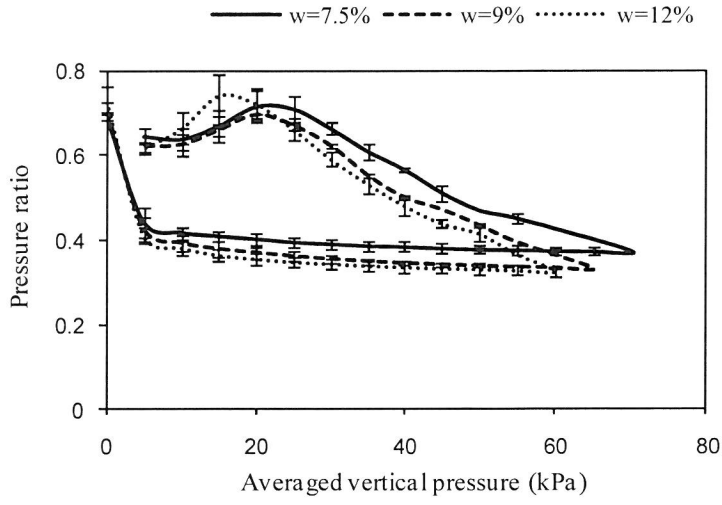

Fig. 77. The pressure ratio in y direction versus vertical pressure for model rapeseed specimens at different moisture content

Qualitative agreement was observed between the effective elastic modulus-vertical pressure curves for physical and numerical grain beddings (Fig. 78). Stiffness of specimens decreased with moisture content increasing.

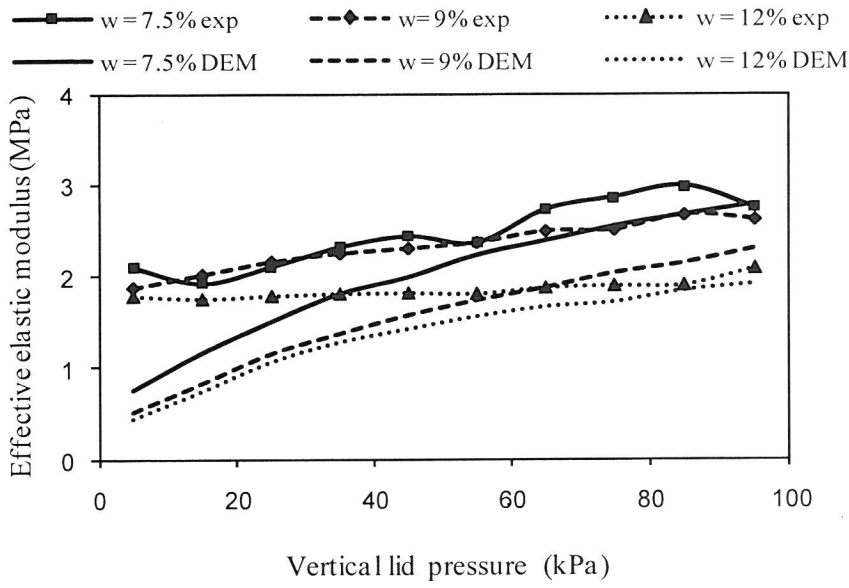

Fig. 78. Effective elastic modulus versus vertical lid pressure for model and real specimens of rapeseed grains at different moisture contents

The differences between the effective elastic moduli obtained for the model and real grain assemblies may have had various sources. The ideal spheres generated in simulations have a high tendency to rotate, which does not take place in real grain systems resulting from grain size deviation and surface roughness. The differences between the mechanical characteristics of specimens obtained in numerical and physical tests are a consequence of high particle rotations in the model systems. Another source of differences between the numerical and experimental results is the inaccuracy of the Hertz–Mindlin contact model applied for DEM simulations. That model does not take into account all effects determining the behaviour of real grains. The lack of quantitative agreement between the numerical and experimental results obtained for grains of various shapes could be a result of representation of particles in simulations. The particle contact stiffness depends on the radii of curvature at the point of contact. Shapes of model grains represented as spheres differ from shapes of rapeseeds, which influences specimen stiffness.

The relationships between pressure ratio and vertical pressure were plotted in Figure 79 for rapeseed grains at different moisture contents. The k_y values estimated for real specimen at w = 7.5 % were higher than the ones obtained for the

model system. Differences between pressure ratios fell within the measurement scatter at vertical pressures higher than 50 kPa. Differences obtained at higher moisture contents lied in the measurement scatter during the whole compression test.

Both, qualitative and quantitative agreement was found between the results obtained from simulations and experimental tests.

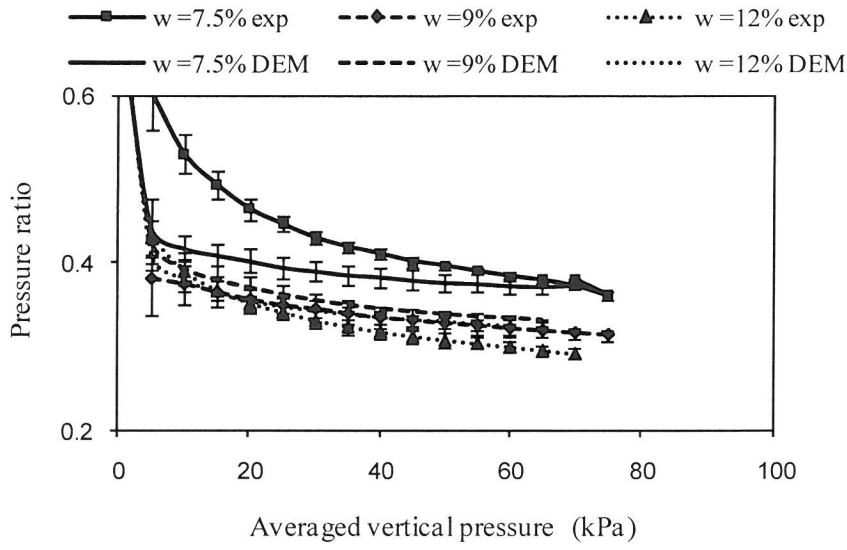

Rys. 79. The pressure ratio in y direction versus vertical pressure for model and real specimens of rapeseed grains (variety Licosmos) at different moisture content

8.2.3. Silo filling and discharge

The silo discharge of wheat grains of moisture content of 12% was modelled with the discrete element method using particles composed of two spheres. The simulations were conducted for a rectangular steel box of one particle diameter thickness, divided into two smaller parts. The initially randomly positioned and orientated 5000 particles generated in the upper part of box settled down under gravity on the bottom of the lower model silo. The following filling procedures were applied: rainfall method (R), central filling (C), extremely eccentric filling (A) and circumferential filling (O) methods.

The material filled from the upper part of model setup through an orifice. The simulations of circumferential filling were done by means of an inset placed above the bottom of the box. The model boxes used in the simulations are presented in Figure 80.

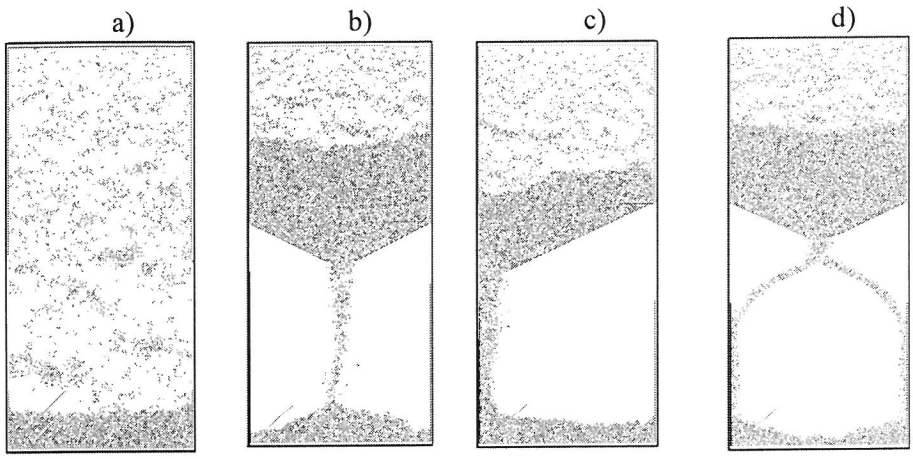

Fig. 80. Model setup used for simulations of silo filling with: a) – rainfall method, b) – central filling, c) – extremely eccentric filling, d) – circumferential filling methods

Figure 81 shows the distributions of particle orientations in the model box filled with various filling procedures.

In all the cases the angles between the longer axis of particles and the bottom of the box estimated for a majority of particles are lower than 30°. The highest number of vertically or nearly vertically oriented clusters was found in the system generated with the rainfall filling method. The longer axes of particles parallel to the generatrix of the cone of natural repose characterised particle assemblies generated with central and eccentric streams. Angles of natural repose equalled 27° and 32° in the former and latter cases, respectively. Generation of the system with circumferential stream resulted in non-uniform distribution of cluster orientations with horizontal orientation distinguished.

Nonuniform distribution of force chains was obtained for each filling procedure. The highest forces in the lower parts of boxes were a result of gravity of material placed above. Propagation of the highest forces with vertically directed chains characterised the assembly created with the rainfall method and central steam. Application of the filling method with eccentric stream resulted in distinguished direction of force transmission parallel to the surface of repose of the material. Generation of the system with circumferential stream resulted in high concentration of vertically oriented force chains in the centre of the box.

Figure 82 shows evolutions of averaged normal forces acting between particles and the bottom of the box along the bottom obtained for investigated particle systems.

High oscillations of forces were observed in each case. The most uniform distribution of forces was obtained for the rainfall filling method. In the case of central

filling the highest forces acted in the centre of the box and in the neighbourhood of its side walls. Increase in force with increase in distance from the left wall where the assembly was the highest was observed for eccentric filing. Significant increase in forces in the centre of the box was a consequence of circumferential filling.

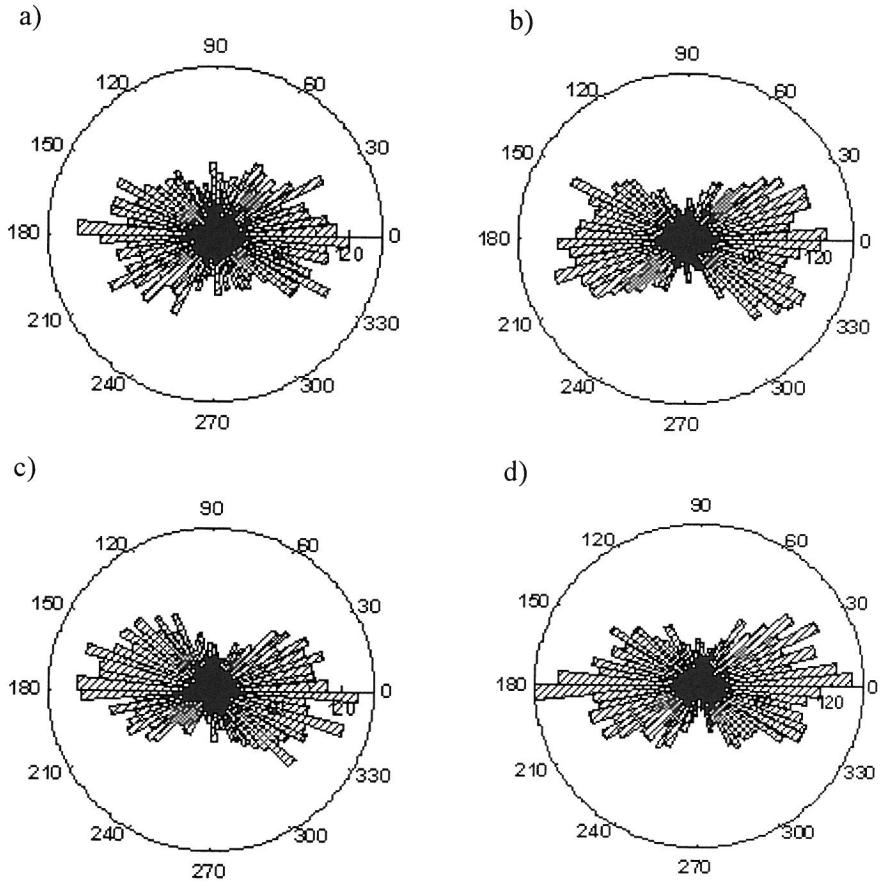

Fig. 81. Distribution of model wheat grains orientations in systems generated with: a) – rainfall, b) – central, c) – extremely eccentric, d) – circumferential filling methods

The mechanism of forces transmission in granular materials is determined by their packing structure. Grain assemblies of close porosities were generated with various methods. The rainfall filling method resulted in the lowest porosity, whilst the highest one was obtained for circumferential filling. Estimated differences between S were lower than 5%.

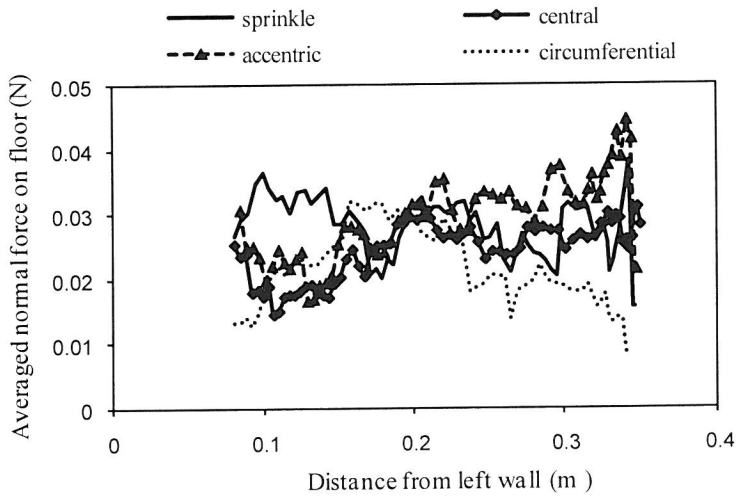

Fig. 82. Evolutions of averaged normal force between particles and bottom of box versus distance from left wall of containers filled with different methods

Comparison of normal stresses exerted on the bottom of the box (σ_{zl}) revealed their dependence on the filling method (Fig. 83). The highest stresses characteried the rainfall filling. A 13% decrease in σ_{zl} value was observed with the central and eccentric filling methods. Filling of the box with circumferential stream decreased normal stress by 50%.

The study of impact of silo filling procedure on normal wall pressure revealed twofold higher pressure in the assembly generated with the rainfall filling method. Such significant differences between stress transmission in examinated particulate systems resulted in nearly 50% difference between their pressure ratios (Fig. 84). The highest k_x values were obtained for rainfall and circumferential filling.

The particle orientations which are also determined by the method of generation of grain system have a high impact on the distribution of tangential stresses in an assembly. The lowest tangential stress was obtained for circumferential filling, which resulted in the lowest ratio of mean tangential to normal pressure (T/F). The values of ratios calculated for different filling methods are shown in Figure 85.

The review of results of physical and numerical testing performed by the authors, given in chapter 8, provided some new information on phenomena occurring in biologically based granular materials from one side, and indicated possible directions of development of DEM for simulation of processes in such media on the other. DEM may explain phenomena that cannot be treated by the mechanics of continuum due to discontinuity or heterogeneity of deposit as well as in the

case of singularities (such as the cusp-like minimum in the relationship of packing fraction against particle aspect ratio (Donev *et al.* 2004). Chances for efficient use of numerical simulations of mechanical processes in research or design increase with an increase of computing power of machines as well as with development of software. Mechanical properties of biologically based materials are strongly influenced by moisture content. As shown in the modelling of the impact of rapeseed against a flat surface (8.2.1), change in moisture content may call for change in the contact model used in simulations. Great wealth of shapes and dimensions of seeds offers a good opportunity for using seed deposits to study the mechanics of granular materials and, on the other hand, for examination of DEM applicability to simulate the mechanical behaviour of various granular materials.

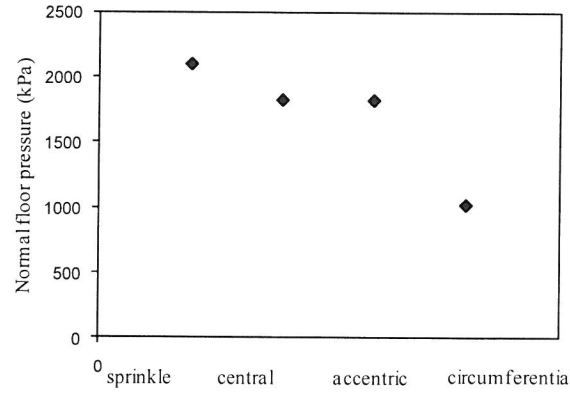

Fig. 83. Normal floor pressure for different filling methods

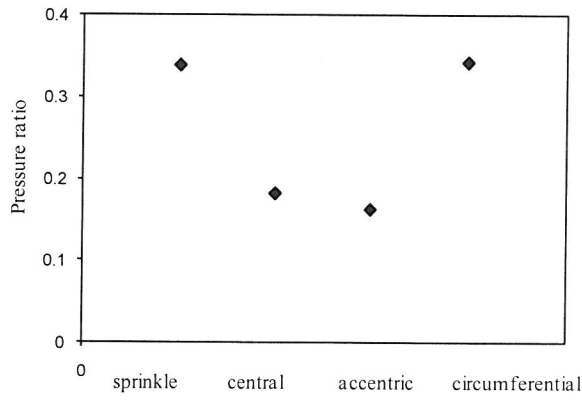

Fig. 84. Pressure ratio for different filling methods

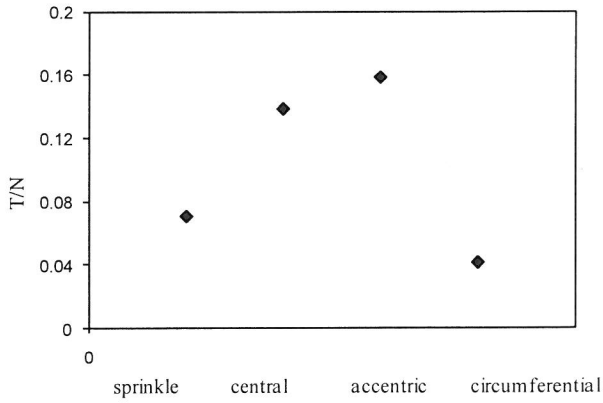

Fig. 85. The ratio of tangential to normal wall pressure for different filling methods

9. REFERENCES

Akin J.E., 1994. Finite Elements for Analysis and Design. Academic Press, Harcourt Brace & Company, Publisher, London.

Allen J.R.L., 1969. Notes towards a theory of concentration of solids in natural sand. Geological Magazine, (106) 4, 309-321.

ASTM – D6128 (2000).Standard Test Method for Shear Testing of Bulk Solids Using the Jenike Shear Cell. American Society for Testing and Materials, West Conshohocken, PA.

Azadi P., Farnood R., Yan N., 2008. Discrete element modeling of the mechanical response of pigment containing coating layers under compression. Computational Materials Science 42, 50-56.

Balassy Z., Horabik J., Molenda M., 1989. On friction properties of wheat grain. Advances of Agricultural Sciences Problem Issues, 378, 11-19.

Barbarosa-Cànovas G.V., Vega-Mercado H., 1996. Physical, chemical and microbiological characteristics of dehydrated foods. Dehydration of Foods, Chapman & Hall, New York.

Bednarski T., 1995. Mechanics of plastic flow (in Polish). PWN Warszawa.

Bijnen F.G.C., H. van Aalst, Baillif P.Y., Blonk J.C.G., Kersten D., Kleinherenbrink F., Lenke R., van der Stappen M.L.M., 2002. In-line structure measurement of food products. Powder Technology, 124, 188-194.

Blair D.L., Mueggenburg N.W., Marshal A.H., Jaeger H.M., Nagel S.R., 2001. Force distributions in three-dimensional granular assemblies: Effects of packing order and interparticle friction. Physical Review E, 63, 041304, 1-8.

Blau P., 2001. The signifficance and use of the friction coefficient. Tribology International, 34, 585-591.

Brilliantov N.V., Pöschel T., 1998. Rolling friction of various sphere on a hard plane. Europhysics Letters, 42, 511-516.

Britton M.G., Moysey E.B., 1986. Grain properties in the proposed new engineering practice on bin loads. ASAE Paper No. 86-4502, St. Joseph, MI.

Brubaker J.E., Pos J., 1965. Determining static coefficients of friction of grains on structural surfaces. Transactions of the ASAE, 1, 53-55.

BS-2955:1958. Glossary of terms relating to powders. British Standards Institution, London, UK.
Buckley D.H., 1981. Surface effects in adhesion, friction, wear and lubrication. Elsevier, Amsterdam- Oxford -New York.
Bucklin R.A., Thompson S.A., Ross I.J., Biggs R.H.,1989. Apparent coefficient of friction of wheat on bin wall material. Transactions of the ASAE, 5, 1769-1773.
Calladine C.R., Greenwood J.A., 1978. Line and point loads on a non-homogeneous incompressible elastic half-space. Quarterly Journal of Mechanics and applied Mathematics, 31, 507.
Campbell C., 2002. Granular shear flows at the elastic limit. Journal of Fluid Mechanics 465, 261-291.
Canadian Farm Building Code, 1977. National Research Council of Canada, Ottawa.
Carr Jr. R.L., 1965. Classifying flow properties of solids. Chemical Engineering, 72, 69-72.
Cassagrande A., 1936. Characteristics of cohesioj less soils affecting the slopes of slopes and earth fills. J. of Boston Society of Civil Engrs., 23, 13-32.
Chang C.S., Converse H.H., Martin C.R., 1983. Bulk properties of grain as affected by self-propelled rotational type grain spreaders. Transactions of the ASAE, 26(5), 1543-1550.
Chang C.S., L. Ma., 1990. Modelling of discrete granulates as micropolar comtinua. Journal of Engineering Mechanics, 116(12), 2703-2721.
Chattopadhyay A., Rao R.K., Parameswaran M.A., 1994. On the Classification of Bulk Solids. Bulk Solids Handling, 14(2), 339-344.
Chung Y.C., 2006. Discrete element modelling and experimental validation of a granular solid subject to different loading conditions. PhD dissertation, University of Edinburgh.
Chung Y.C., Ooi J. Y., Favier J., 2005 Measurement and modeling of a particulate assembly under confined compression. Particulate Systems Analysis 2005, Stratford-upon-Avon, UK.
Cleary P., Sawley M.L., 2002. DEM modeling of industrial granular flows: 3D case studies and the effect of particle shape on hopper discharge. Applied Mathematical Modelling, 26, 89-111.
Clower R.E., Ross I.J., White G.M., 1973. Properties of compressible granular materials as related to forces in bulk storage structures. Transactions of the ASAE, 478-481.
Cudny M, Binder K., 2005. Kryteria wytrzymałości gruntu na ścinanie w zagadnieniach geotechniki, http://www.pg.gda.pl/~mcud/publications/content/documents/IMG_2_2005.pdf
Cundall P.A., Strack O.D., 1979. A discrete element model for granular assemblies. Géotehnique, 29(1), 47-65.
Cyrus P., 1985. Tribometer for measuring the friction coefficient of grain during the shearing on sliding support plate. Proceedings of the '85 conference on mechanics VSZ in Prague, 17-23.
Delwiche S.R., 2000. Wheat endosperm strength properties as affected by miosture. Trans. of the ASAE 43(2), 365-373.
Desai C.S., Abel J.F., 1972. Introduction to the finite element method. A numerical method for engineering analysis, VNR New York.
Dobrzański B., 1990. Metodical aspects of estimation of mechanical properties of pea seeds (in Polish). PhD dissertation. Institute of Agrophysics PAS, Lublin, Poland.
Donev A., Cisse I., Sachs D., Variano E.A., Stillinger F.H., Connelly R., Torquato S., Chaikin P.M., 2004. Improving the Density of Jammed Disordered Packings Using Ellipsoids. Science, 303, 990.
Drescher A., 1991. Analytical methods in bin-load analysis. Elsevier, Amsterdam-Oxford-New York-Tokyo.
Drozdow J.N., Pawlow W.G., Puczkow W.N., 1986. Friction and wear in extremal conditions (in Czech). Moskwa: Maszinostrojenie.
Eurocode 1, 2003. Basis of design and actions on structures – Part 4: Actions in silos and tanks. European Committee for Standarization. Central Secretariat: rue de Stassart 36, B-1050 Brussels.

Falcon E, Laroche C, Fauve S and Coste C. 1998. Behavior of once elastic ball bouncing repeatedly off the ground. The European Physical Journal B, 3,45-57.

Feda J., 1977. Mechanics of particulate solids (in Czech). Academia, Praha.

Fiala J., 1965. Friction of agricultural materials (in Czech). Zemedelska Technika, 4, 205-220.

Frontczak J., Metzger T., 1985. The studies on the slip angle geometrical features of corn grain in the moisture function. Proceedings of the '85 conference on mechanics VSZ in Prague, 225-238.

Glenn G.M., Younce F.L., Pitts M.J., 1991. Fundamental physical properties characterizing the hardness of wheat endosperm. Journal of Cereal Science, 13, 179-194.

Goodey R.J., Brown C.J., Rotter J.M., 2003. Verification of a 3-dimensional model for filling pressures in square thin-wall silos. Engineering Structures, 25, 1773-1783.

Gröger T., Katterfeld A., 2007. Application of the Discrete Element Method in Materials Handling, Part 1: Basics and Calibration, Bulk Solids Handling, 27 (1), 17-23.

Grundas S., Hnilica P., 1987. Types of wheat endosperm and its mechanical properties (in Polish). Zesz. Probl. Post. Nauk Roln., 320, 127-133.

Gu Z.H., Arnold P.C., McLean A.G., 1992. Consolidation- related density and permeability models for bulk solids. Powder Technology, 72, 39-44.

Hanzelik F., Keleman P., Tomovcik J., 1968. Deformation and friction of of wheat grains. Acta Technologica Agriculturae, Nitra, 30-42.

Harvill T.L., Hoog J.H., Holve D.J., 1995. In-process particle size distribution measurement for pharmaceutical applications. Powder Handling and Processing, 7(2), 139-141.

Hassanpour A., Antonya S.J., Ghadiri M., 2008. Influence of interface energy of primary particles on the deformation and breakage behaviour of agglomerates sheared in a powder bed. Chemical Engineering Science, 63 (23), 5593-5599.

Hebda M., Wachal A., 1980. Trybologia, WNT, Warszawa.

Herle I., Gudehus G., 1999. Determination of parameters of a hypoplastic constitutive model from properties of grain assemblies, Mechanics of Cohesive – Frictional Materials, 4, 461-486.

Herrmann H.J., 2002. Granular matter, Physica A, 313, 188-210(23).

Hertz H., 1882. Über die Berührung fester elastischer Körper. J. Reine und Angewandte Mathematik, 92, 156-171.

Horabik J., 2001. Characteristics of physical properties of granular plant materials for storage purposes (in Polish). Acta Agrophysica, 54.

Horabik J., Łukaszuk J., Grochowicz M., 2000. Formation of shear band in a granural material during triaxial comression test. Int. Agrophysics, 14, 273-278.

Horabik J., M. Molenda., 2002. Physical properties of granular food materials (in Polish). Acta Agrophysica, 74.

Horabik J., Molenda M., 1989. True contact area between wheat grain and a flat surface. Zesz. Probl. Post. Nauk Roln., 378, 63-68.

Hueckel T., Dresher A., 1972. Nonlinear description of deformation of elastoplastic particulated materials (in Polish). Prace Instytutu Podstawowych Problemów Techniki PAN, 65.

Iwashita K., Oda M., 2000. Micro-deformation mechanism of shear banding process based on modified distinct element method. Powder Technology, 109, 192-205.

Jaeger H.M., Nagel S.R., Behringer R.P., 1996. Granular solids, liquids and gases. Reviews of Modern Physics, 68(4), 1259-1273.

Janssen H.A., 1895. Investigations of pressureof grain in silo (in German). Verein Deutscher Ingenieure, Zeitschrift (Dusseldorf), 39, 1045-1049.

Jenike & Johanson, 2005. Inc. Bulk Solids: Science/Engineering/Design; http://www.jenike.com/, 2005.

Jenike A.W., 1961. Gravity Flow of Bulk Solids. Bulletin of the University of Utah (52)29, Salt Lake City, Utah.

Jenike A.W., 1964. Storage and flow of solids. Bull.123, Eng. Expt. Sta., Utah State Univ.

Ji S., Shen H.H., 2004. Contact Force Models for Granular Flows, Report No 04-02.

Johnson K.L., 2004. Contact Mechanics, Cambridge University Press.

Kanatani K., 1981. A theory of contact force distribution in granular materials. Powder Technology, 28(2), 167-172.

Kanatani K., 1984. Distribution of directional data and fabric tensors. International Journal of Engineering Science, 22(2), 149-164.

Kezdi A., 1974. Handbook of soil mechanics. Akademiai Kiado. Budapest,

Kleiber M., 1995. Technical mechanics. Computational methods for mechanics of solids (in Polish). PWN, Warszawa.

Kolymbas D., 2000. Constitutive Modelling of Granular Materials, Springer-Verlag Berlin.

Kondic L., 1999. Statistical physics, plasmas, fluids, and related interdisciplinary topics. Physical Review. E, 60(1), 751-770.

Konishi J., Oda M., Nemat-Nasser S., 1982. Inherent anisotropy and shear strength of assembly of oval cross- sectional rods. Deformation and failure of granular materials. A.A. BALKEMA/Rotterdam.

Koper R., Grundas S., 1987. Young modulus and strain absorption in wheat grain of differentiated moisture content (in Polish). Zesz. Probl. Post. Nauk Roln., 320, 151-157.

Kragelsky I.V., Dobytchin M.N., Kombalov V.S., 1977. Principles of calculation of friction and wear (in Russian). Moskva, Maschinostroenie.

Kruggel-Emden H., Simek E., Rickelt S., Wirtz S., Scherer V., 2007. Review and extension of normal forcemodels for the discrete element method, Powder Technology, 171, 157-173.

Kutzbach H.D., Scherer R., 1977. Internal friction of cereal grain- review (in German). Landtechnik, 6, 213-219.

Kuwabara G., Kono K., 1987. Restitution coefficient in a collision between 2 spheres. Japanese Journal of Applied Physics, 26, 1230-1233.

Lade P. V., Nelson R. B., Ito Y. M., 1987. Nonassociated flow and stability of granular materials. Journal of Engineering Mechanics, 113(9), 1302-1318.

Landry J.W., Grest G.S., Silbert L.E., Plimpton S.J., 2003. Confined granular packings: structure, stress, and forces, arxiv:cond-mat/0211218v2.

Langston P.A., Tüzün U., Heyes D.M., 1995. Discrete element simulation of internal stress and flow fields in funnel flow hoppers. Powder Technology, 85, 153-169.

Łapko A., 1989. Effects of interaction of granular material on reinforced concrete walls in grain silos. Advences in Research of Technical University of Bialostok, 71, Białystok.

Łapko A., Prusiel J.A., 2000. Investigation on thermal effects in reinforced concrete cylindrical silo structures. Proc. of the 3rd Israeli Conference for Conveying and Handling of Particulate Solids1, 4.25-4.30.

Lawton P.J., 1980. Coefficients of friction between cereal grain and various silo wall materials. J. Agric. Engng Res., 25, 75-86.

Li Y., Zang Q., Puri V.M., Manbeck H.B., 1989. Physical properties effect on stress-strain behavior of wheat en masse – Part 1, load response dependence on initial bulk density and moisture content. Transactions of the ASAE, 32(1),194-202.

Lin X., Ng T-T., 1997. A three-dimensional discrete element model using arrays of ellipsoids, Géotechnique, 47(2), 319-329.

Liu X.L., Lemos J.V, 2001. Procedure of contact detection in discrete element analysis. Advances in Engineering Software, 32, 409-415.

Lobotka J., 1967. Coefficient of friction of chopped feed (in Czech). Zemedelska Technika, 13, 81-93.

Loewer Jr. O. J., Ross I.J., Kratzer D.D., Walker .N., 1977. Properties of ground shelled corn as related to forces in bulk storage structures. Transactions of the ASAE, 20(1), 155-156.

Lu Z., Negi S.C., Jofriet J.C., 1997. A Numerical Model Flow of Granular Materials in Silos. Part 1,2,3. Journal of Agricultural Engineering Research, 68, 223-229, 231-236, 237-246.

Łukaszuk J., Horabik J., 2002. Determination of angle of internal friction of plant granular solids (in Polish). Acta Agrophysica, 64, 1-94.

Maltby L.P., G.G. Enstad G.G., 1993. Uniaxial tester for quality control and flow property characterization of powders. Bulk Solids Handling, 13(1), 135-139.

Mark J., Holst F.G., Rotter J. M., Ooi J. Y., Rong G.H., 1999. Numerical Modeling of Silo Filling, I, Journal of Food Engineering and Mechanics, 125, 104-110.

Masson S., Martinez J., 2000. Multiscale simulations of the mechanical behaviourof an ensiled granular material, Mechanics of Cohesive-Frictional materials, Mech. Cohs.-Frict. Matter 5, 425-442.

Mindlin R.D., 1949. Compliance of elastic bodies in contact. J. Appl. Mechanics, 16, 259-268.

Mindlin R.D., Deresiewicz H., 1953. Elastic spheres in contact under varying oblique forces, Trans. ASME, Series E, Journal of Applied Mechanics, 20, 327.

Mishra B. K., Murty C.V. R., 2001. On the determination of contact parameters for realistic DEM simulations of ball mills. Powder Technology, 115, 290-297.

Mohsenin N.N., 1978. Physical properties of plant and animal materials. New York - London - Paris: Gordon and Breach Science Publishers.

Molenda M., Horabik J., 1998. Lateral to vertical pressure ratio in a model grain silo. Proceedings of the Seminar "Operations on granular materials", Lublin, 31-39.

Molenda M., Horabik J., Grochowicz J., Szot B., 1995. Friction of wheat grain (in Polish). Acta Agrophysicsa, 4.

Molenda M., Horabik J., Ross I.J., 1998. Stress and deformation of wheat in direct shear test. International Agrophysics, 12(2), 115-118.

Molenda M., Thompson S.A., Ross I.J., 2000. Friction of wheat on corrugated and smooth galvanized steel surfaces. Journal of Agricultural Engineering Research, 77(2), 209-219.

Molenda, M., Horabik, J., Ross, I.J., 1996. Effect of filling method on load distribution in model grain bins. Transactions of the ASAE, 39, 219-224.

Moore D.W., White G.M., Ross I.J., 1984. Friction of wheat on corrugated metal surfaces. Transactions of the ASAE, 6, 1842-1847.

Morland L.W., Sawicki A., Milne P.C., 1993. Uni-axial compaction of a granular material. J. Mech. Phys. Solids, 41(11), 1755-1779.

Morris J., Glenn L., Blair S., Heuze F., 2001. The Distinct Element Method – Application to Structures in Jointed Rock. International Workshop Meshfree Methods of Partial Differential Equations, Bonn, Germany, 11-14.09.2001.

Moysey E.B., 1984. The effect of grain sopreaders on grain friction and bin wall preasures. J. Agric. Engng. Res., 30, 149-156.

Moysey E.B., Hiltz S., 1985. Friction properties of fertilizers. Canadian Agricultural Engineering, 2, 79-83.

Mühlhaus H.B., Vardoulakis I., 1987. The thickness of shear bands in granular materials. Géotechnique, 37(3), 271-283.

Nedderman R.M., Laohakul C., 1980. The thickness of the shear zone of flowing granular materials. Powder Technology, 25, 91-100.

O'Sullivan C., Bray J.D., 2004. Selecting a suitable time step for discrete element simulations that use the central difference time integration scheme, Engineering Computations, 21(2/3/4), 278-303.

O'Sullivan C., Bray J.D., Riemer M., 2002. Influence of Particle Shape and Surface Friction Variability on Response of Rod-Shaped Particulate Media, Journal of Engineering Mechanics, 128, 11.

Oda M., 1976. Fabrics and their effects on the deformation behaviours of sand. Dept. Found. Engng. Fac. Engng. Saitama University, Special Issue.

Oda M., 1977. Coordination Number and its Relation to Shear Strength of granular material. Soil and Foundations, 17(2), 29-42.

Oda M., 1978. Significance of fabric in granular mechanics. Proc. US-Japan Seminar, Sendai, Japan, 7-26.

Oda M., Deformation mechanism of sand in triaxial compression tests. Soil and Foundations, 12(4), 45-63.

Oda M., Konishi J., Nemat-Nasser S., 1980. Some experimentally based fundamental results on the mechanical behaviour of granular materials. Geotechnique 30, 479-495.

Peleg M., 1985. The role of water in rheology of hygroscopic food powders. In: properties of water in Foods. Red. D. Simataos, J.L. Multon. Martinus Nijhoff Publishers Dordrecht, 394-404.

Peschl I.A.S.Z., 1989. Equipment for the measurement of mechanical properties of bulk materials. Powder Handling and Processing, (1) 1, 73-81.

Peschl I.A.S.Z., 1989. Measurement and evaluation of mechanical properties of powders. Powder Handling and Processing, (1) 2, 135-141.

Peschl I.A.S.Z., 1989. Quality control of powders for industrial application. Powder Handling and Processing, (1) 4, 357-363.

Ploof D.A., Carson J.W., 1994. Quality control tester to measure relative flowability of powders. Bulk Solids Handling, 14(1), 127-132.

PN-73/R-74007. Polish Standard. Cereal grains. Determination of density. Wydawnictwa Normalizacyjne "ALFA".

PN-74/Z-04002.07. Polish Standard. Air purity protection. Tests of dust physical properties. Determination of angle of repose dust. Polish Committee for Standarization, Measures and Quality.

PN-B-03254-2002: Concrete bins for granular materials. Calculation, design, performace and operation (in Polish).

Prusiel J.A., Nikitin W., 2000. Analisies of thermal effects in cylindrical concrete silos for bulk solids (in Polish). Proceedings from XI Conference „Reinforced and prestressed containers for granular materials", 161-168, Świeradów Zdrój.

Raji A.O., Favier J.F., 2004. Model for the deformation in agricultural and food particulate materials under bulk compressive loading using discrete element method. II: Compression of oilseeds, Journal of Food Engineering 64, 373-380.

Raltchev A., Barov W., 1970. New apparatus for determination of coefficient of internal friction (in Czech). Problemy Obrabotki Poczwy, Sofia, 169-177.

Richter D.W., 1954. Friction coefficients of some agricultural materials. Agricultural Engineering, June, 411-413.

Roscoe K.H., 1970. The influence of strains in soil mechanics. 10th Rankine Lecture. Géotechnique, 20(2), 127-170.

Rowe P.W., 1969. The relation between the shear strength of sands in triaxial compression, plane strain and direct shear. Geotechnique, 19(1), 75-86.

Rusinek R., Molenda M., Sykut J., Pits N., Tys J., 2007. Uniaxial compression of rapeseed using apparatus with cuboid chamber, Acta Agrophysica 10(3), 677-685.

Rymarz C., 1993. Mechanics of continuum. PWN Warszawa .

Sawicki A., 1994. Elasto-plastic interpretation of oedometric test., Archives of Hydro-Engineering and Environmental Mechanics, 41(1-2), 111-131.

Sawicki A., Świdziński W., 1995. Cyclic compaction of soils, grains and powders. Powder Technology, 85, 97-104.

Sawley M.L., Cleary P.W., 1999. A parallel Discrete Element Method for Industrial Granular Flow Simulations, EPFL Supercomputing Review EPFL-SCR, 11.

Scherer R., Kutzbach H.D., 1978. Mechanishe Eigenshaften von Kornerfruchten. Grundlagen Landtechnik, 1, 6-12.

Schott R.W, Britton M.B., 1984. Plane strain behaviour of bulk grain. Paper No. NCR84-503, ASAE St. Joseph, MI.

Schwedes J., 1975. Shearing behaviour of slightly compressed cohesive granular materials. Powder Technol., 11, 59-67.

Sitkei G., 1986. Mechanics of Agricultural Materials, Akadémiai Kiadó, Budapest.

Ślaska-Grzywna B., 1995. Method of determination of limit values of compaction of granular materials (in Polish). PhD dissertation. University of Life Sciences in Lublin, Poland.

Snyder L.H., Roller W.L., Hall G.E., 1967. Coefficients of kinetic friction of wheat on various metal surfaces. Transactions of the ASAE, 3, 411-419.

Stasiak M., Molenda M., 2001. Influence of moisture content on stress-strain relationship of wheat bed (in Polish). VI International Conference "Food Mechanical Engineering", 75-80, Bydgoszcz.

Stephens L.E. and Foster G.H., 1976. Grain bulk properties as affected by mechanical grain spreaders. Transactions of the ASAE 19(2), 354-358.

Stępniewski A., 1997. Influence of moisture content and temperature on variability of mechanical properties of rapeseeds (in Polish). PhD dissertation, Institute of Agrophysics PAS, Lublin, Poland.

Stewart B.R., Hossain Q.A., Kunze O.R., 1969. Friction coefficients of sorghum grain on steel, teflon and concrete surfaces. Transactions of the ASAE, 4, 415-418.

Stronge W.J., 2000. Impact Mechanics. Cambrige University Press, Cambrige, UK.

Sykut J., Molenda M., Horabik J., 2008. DEM simulation of the packing structure and wall load in a 2-dimensional silo. Granular Matter, 10, 273-278.

Tejchman J., 1998. Numerical simulation of filling in silos with a polar hypoplastic constitutive model. Powder Technology, 96, 227- 239.

Tejchman J., Wu W., 1995. Experimental and numerical study of sand – steel interfaces. International Journal for Numerical and Analytical Methods in Geomechanics, 19, 513- 536.

Thompson S.A., Ross I.J., 1983. Compressibility and frictional coefficient of wheat. Transactions of the ASAE, 26(4), 1171-1176.

Thornton C., 2000. Numerical simulations of deviatronic shear deformation of granular media. Géotechnique, 50(1), 43-53.

Thornton C., Ning Z., 1998. A theoretical model for the stick/bounce behaviour of adhesive, elastic-plastic spheres., Powder Technology, 99, 154-162.

Tijskens E., Ramon H., De Baerdemacker J., 2003. Discrete element modeling for process simulation in agriculture. Journal of Sound and Vibration, 266, 493-514.

Timoshenko S.P., Goodier J.N., 1934. Theory of elasticity, New York, McGraw-Hill.

Tsang-Mui-Chung M., Verma L. Lalit, Wright M.E., 1984. A device for friction measurement of grains. Transactions of the ASAE, 4, 1938-1944.

Tsuji Y., 1993. Simulation of particle motion in processes. IFPRI Annual Meeting, Pasadena, June.

Versavel P.A., Britton M.G., 1984. In-bin bulk density of grain. Paper No. 84-4004, ASAE, St. Joseph, MI.

Voyiadjis G.Z., Thiagarajan G., Petrakis E., 1995. Constitutive modelling for granular media using an anisotropic distortional yield model. Acta Mechanica, 110, 151-171.

Vu-Quoc L., Zhang X., Walton O.R., 2000. A 3-D discrete-element method for dry granular flows of ellipsoidal particles. Computer Methods in Applied Mechanics and Engineering, 187, 483-528.

Walton K., 1987. The effective elastic moduli of a random packing of spheres. J. of Mech. Phys. of Solids, 35(2), 213-226.

Willis J.R., 1966. Hertzian contact of anisotropic bodies. Journal of the Mechanics and Physics of Solids, 14, 163-176.

Wilms H., 1991. Criteria for evaluation of silo design codes. Bulk Solids Handling, 11 (1), 55-61.

Wojtkowski M., Pecen J., Horabik J., Molenda M., 2010. Rapeseed impact against a flat surface: Physical testing and DEM simulation with two contact models. Powder Technology, 198, 61-68.

Woźniak W., 1998. The effect of moisture treatment on mechanical properties of wheat grain. Proceedings of the Ninth Seminar "Properties of water in foods", 62-70, Zakopane.

Yu A.B., 2004. Discrete element method. An effective way for particle scale research of particulate matter. Engineering Computations, 21(2/3/4), 205-214.

Zahlan N., Knight D.T., Backhouse A., Leiper G.A., 2001. Modelling powder compaction and pressure cycling. Powder Technology, 114, 112-117.

Zhang D., Whiten W.J., 2001. Step size control for efficient discrete element simulation, Materials Engineering, 14(10), 1341-1346.

Zhang L., 2003. The behaviour of granular material in pure shear, direct shear and simple shear, PhD dissertation, Aston University.

Zhang Q., Britton M.G., Kieper R.J., 1994. Interactions between wheat and a corrugated steel surface. Trans. ASAE, 37(3), 951-956.

Zhang Q., Puri V.M., Manbeck H.B., 1986. Determination of elastoplastic constitutive parameters for wheat en masse. Transactions of the ASAE, 29(6), 1739-1746.

Zhang Q., Puri V.M., Manbeck H.B., 1988. Model for frictional behaviour of wheat on structural materials. Transactions of the ASAE, 3, 898-903.

Zhang Q., Puri V.M., Manbeck H.B., 1994. Applicability of a two-parameter failure criterion to wheat en masse. Transactions of the ASAE, 37(2), 571-575.

Zhang Y.H., Jofriet J.C., 1993. Equivalent stress-strain relationship for soybean and corn. ASAE Paper No. 934506. ASAE, St. Joseph, MI 49085.

9. SUMMARY

The main objective of the authors of that book was to present the current state of study of mechanical properties of granular solids with special focus on agro and food biologically based granular materials. The main features of biologically based materials that make them different from mineral materials are: strong influence of moisture content on mechanical behavior and high deformability of granules. These differences bring about certain peculiar behaviors and enforce adjustments of contact models and calculation techniques. This work review currently available solutions and present problems that have a chance to be solved in the nearest future. Out of these only narrow portions of knowledge were presented in this book that are directly tight with the phenomena encountered by the authors in their laboratory examinations or in practice.

The main theoretical approaches – continuum and discrete ones were presented in that book. The continuum theory that consider a volume of material as as a solid body or a liquid, was the earliest approach of scientists for predicting behaviors of bulk solids. Continuum approach led to solutions of numerous problems of technology but it failed in the cases where interactions between grains were important. Thus, the opposite option is to model every single grain using discrete approach. The computational technique which allows tracking the motion of each individual particle and obtaining detailed information about the system behavior is the Discrete (or Distinct) Element Method (DEM). For simulations, the trajectory and rotation of each particle in a system are obtained using a numerical time integration scheme. Today simulations of several thousands of 3D spheres or ellipsoids are conducted. Still long way remains to come regarding that the mass of 1000 seeds of wheat is approximately 40 g, thus 40 kg sack contains approximately one million kernels. Success of DEM examination of granular material rely on proper use of concepts from several branches of science and engineering, such as: mechanics of continuum, impact mechanics, contact mechanics, strength of materials and programming.

The presented work contains brief description of the most popular theoretical approaches, presents popular methods and equipment for determination of material parameters and interesting results of discrete element modeling of behavior of granular plant materials.

Keywords: granular plant materials, mechanics of granular solids, discrete element method

10. STRESZCZENIE

MECHANICZNE WŁAŚCIWOŚCI ROŚLINNYCH MATERIAŁÓW SYPKICH. UJĘCIE CIĘGLE I DYSKRETNE

Celem niniejszego opracowania było przedstawienie obecnego stanu wiedzy na temat mechanicznych właściwości materiałów rozdrobnionych, ze szczególnym uwzględnieniem materiałów pochodzenia roślinnego. Głównymi cechami odróżniającymi materiały sypkie pochodzenia biologicznego od materiałów mineralnych są: silny wpływ współczynnika wilgotności nasion na ich właściwości mechaniczne oraz duża odkształcalność nasion. Wspomniane różnice stanowią źródło pewnych szczególnych zachowań materiałów oraz determinują wybór modelu kontaktu i techniki obliczeniowej w badaniu ośrodków rozdrobnionych pochodzenia roślinnego. Niniejsze opracowanie prezentuje wąski zakres wiedzy, odnoszącej się do zjawisk i procesów badanych przez autorów podczas badań laboratoryjnych oraz niezbędnej w rozwiązaniach praktycznych.

W opracowaniu przedstawiono główne teoretyczne podejścia – ciągłe (*continuum*) i dyskretne. Teoria *continuum*, która traktuje złoże materiału jako całość, jako ciało stałe lub ciecz, jest najstarszym podejściem naukowym wykorzystywanym do przewidywania zachowań ośrodków rozdrobnionych. Podejście ciągłe umożliwiło rozwiązanie wielu problemów technologicznych, jednak nie może być ono stosowane gdy przebieg analizowanego procesu determinowany jest przez oddziaływania zachodzące między elementami ośrodka. Modelowanie pojedynczych elementów złożonego ośrodka umożliwia podejście dyskretne. Techniką numeryczną, pozwalającą na analizę ruchu każdej z cząstek ośrodka oraz dostarczającą szczegółowych informacji o zachowaniu elementów złoża jest, zaproponowana w 1979 roku, Metoda Elementów Dyskretnych (DEM). Trajektorie ruchu oraz obroty cząstek wyznaczane są poprzez numeryczne całkowanie równań ruchu względem czasu. Moc obliczeniowa dostępnych dziś procesorów umożliwia realizację symulacji procesów w ośrodkach tworzonych przez kilkadziesiąt tysięcy sfer lub elipsoid. Zważywszy na fakt, iż masa 1000 nasion pszenicy wynosi w przybliżeniu 40 g, zaś ośrodek o masie 40 kg zawiera około 1 miliona nasion, poszukiwanie metod ograniczania czasu symulacji oraz wymaganej mocy obliczeniowej pozostaje wciąż dużym wyzwaniem. Źródłem sukcesu badania zachowania materiałów sypkich poprzez użycie Metody Elementów Dyskretnych jest prawidłowe zastosowanie koncepcji wywodzących się z różnych dziedzin nauki i inżynierii: mechaniki ośrodków ciągłych, mechaniki zderzenia, mechaniki kontaktu, wytrzymałości materiałów oraz programowania.

Niniejsza praca zawiera krótki opis najbardziej popularnych podejść teoretycznych, przedstawia znane metody i urządzenia wykorzystywane do wyznacza-

nia parametrów materiałowych oraz interesujące wyniki modelowania roślinnych materiałów roślinnych metodą elementów dyskretnych.

Słowa kluczowe: roślinne materiały sypkie, mechanika materiałów sypkich, metoda elementów dyskretnych

Address of Authors:
Joanna Wiącek, Marek Molenda, Józef Horabik
Institute of Agrophysics, Polish Academy of Sciences
ul. Doświadczalna 4
20-290 Lublin
e-mail: jwiacek@ipan.lublin.pl

Adresy autorów
Joanna Wiącek, Marek Molenda, Józef Horabik
Instytut Agrofizyki im. Bohdana Dobrzańskiego PAN
ul. Doświadczalna 4
20-290 Lublin
e-mail: jwiacek@ipan.lublin.pl